
IGT-OMD: Implicit Gradient Transport for Decision-Focused Learning under Delayed Feedback

Benjamin Amoh Geoffrey Parker Wesley Marrero
 Thayer School of Engineering, Dartmouth College
 benjamin.k.amoh.th@dartmouth.edu

Abstract

Decision-focused learning trains predictive models end-to-end against downstream decision loss, but online settings suffer delayed feedback: outcomes may not arrive for many environment interactions. We identify *staleness amplification*, a failure mode unique to bilevel optimization under delay, in which gradient staleness couples with inner-solver sensitivity to inflate regret beyond single-level delay theory. We prove that any black-box delayed optimizer incurs an irreducible regret cost from inner-solver approximation error, and that gradient staleness contributes a quadratically growing transport error without bilevel-aware correction. Our algorithm, **IGT-OMD**, applies Implicit Gradient Transport to hypergradients within Online Mirror Descent, re-evaluating stale gradients at the current parameters using stored inner solutions. This method reduces transport error from a quadratic to a linear dependence on delay and achieves the first sublinear regret bound for delayed bilevel optimization with queue-length-adaptive step sizes. Controlled experiments provide a *mechanistic fingerprint*: transport benefit is exactly 0.0% (by construction) at unit delay and grows monotonically to 9.5% at fifty rounds ($p < 0.001$), isolating the correction’s effect. On Warcraft shortest-path, IGT-OMD reduces decision-loss optimality gap by 15–36% over D-FTRL/2-Stage baselines; on Linear Quadratic Regulator benchmark it maintains a constant maximum stable learning rate across delays where bilevel-unaware methods degrade by up to $9.3\times$.

1 Introduction

In many operational settings (from inventory management to energy dispatch to personalized medicine), a predictive model feeds its forecast into a downstream optimization solver whose solution is then deployed. Decision-Focused Learning (DFL) trains such models end-to-end against a *decision loss* rather than a surrogate prediction error [1, 2, 3]. The resulting training problem is inherently bilevel: the *outer level* adjusts the predictor parameters θ (e.g., neural-network weights), while the *inner level* solves for an optimal decision $w^*(\theta)$ (e.g., a control policy or a transport plan).

In online deployments, feedback is often delayed. A decision made at environment interaction (i.e., round) t yields observable outcome feedback only at round $t+d_t$, where the delay d_t may vary. At any given round, several past decisions may still be awaiting feedback; we call this set the *queue* with size (i.e., *queue length*) σ_t , and write σ_{\max} for its worst-case value. Single-level delayed optimizers such as Delayed Follow-the-Regularized-Leader (D-FTRL; 4, [5]) and Robust Online Mirror Descent (OMD) (OMD; 6) handle this challenge by correcting for the outer-parameter drift $\|\theta_t - \theta_{t-d_t}\|$.

Staleness amplification: why bilevel delay is harder. In single-level Online Convex Optimization (OCO), a stale gradient is a bounded perturbation independent of optimizer state. The bilevel setting is structurally different: the hypergradient of $F(\theta) = \mathcal{L}_{\text{true}}(w^*(\theta); \theta)$ depends on the inner minimizer $w^*(\theta)$, which drifts as θ changes. Feedback generated by an inner solution that has since drifted introduces gradient error proportional to accumulated outer-parameter change—*staleness amplification*.

Table 1: Comparison with related work. IGT-OMD is the first bilevel delayed optimizer.

Category	Method	Delay	Bilevel	Adaptive	Open Gap
Task-driven bilevel	SPO+ [1]	✗	✓	✗	No delays
	Online DFL [11]	✗	✓	✓	No delays
	Control-oriented MBRL [12]	✗	✓	✗	No delays
Single-level delayed OCO	D-FTRL [4]	✓	✗	✓	Staleness amplification
	Robust OMD [6]	✓	✗	✓	No bilevel
	DORM+ [13]	✓	✗	✓	Single-level
General Bilevel (no delays)	Online bilevel [18]	✗	✓	✗	No delays
	BSA [17]	✗	✓	✗	Offline
Grad. transport	IGT [7]	✓	✗	✗	Single-level RL
DDE analysis	Differential Delay Analysis [8]	✓	✗	✗	Distributed SGD
Ours	IGT-OMD	✓	✓	✓	—

This has two structural effects formalized in Theorem 2: an irreducible inner-solver floor on regret, and a per-round transport error that is quadratic in queue length without bilevel-aware correction.

IGT-OMD: how we fix it. The key idea of our algorithm is to *re-evaluate* stale hypergradients at the current parameters rather than using them as-is. When feedback from a past round s arrives, our algorithm has already stored an inner solution w_s and adjoint vector v_s^* to cheaply recompute the hypergradient at the current θ_t without re-solving the inner problem. Accumulating these corrections via Implicit Gradient Transport (IGT) [7] replaces the squared total drift $\|\theta_t - \theta_{t-d_t}\|^2$ with a sum of squared per-step changes $\sum_s \|\theta_{s+1} - \theta_s\|^2$, which is a factor σ_{\max} smaller. Embedding this corrected gradient in OMD with a step size that tracks the running queue envelope—motivated by Delay Differential Equation (DDE) stability analysis [8]—yields our algorithm, **IGT-OMD**.

Contributions. (1) *Algorithm.* IGT-OMD corrects stale hypergradients at $O(p)$ cost per outstanding round without re-solving inner problems (Algorithm 1). (2) *Analysis.* We prove the first bilevel-delayed regret bound $O(\sqrt{T}\sigma_{\max} + T\epsilon_{\text{inner}}^2)$ (Theorem 1), a staleness amplification lower bound showing $\Omega(T\epsilon_{\text{inner}}^2)$ is tight (Theorem 2), an inner-loop apathy decomposition decoupling staleness from inner-solver quality (Theorem 3), and DDE stability analysis (Propositions 1–2). (3) *Experiments.* On LQR, IGT-OMD maintains constant stability across all delays; on Warcraft, it reduces optimality gap by 15–36% over D-FTRL/2-Stage baselines. A controlled optimizer experiment confirms the predicted mechanistic signature with 9.5% improvement at $d = 50$ ($p < 0.001$).

1.1 Related Work

Table 1 positions IGT-OMD against relevant prior work. Previous DFL methods [1, 9, 2, 10, 11] solve the bilevel training problem but assume immediate feedback. Conceptually, DFL is a task-driven subclass of bilevel optimization: the inner problem is the downstream decision layer, and the outer model is trained on realized decision loss. Under this lens, we view [12] as closer to DFL-style prior work than general-purpose bilevel optimization. Single-level delayed optimizers [4, 6, 13, 14, 15, 16] correct for outer-parameter drift but treat the objective as a black-box function, making them vulnerable to staleness amplification when applied to bilevel problems (Theorem 2). Bilevel optimization methods [17, 18, 19, 20, 21] handle the nested structure but assume synchronous updates. Gradient transport [7] was originally developed for single-level reinforcement learning; DDE stability analysis [8] was applied to distributed stochastic gradient descent. No prior method handles both bilevel structure and delayed feedback. While some single-level delayed methods employ *delay-adaptive* step sizes (scaled by round or cumulative delay), their schedules do not account for inner-solver sensitivity—a factor unique to bilevel objectives. Our algorithm fills this gap by extending gradient transport from single-level policy gradients to bilevel hypergradients and embedding the result in OMD with *queue-length-adaptive* step sizes calibrated to the bilevel structure.

2 Problem Formulation

We now formalize the online bilevel optimization problem under delayed feedback. Our notation is summarized in Table 5 in Appendix A.

2.1 Online Bilevel Optimization with Delayed Feedback

Consider a learner that adjusts a predictive model each round, but outcome feedback arrives only after several rounds. The gradient signal for each update is therefore based on parameters from the past—the delayed bilevel feedback loop we formalize below.

At each interaction with the environment (i.e., round) $t = 1, \dots, T$, the learner holds outer-level predictor parameters $\theta_t \in \Theta \subseteq \mathbb{R}^p$ and approximately solves the inner problem $w^*(\theta_t) = \operatorname{argmin}_{w \in \mathcal{W} \subseteq \mathbb{R}^q} \mathcal{L}_{\text{model}}(w; \theta_t)$, where $\mathcal{L}_{\text{model}}$ is the model-based decision objective, p is the predictor dimension, and q is the decision dimension. The approximate solution w_t is obtained by running $K \in \mathbb{N}_{>0}$ gradient descent steps from the previous solution w_{t-1} , yielding inner-solver error $\|w_t - w^*(\theta_t)\| \leq \epsilon_{\text{inner}}$. The learner executes w_t , and after $d_t \geq 0$ rounds the environment reveals an outcome object z_t that determines the realized loss. At round t , newly arrived feedback is $A_t = \{s : s + d_s = t\}$, the set of arrived observations is $\mathcal{O}_t = \{(s, z_s) : s + d_s \leq t\}$, and the queue of rounds still awaiting feedback is $Q_t = \{s \leq t : s + d_s > t\}$, with queue length $\sigma_t = |Q_t|$ and envelope $\bar{\sigma}_t = \max_{r \leq t} \sigma_r$. Using only arrived feedback, the learner updates θ_{t+1} . The performance measure is *decision regret*:

$$\text{Regret}_T^{\text{dec}} = \sum_{t=1}^T \mathcal{L}_{\text{true}}(w_t; \theta_t) - \min_{\theta \in \Theta} \sum_{t=1}^T \mathcal{L}_{\text{true}}(w^*(\theta); \theta)$$

which compares the learner’s cumulative decision loss to that of the best fixed predictor in hindsight.

2.2 Hypergradient Computation via Implicit Differentiation

The hypergradient—the derivative of the decision loss with respect to the predictor parameters—decomposes via the Implicit Function Theorem [22] into an explicit (direct) and an implicit (through the inner solver) component. To avoid the $O(q^3)$ cost of a full Jacobian inversion, we follow [12] and introduce an adjoint vector $v^* \in \mathbb{R}^q$ that satisfies the linear system $H_w v^* = \nabla_w \mathcal{L}_{\text{true}}(w^*; \theta)$, where $H_w := \nabla_{ww}^2 \mathcal{L}_{\text{model}}(w^*; \theta)$ is the Hessian of the inner objective. The adjoint is computed approximately via Conjugate Gradient [23]. The hypergradient is then:

$$g_t(\theta) = \nabla_{\theta} \mathcal{L}_{\text{true}} \Big|_{w \text{ fixed}} - [\nabla_{\theta} \nabla_w \mathcal{L}_{\text{model}}(w^*; \theta)]^{\top} v^*, \quad (1)$$

where the first term captures the direct effect of θ on the loss and the second captures the indirect effect through how the inner solver’s decision changes with θ .

Re-evaluation under delay. When feedback from a past round s arrives at round $t > s$, the algorithm can re-evaluate the hypergradient at the current parameters θ_t using the stored inner solution w_s , observed feedback z_s , and adjoint v_s^* at $O(pq)$ cost, without re-solving the inner problem:

$$g_s(\theta_t) = \nabla_{\theta} \mathcal{L}_{\text{true}}(w_s; \theta_t) \Big|_{w \text{ fixed}} - [\nabla_{\theta} \nabla_w \mathcal{L}_{\text{model}}(w_s; \theta_t)]^{\top} v_s^*. \quad (2)$$

This is an approximation: the cached adjoint was computed at θ_s , so the re-evaluation holds (w_s, v_s^*) fixed and updates only the explicit θ_t -dependence. The resulting residual is controlled in Appendix E.1.

3 IGT-OMD Algorithm

IGT-OMD assembles three pieces, hypergradient transport (IGT), mirror-descent updates (OMD), and a queue-length-adaptive step size, into a single procedure that costs $O(pq)$ per outstanding round.

3.1 Building Blocks

Implicit Gradient Transport. IGT [7] is a mechanism to reevaluate a stale gradient via a telescoping sum. Given a gradient computed at a past iterate $g_s(\theta_s)$, the gradient estimate at

the current θ_t is $g_s^{\text{IGT}}(\theta_t) = g_s(\theta_s) + \sum_{k=s}^{t-1} [g_s(\theta_{k+1}) - g_s(\theta_k)]$. This estimate accumulates the one-step gradient changes along the trajectory from θ_s to θ_t . For the frozen surrogate $g_s(\cdot)$, the telescope is exact; under L -smoothness, the transported path variation satisfies $\sum_{k=s}^{t-1} \|g_s(\theta_{k+1}) - g_s(\theta_k)\|^2 \leq L^2 \sum_{k=s}^{t-1} \|\theta_{k+1} - \theta_k\|^2$, a *sum of squared per-step changes*. By contrast, the naïve stale-gradient surrogate uses $L^2 \|\theta_t - \theta_s\|^2$ (squared total displacement), which by the Cauchy–Schwarz inequality [24] is up to σ_t times larger. See Appendix B for details.

Online Mirror Descent. OMD [25] generalizes projected gradient descent via a Bregman divergence [26] $D_\psi(\theta, \theta') = \psi(\theta) - \psi(\theta') - \langle \nabla \psi(\theta'), \theta - \theta' \rangle$ generated by a strongly convex mirror map ψ :

$$\theta_{t+1} = \operatorname{argmin}_{\theta \in \Theta} \langle g_t, \theta \rangle + \frac{1}{\eta_t} D_\psi(\theta, \theta_t), \quad (3)$$

where η_t is a step size. When $\psi(\theta) = \frac{1}{2} \|\cdot\|^2$ (the squared Euclidean norm) the update recovers projected gradient descent. This method accommodates non-Euclidean geometries and admits $O(\sqrt{T})$ regret bounds extending to the delayed setting [4, 6]. See Appendix B for details.

3.2 IGT-OMD’s Per-Round Procedure

For each arrived round selected for transport, our algorithm maintains a replay buffer \mathcal{B} that stores the inner solution w_s , adjoint vector v_s^* , and the most recently transported hypergradient $g_s(\theta_{t-1})$. Algorithm 1 details our procedure. Each round t proceeds in three phases.

Phase 1: Solve and execute (lines 4–9). The learner runs K warm-started gradient-descent steps on $\mathcal{L}_{\text{model}}(\cdot; \theta_t)$ from w_{t-1} to obtain $w_t \approx w^*(\theta_t)$ with $\|w_t - w^*(\theta_t)\| \leq \epsilon_{\text{inner}}$, then executes w_t . No true-loss hypergradient for this decision is computed until its feedback arrives.

Phase 2: Transport (lines 11–18). When feedback arrives for rounds $s \in A_t$, the algorithm solves the corresponding adjoints, forms the arrival gradient, and re-evaluates earlier arrived gradients in the transport buffer. Aggregating the arrival term with these one-step corrections yields the IGT-corrected hypergradient:

$$g_t^{\text{IGT}} = g_{A_t}(\theta_t) + \sum_{s \in \mathcal{B}_t} [g_s(\theta_t) - g_s(\theta_{t-1})], \quad (4)$$

which is a causal telescoping update driven only by arrived feedback. Crucially, transport reuses the stored (w_s, v_s^*) and the inner problem is *not* re-solved during transport.

Phase 3: Adaptive update (lines 10 and 20). The learner takes an OMD step (3) with the corrected gradient and a queue-envelope-adaptive step size $\eta_t = \eta_0 / \sqrt{1 + \beta \bar{\sigma}_t}$, where $\eta_0 > 0$ is the base learning rate and $\beta = \|L_{\text{IGT}}\| / \lambda_{\min}(H_F)$ is the delay-sensitivity ratio (set to 1.0 when unknown). When the envelope is short, $\eta_t \approx \eta_0$ recovers the non-delayed rate; when long, η_t shrinks as $1/\sqrt{\bar{\sigma}_t}$.

3.3 Cost and Memory Analysis

The per-round cost is $O(Kpq + |A_t|q^2\kappa_w + |\mathcal{B}_t|pq)$ —a $\min(K, \kappa_w)$ -factor savings over re-solving each delayed inner problem; buffer memory is $O(\sigma_{\max}(p + 2q))$ (Appendix C).

Remark 1 (Optimizer-agnostic transport). *The transport correction (4) depends only on the parameter trajectory $\{\theta_s\}_{s \in Q_t}$, not on the specific update rule. Any optimizer—Adam, SGD, D-FTRL—that supplies iterates to the re-evaluation loop inherits the σ_{\max} -factor improvement. We validate this observation by evaluating Adam+IGT in Section 5.4 and D-FTRL+IGT in Appendix G.2.*

4 Theoretical Analysis

Our main results follow with their full proofs in Appendix E.1 - E.5.

4.1 Assumptions

We assume seven standard regularity conditions from bilevel optimization [17, 18] and delayed OCO [4, 6]: (A1–A2) inner strong convexity and smoothness; (A3) bounded solver error ϵ_{inner} ; (A4) bounded queue length σ_{\max} ; (A5) Lipschitz cross-partial (enables hypergradient re-evaluation in (2)); (A6) bounded hypergradients G ; and (A7) bilevel strong convexity; detailed in Appendix D

Algorithm 1 IGT-OMD: Implicit Gradient Transport for Bilevel Delayed Optimization

```

1: Input: Base step size  $\eta_0$ , damping  $\beta$ , inner steps  $K$ , inner step size  $\eta_w$ ; loss functions  $\mathcal{L}_{\text{model}} : \Theta \times \mathcal{W} \rightarrow \mathbb{R}$  (inner),
    $\mathcal{L}_{\text{true}} : \Theta \times \mathcal{W} \rightarrow \mathbb{R}$  (outer)
2: Initialize:  $\theta_1 \in \Theta$ ,  $w_0 \in \mathcal{W}$ , buffer  $\mathcal{B} \leftarrow \emptyset$ , queue  $Q_0 \leftarrow \emptyset$ , envelope  $\bar{\sigma}_0 \leftarrow 0$ 
3: for  $t = 1, \dots, T$  do
4:    $w_{t,0} \leftarrow w_{t-1}$  // warm-start
5:   for  $k = 0, \dots, K - 1$  do
6:      $w_{t,k+1} \leftarrow w_{t,k} - \eta_w \nabla_w \mathcal{L}_{\text{model}}(w_{t,k}; \theta_t)$  // inner GD
7:   end for
8:    $w_t \leftarrow w_{t,K}$ 
9:   Execute  $w_t$ ; receive arrivals  $A_t = \{s : s + d_s = t\}$  and update  $Q_t \leftarrow Q_{t-1} \cup \{t\} \setminus A_t$ 
10:   $\sigma_t \leftarrow |Q_t|$ ;  $\bar{\sigma}_t \leftarrow \max(\bar{\sigma}_{t-1}, \sigma_t)$ ;  $\eta_t \leftarrow \eta_0 / \sqrt{1 + \beta \bar{\sigma}_t}$ 
11:   $g^{\text{IGT}} \leftarrow 0$ 
12:  for  $s \in A_t$  do
13:    Solve  $H_w v_s^* = \nabla_w \mathcal{L}_{\text{true}}(w_s; \theta_t)$  and compute  $g_s(\theta_t)$  // arrival gradient
14:     $g^{\text{IGT}} \leftarrow g^{\text{IGT}} + g_s(\theta_t)$ ; store  $(w_s, v_s^*, g_s(\theta_t))$  in  $\mathcal{B}$ 
15:  end for
16:  for  $s \in \mathcal{B}$  do
17:    Re-evaluate  $g_s(\theta_t)$  and add  $g_s(\theta_t) - g_s(\theta_{t-1})$  to  $g^{\text{IGT}}$  // transport step
18:    Update cached  $g_s(\theta_t)$  in  $\mathcal{B}$ 
19:  end for
20:   $\theta_{t+1} \leftarrow \theta_t - \eta_t g^{\text{IGT}}$  // OMD update (3)
21:  Evict oldest entries if  $|\mathcal{B}| > \sigma_{\max}$ 
22: end for
23: Return:  $\{\theta_t\}_{t=1}^T$ 

```

4.2 Convergence of IGT-OMD

Our first question is whether IGT-OMD achieves sublinear regret, and whether inner-solver error and delay amplify each other. The theorem shows the coupling is additive, enabling independent control of both error sources.

Theorem 1 (Bilevel convergence under delay). *Under Assumptions 1–7, define $\rho_{\text{cpl}} := L_{w\theta}^2 / (\mu_w^2 \mu_F) < 1$ and $C_\rho = (1 - \rho_{\text{cpl}})^{-1}$. Algorithm 1 with step size η_t attains decision regret:*

$$\text{Regret}_T^{\text{dec}} \leq C_\rho \left[\frac{2D_\psi \sqrt{1 + \beta \sigma_{\max}}}{\eta_0} + \frac{\eta_0 G^2 T}{2} + 2T \epsilon_{\text{inner}}^2 + L_F \sum_{t=1}^T \sum_{k \in W_t} \|\theta_{k+1} - \theta_k\|^2 \right], \quad (5)$$

where D_ψ is the Bregman diameter of the feasible set. Setting $\eta_0 = c/\sqrt{T}$ yields $\text{Regret}_T^{\text{dec}} = O(\sqrt{T} \sigma_{\max} + T \epsilon_{\text{inner}}^2)$, where $c = 2D_\psi^{1/2} (1 + \beta \sigma_{\max})^{1/4} / G$ balances the first two terms of (5).

Single-level D-FTRL [4] and Robust OMD [6] attain $O(\sqrt{T} d_{\text{tot}})$ regret ($d_{\text{tot}} = \sum_t d_t = \text{total delay}$); we match this with σ_{\max} in place of d_{tot} —a strictly tighter measure since $\sigma_{\max} \leq d_{\max} \ll d_{\text{tot}}$ is possible [15]. Here $W_t = \{k : \max(1, t - \sigma_t) \leq k \leq t - 1\}$ is the active transport window. The $T \epsilon_{\text{inner}}^2$ penalty is additive, not multiplicative, so delay and inner-solver precision can be tuned independently.

4.3 Staleness amplification Lower Bound

We now ask how much delayed feedback penalizes bilevel optimization relative to single-level: is the $O(\sigma_{\max}^2)$ transport error growth a fundamental barrier, or a proof artifact? This matters to decision quality. The structural source of the barrier is the Implicit Function Theorem (IFT) coupling between the outer and inner problems: the bilevel Lipschitz constant $L_F = L_\theta + L_{w\theta}^2 / \mu_w$ —where $L_\theta = \|\nabla_\theta^2 \mathcal{L}_{\text{true}}\|$, $L_{w\theta} = \|\nabla_{w\theta}^2 \mathcal{L}_{\text{model}}\|$, and μ_w is the inner strong-convexity constant—encodes how sensitively $w^*(\theta)$ tracks outer-parameter changes. The coupling constant $C_0 = L_{w\theta} / \mu_w$ measures how inner-solver error propagates into the hypergradient. Theorem 2 formalizes three consequences of this coupling; part (b) constructs a hard quadratic instance confirming the lower bound is tight.

Theorem 2 (Staleness amplification). *Let \mathcal{A} be any delayed optimizer treating $F(\theta)$ as a black-box convex function using stale bilevel gradients without bilevel-aware correction. Then:*

(a) *The gradient mismatch satisfies $\|\hat{g} - \nabla F(\theta_t)\| \leq L_F \|\theta_t - \theta_{t-d_t}\| + C_0 \epsilon_{\text{inner}}$.*

- (b) On a hard quadratic bilevel instance, $\text{Regret}_T(\mathcal{A}) \geq \Omega(T\epsilon_{\text{inner}}^2)$, regardless of step-size schedule, delay handling strategy, or queue length adaptation.
- (c) Bilevel aware correction reduces the transport error from $O(\sigma_{\text{max}}^2\eta^2G^2)$ to $O(\sigma_{\text{max}}\eta^2G^2)$ per round—a factor σ_{max} improvement.

Statement (a) of Theorem 2 reveals staleness amplification: staleness couples with the bilevel Lipschitz constant L_F which is absent in single-level OCO. Statement (b) shows the $T\epsilon_{\text{inner}}^2$ term in Theorem 1 is tight. Lastly, statement (c) demonstrates that the effect of replacing the squared total drift with a sum of squared per-step changes through our telescoping correction is exactly σ_t by the Cauchy–Schwarz inequality [24] (confirmed numerically at $R^2 > 0.99$ in Section 5.3).

4.4 Inner-Loop Apathy Decomposition

Our third question is whether the delay error and the inner-solver error interact. The following decomposition shows that they do not, as transport decouples them.

Theorem 3 (Inner-loop apathy). *Under Assumptions 1–7, the decision regret decomposes as:*

$$\text{Regret}_T^{\text{dec}} = \underbrace{O(\eta_0^2 G^2 T \sigma_{\text{max}})}_{\text{delay error } (R_1)} + \underbrace{O(T \epsilon_{\text{inner}}^2)}_{\text{inner bias } (R_2)} + \underbrace{O\left(C_{\text{ap}} \sum_{t=1}^T \sum_{k \in W_t} \|\theta_{k+1} - \theta_k\|^2\right)}_{\text{interaction } (R_3)}. \quad (6)$$

The interaction R_3 uses per-step squared changes ($\sigma_t \eta^2 G^2$) instead of squared total drift ($\sigma_t^2 \eta^2 G^2$)—a σ_t factor improvement; here C_{ap} is an explicit bounded constant, so ϵ_{inner} remains additive rather than multiplied by delay.

This theorem implies that the optimizer becomes insensitive to the inner solver precision, suggesting “inner-loop apathy.” Moreover, IGT decouples the outer staleness from the inner-solver quality, with ϵ_{inner} entering additively.

4.5 DDE Stability and Discrete Consistency

The adaptive step size η_t is not heuristic: it arises from a stability analysis of the continuous-time limit. Taking $\eta \rightarrow 0$ in a bounded active-window embedding, the IGT-OMD iterates (3) converge to a DDE whose characteristic roots determine a sufficient stability certificate.

Proposition 1 (DDE stability region). *Suppose $\sigma_{\text{max}} < 1/\beta$ and $\theta^* \in \text{relint}(\Theta)$. Consider the continuous-time limit of IGT-OMD, $\dot{\theta}(t) = -\eta(t) g^{\text{IGT}}(\theta(t), \{\theta(t - \tau_s)\}_{s \in Q(t)})$, with $\eta(t) = \eta_0 / \sqrt{1 + \beta \bar{\sigma}(t)}$. Linearizing around θ^* , the system is asymptotically stable whenever $\eta_0 < \min\{1/(\|H_F\| \sqrt{1 + \beta \sigma_{\text{max}}}), \sqrt{1 + \beta \sigma_{\text{max}}} / (\sigma_{\text{max}} \sqrt{\|L_{\text{IGT}}\|})\}$, where $\|H_F\|$ denotes its spectral norm (equal to $\lambda_{\text{max}}(H_F)$; $H_F \succ 0$). This is a sufficient local certificate for the bounded active-window embedding used in the analysis.*

This result provides *local* asymptotic stability for the linearized, homogeneous system ($\epsilon_{\text{inner}} = 0$). In the analyzed embedding, the certificate is indexed by queue length σ_{max} rather than raw delay, matching the constant $\eta_{\text{max}} = 0.093$ observed across $\sigma \in \{1, \dots, 100\}$ in Table 2.

Proposition 2 (Discrete-continuous consistency). *Let θ_k^{disc} denote IGT-OMD iterates and $\theta^{\text{cont}}(t)$ the solution to the DDE in Proposition 1 with the same initial history. Under the assumptions of Proposition 1 and a uniform step bound $\eta_t \leq \eta_{\text{max}}$, the discrete trajectory tracks the continuous solution: $\sup_{k \leq T} \|\theta_k^{\text{disc}} - \theta^{\text{cont}}(t_k)\| \leq C \eta_{\text{max}}$, with $t_k = \sum_{s \leq k} \eta_s$ and a constant C depending on T , $\|H_F\|$, $\|L_{\text{IGT}}\|$, and σ_{max} but not on the discretization. Consequently, the discrete iterates inherit the asymptotic stability and contraction rate of the DDE up to $O(\eta_{\text{max}})$ error.*

Proposition 2 follows because Algorithm 1 is a forward-Euler discretization of the DDE. This result shows the stability region and contraction rate from the continuous-time system—particularly the η_{max} -dependent step size calibration of (3.2)—transfer to discrete iterates in practice, with error vanishing in η_{max} .

Remark 2 (Interior equilibrium). *Both propositions require $\theta^* \in \text{relint}(\Theta)$ for DDE linearization; the regret bounds (Theorems 1–3) hold without this restriction. The boundary case is handled by the OMD projection in (3).*

Table 2: LQR stability boundary: maximum stable learning rate η_{\max} vs. queue length σ . IGT-OMD maintains constant η_{\max} across all delays; bilevel-unaware methods (2-Stage, SPO+) degrade earliest.

Algorithm		$\sigma=1$	$\sigma=10$	$\sigma=20$	$\sigma=40$	$\sigma=60$	$\sigma=80$	$\sigma=100$
Bilevel	IGT-OMD (ours)	0.093	0.093	0.093	0.093	0.093	0.093	0.093
	2-Stage (MSE)	0.093	0.075	0.039	0.022	0.015	0.012	0.010
	SPO+	0.093	0.081	0.039	0.021	0.013	0.011	0.009
Single	D-FTRL	0.093	0.093	0.093	0.093	0.065	0.060	0.052
	Robust OMD	0.093	0.093	0.093	0.093	0.075	0.060	0.056
	Stale OMD	0.093	0.093	0.093	0.093	0.070	0.056	0.052

5 Experiments

We evaluate IGT-OMD across four environments that jointly test our theoretical claims: (i) LQR for stability under delay, (ii) Warcraft for staleness amplification, (iii) Sinkhorn OT for the σ_{\max} -factor transport error scaling, and (iv) a controlled experiment isolating the transport contribution with optimizer choice held fixed. Our baselines span a 2×2 matrix (bilevel-aware vs. single-level \times delay-aware vs. delay-unaware): 2-Stage (MSE), SPO+ [1], D-FTRL [4], Robust OMD [6], and Stale OMD [25]. Additional details on our experiments and additional analyses are in Appendices F and G. All experiments use 5–10 seeds; error bars report ± 1 standard deviation.

5.1 Linear Quadratic Regulator Stability Boundary

Setup. An LQR provides a clean bilevel stability testbed: the inner problem computes a linear gain for a learned dynamics model, with the inner configuration held fixed to isolate delay handling. We use true dynamics $x_{t+1} = A_{\text{true}}x_t + B_{\text{true}}u_t + \xi_t$ and learned parameters $\theta = (\hat{A}, \hat{B}) \in \mathbb{R}^{10 \times 13}$. Constant delays $d \in \{1, 10, 20, 40, 60, 80, 100\}$ span both the stable regime ($d \leq 40$, all methods converge) and the phase-transition region predicted by Proposition 1 ($d \geq 60$, bilevel-unaware methods degrade); beyond $d = 100$ baselines diverge entirely. The maximum stable learning rate η_{\max} is found via binary search.

Results. Table 2 reveals a two-regime structure: IGT-OMD maintains constant $\eta_{\max} = 0.093$ across all $\sigma \leq 100$ (Proposition 1), while bilevel-unaware methods (2-Stage, SPO+) degrade to 0.010 at $\sigma = 100$ (89% reduction). Single-level delay-aware methods degrade more slowly but still fall to 0.052 (44%). IGT-OMD’s achieves $9.3\times$ and $1.8\times$ gains over 2-Stage and D-FTRL respectively.

Remark 3 (Constant delay as adversarial worst case). *Constant $d_t = d$ gives $\sigma_{\max} = d$ and maximizes $\sum_t \sigma_t$ among all delay patterns with the same total feedback budget. Hence, our constant-delay experiments are adversarial; variable delays can only improve on these bounds. We additionally validate under uniform delays in Appendix G.3.*

5.2 Warcraft Shortest Path: A structural contrast

Having established stability in a linear setting, we turn to a combinatorial optimization benchmark to test whether staleness amplification degrades the quality of real decisions.

Setup. We study shortest-path planning on 12×12 grids from Warcraft II maps with four terrain types. The outer parameters $\theta \in \mathbb{R}^{128}$ index the trainable hidden-layer column of a 2-layer neural network predicting per-cell traversal costs, and outer gradients are computed with the differentiable perturbation surrogate of Vlastelica et al. [9]. The inner problem runs Dijkstra’s algorithm to find the shortest path—an exact solver, so $\epsilon_{\text{inner}} = 0$. The decision loss evaluates the chosen path under true terrain costs; the *optimality gap* measures the excess cost over the oracle shortest path. We test constant delays $d \in \{0, 10, 50, 100\}$ and stochastic Poisson delays with mean $\lambda \in \{10, 25, 50, 100\}$ under OU edge-cost drift rate 0.05. We use 10 seeds over $T = 5,000$ rounds.

Results. Table 3 reveals three structural findings. First, IGT-OMD achieves the lowest optimality gap across all delay configurations: at $d=100$, gap 1.56 vs. 1.83 for D-FTRL (14.8% reduction) and 2.42 for 2-Stage (35.5% reduction), confirming staleness amplification (Theorem 2(a)). Second, methods without bilevel awareness (2-Stage, SPO+) degrade most severely (1.6–3.4 \times gap relative to IGT-OMD), showing that ignoring the inner solver’s sensitivity has dramatic consequences under

Table 3: Warcraft shortest path: optimality gap (mean over last 200 rounds, ± 1 s.d.) vs. delay configuration. IGT-OMD achieves the smallest gap across all settings.

Algorithm		Constant Delay		Poisson Delay	
		$d = 50$	$d = 100$	$\lambda = 50$	$\lambda = 100$
Bilevel	IGT-OMD (ours)	1.52\pm0.21	1.56\pm0.27	1.70\pm0.18	1.53\pm0.16
	2-Stage (MSE)	2.17 \pm 0.42	2.42 \pm 0.42	2.46 \pm 0.44	2.39 \pm 0.43
	SPO+	4.10 \pm 1.76	4.11 \pm 1.94	5.76 \pm 0.99	4.26 \pm 1.58
Single	D-FTRL	1.97 \pm 0.50	1.83 \pm 0.15	1.91 \pm 0.31	1.94 \pm 0.18
	Robust OMD	1.86 \pm 0.34	1.77 \pm 0.15	1.85 \pm 0.28	1.81 \pm 0.39
	Stale OMD	1.82 \pm 0.33	1.77 \pm 0.23	1.89 \pm 0.42	1.80 \pm 0.33

delay. Third, because the inner solver is exact ($\epsilon_{\text{inner}} = 0$), the inner-loop apathy benefit (Theorem 3) is inoperative here. The reduction over delay-aware methods (12–21%) is correspondingly smaller than on Sinkhorn, where $\epsilon_{\text{inner}} > 0$ —a structural prediction of the theory.

5.3 Transport Error Scaling (Sinkhorn Optimal Transport)

Warcraft uses an exact inner solver, so the inner-solver error channel (R_2 in Theorem 3) is zero. To test the full $R_1 + R_2 + R_3$ decomposition, we need an environment where $\epsilon_{\text{inner}} > 0$.

Setup. We use a Sinkhorn (OT) task—computing a minimum-cost coupling between two discrete distributions via differentiable entropic regularization ($n = 10$, $K = 10$ inner Sinkhorn iterations, OU drift)—with constant delays $d \in \{1, 2, 5, 10, 20, 50\}$, $T = 1,000$, 5 seeds, to test the transport error scaling claims of Theorems 2(c) and 3. We compute two error surrogates: $R_{\text{sq}} = \sum_t \|\theta_t - \theta_{t-d}\|^2$ (squared total drift, the quantity naïve methods pay) and $R_3 = \sum_t \sum_{s \in Q_t} \|\theta_{s+1} - \theta_s\|^2$ (sum of per-step squared changes, the quantity IGT pays).

Results. The ratio R_{sq}/R_3 tracks σ_{max} with near-perfect fidelity across all four algorithms: ratio ≈ 9.99 at $d = 10$, ≈ 19.9 at $d = 20$, ≈ 49.3 at $d = 50$ (Table 8 in Appendix F.3). Log-log regression in Figure 1 confirms the theoretical slopes: $R_3 \propto \sigma^{0.99}$ and $R_{\text{sq}} \propto \sigma^{1.99}$ (both $R^2 > 0.99$). This consistent ratio is not an algorithmic artifact—it holds identically for IGT-OMD, D-FTRL, Robust OMD, and Stale OMD—because the σ_{max} -factor improvement follows from a *geometric* identity (Cauchy–Schwarz [24]) of the parameter trajectory.

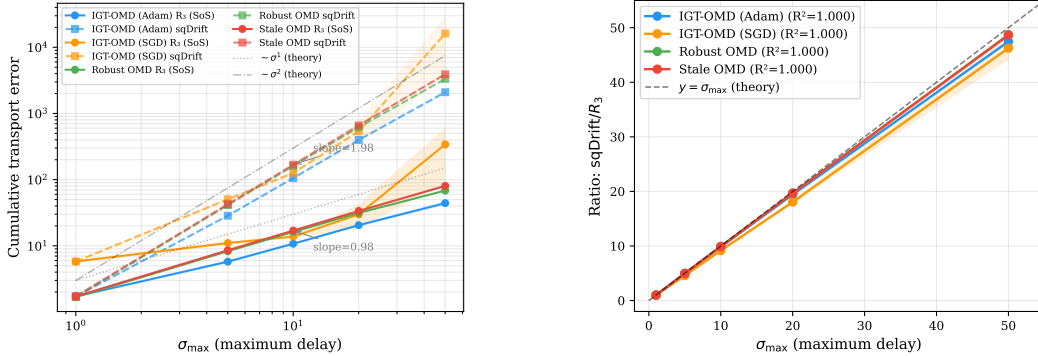


Figure 1: **Transport error scaling validates Theorem 2(c).** *Left:* Log-log regression of cumulative R_3 (slope ≈ 1) and R_{sq} (slope ≈ 2) against σ_{max} , confirming linear vs. quadratic scaling. *Right:* The ratio R_{sq}/R_3 tracks σ_{max} with near-perfect agreement across all algorithms.

5.4 Isolating Transport Contribution with Adam

Algorithm 1 with SGD does not outperform Adam baselines (i.e., Robust OMD, and Stale OMD) on the Sinkhorn OT non-convex task—the transport corrections are exact, but the base optimizer’s convergence properties also matter. To disentangle these effects, we hold the Adam optimizer [27] fixed in this experiment.

Table 4: Sinkhorn OT: cumulative regret ($T = 1,000$, 5 seeds). Adam+IGT vs. Stale OMD isolates the transport contribution; improvement grows monotonically with delay ($p < 0.01$ for $d \geq 10$).

Algorithm	$d = 1$	$d = 5$	$d = 10$	$d = 20$	$d = 50$
Adam+IGT (ours)	579±15	557±14	551±12	553±10	568±12
Stale OMD (Adam)	579±15	583±14	589±14	601±14	628±13
Robust OMD (Adam)	581±15	586±16	594±16	606±14	634±15
Improvement (%)	0.0%	+4.6%	+6.5%	+7.9%	+9.5%
<i>p</i> -value	–	0.029	0.004	<0.001	<0.001

Setup. To isolate IGT transport from optimizer choice, both treatment (IGT-OMD) and control (Stale OMD) use identical Adam ($\eta = 10^{-3}$, $\beta_1 = 0.9$, $\beta_2 = 0.999$). We refer to the modification of IGT-OMD with Adam as Adam+IGT. Our experiment uses the same Sinkhorn environment with $d \in \{1, 5, 10, 20, 50\}$, $T = 1,000$, and 5 seeds.

Results. Table 4 shows a monotonically growing transport benefit: 0.0% at $d = 1$ (by construction), +4.6% at $d = 5$, +7.9% at $d = 20$ ($p < 0.001$), +9.5% at $d = 50$ ($p < 0.0001$). The $d = 1$ zero is a designed negative control: when $|Q_t| = 1$, the sum-of-squares and squared-total-drift are identical, so IGT is vacuous. The monotonic growth is the signature of Theorem 2(c). Adam+IGT’s regret remains statistically flat across delays, while Stale OMD’s regret monotonically increases.

2×2 factorial. In a 2×2 factorial over optimizer and transport, we find cumulative regret grows modestly without transport (+7.3% for SGD and +8.4% for Adam as delay increased from $d = 1$ to $d = 50$). However, the interaction is non-additive: IGT+SGD *worsens* degradation to +28.8%, while IGT+Adam *eliminates* it (−1.8%, $p = 0.29$). Transport corrections and adaptive scaling are synergistic—neither alone achieves zero degradation.

Remark 4 (Trajectory stability as hidden requirement). *Adam’s per-coordinate scaling constrains step magnitudes, ensuring transported gradients $g_s(\theta_t)$ remain accurate corrections. SGD lacks this preconditioning, so transport introduces noise in high-curvature directions. See Appendix G.2.*

D-FTRL+IGT. Repeating with D-FTRL as the base optimizer yields a near-identical improvement curve (0.0% at $d = 1$ to +9.8% at $d = 50$; Table 11 in Appendix G.2), confirming the optimizer-agnostic transport benefit (Remark 1).

Summary. A unified table mapping results to theorems is in Appendix F; Appendix G.1 reports a non-convex HalfCheetah MPC stress test reserved for the non-convex extension. Across assumption-aligned benchmarks, the results confirm each theoretical claim: constant stability across delays (Proposition 1), staleness amplification in bilevel-unaware methods (Theorem 2(a)), the σ_{\max} -factor improvement as a geometric identity (Theorem 2(c)), and additive decoupling of inner-solver error from delay (Theorem 3).

6 Conclusion

We introduced IGT-OMD, the first delayed optimizer for bilevel predict-then-optimize pipelines. Our analysis identifies staleness amplification—the coupling between outer-parameter staleness and inner-solver sensitivity—as a failure mode unique to bilevel delay (Theorem 2), establishes a matching lower bound, and shows IGT reduces transport error by a factor σ_{\max} . Adam+IGT achieves 9.5% lower regret than Stale OMD at $d=50$ ($p < 0.001$), with the improvement growing monotonically with delay, as predicted, and vanishing at $d=1$ as a designed negative control. A 2×2 factorial confirms transport and adaptive scaling are synergistic—only their combination eliminates delay degradation. Our broader impacts are summarized in Appendix H.

Limitations and Future Work. Strong convexity of $\mathcal{L}_{\text{model}}$ (Assumption 1) may not hold for neural predictors; a formal non-convex analysis remains open. Our 2×2 factorial analysis shows that transport corrections require trajectory stability (Adam) and can *amplify* degradation without it (SGD)—an interaction not captured by the current theory. Per-round cost $O(Kpq + \sigma_{\max}pq + q^2\kappa_w)$ may be prohibitive for large q ; low-rank Hessian approximations could help. Natural extensions include non-convex inner objectives via fixed-point implicit differentiation applications, applications in reinforcement learning with delayed rewards, and federated settings with communication delays.

References

- [1] Adam N. Elmachtoub and Paul Grigas. Smart “Predict, then Optimize”. *Management Science*, 68(1):9–26, 2022. doi: 10.1287/mnsc.2020.3922.
- [2] Bryan Wilder, Bistra Dilkina, and Milind Tambe. Melding the data-decisions pipeline: Decision-focused learning for combinatorial optimization. In *Proceedings of the AAAI Conference on Artificial Intelligence*, volume 33 (01), pages 1658–1665, 2019. doi: 10.1609/aaai.v33i01.33011658.
- [3] Jayanta Mandi, James Kotary, Senne Berden, Maxime Mulamba, Victor Bucarey, Tias Guns, and Ferdinando Fioretto. Decision-focused learning: Foundations, state of the art, benchmark and future opportunities. *Journal of Artificial Intelligence Research*, 81:1623–1701, 2024.
- [4] Pooria Joulani, András György, and Csaba Szepesvári. Online learning under delayed feedback. In *International Conference on Machine Learning*, pages 1453–1461. PMLR, 2013.
- [5] Shai Shalev-Shwartz. Online learning and online convex optimization. *Foundations and Trends in Machine Learning*, 4(2):107–194, 2012.
- [6] Kent Quanrud and Daniel Khashabi. Online learning with adversarial delays. In *Advances in Neural Information Processing Systems*, volume 28, pages 1270–1278. Curran Associates, Inc., 2015. URL <https://neurips.cc>.
- [7] Sébastien M.R. Arnold, Pierre-Antoine Manzagol, Reza Babanezhad, Ioannis Mitliagkas, and Nicolas Le Roux. Reducing the variance in online optimization by transporting past gradients. In *Advances in Neural Information Processing Systems*, volume 32, 2019.
- [8] Siyuan Yu, Wei Chen, and H. Vincent Poor. Distributed stochastic gradient descent with staleness: A stochastic delay differential equation based framework. *IEEE Transactions on Signal Processing*, 2025. doi: 10.48550/arxiv.2406.11159. Accepted. arXiv:2406.11159.
- [9] Marin Vlastelica, Anselm Paulus, Vít Musil, Georg Martius, and Michal Rolínek. Differentiation of blackbox combinatorial solvers. In *International Conference on Learning Representations*, 2020.
- [10] Bo Tang and Elias B. Khalil. PyEPO: A PyTorch-based end-to-end predict-then-optimize library for linear and integer programming. *arXiv preprint arXiv:2206.14234*, 2022. doi: 10.48550/arXiv.2206.14234. URL <https://arxiv.org>.
- [11] Aymeric Capitaine, Maxime Haddouche, Eric Moulines, Michael I. Jordan, Etienne Boursier, and Alain Durmus. Online decision-focused learning. *arXiv preprint arXiv:2505.13564*, 2025. URL <https://arxiv.org>.
- [12] Evgenii Nikishin, Remo Abachi, Rishabh Agarwal, and Pierre-Luc Bacon. Control-oriented model-based reinforcement learning with implicit differentiation. In *Proceedings of the AAAI Conference on Artificial Intelligence*, volume 36(7), pages 7886–7894, 2022. doi: 10.1609/aaai.v36i7.20758.
- [13] Genevieve Flaspohler, Francesco Orabona, Judah Cohen, Soukayna Mouatadid, Miruna Oprescu, Paulo Orenstein, and Lester Mackey. Online learning with optimism and delay. In *Proceedings of the 38th International Conference on Machine Learning*, volume 139 of *Proceedings of Machine Learning Research*, pages 3363–3373. PMLR, 2021. URL <https://mlr.press>.
- [14] Jiatai Huang, Yan Dai, and Longbo Huang. Banker online mirror descent: A universal approach for delayed online bandit learning. In *Proceedings of the 40th International Conference on Machine Learning*, volume 202 of *Proceedings of Machine Learning Research*, pages 13818–13847. PMLR, 2023. URL <https://proceedings.mlr.press/v202/huang23e/huang23e.pdf>.
- [15] Alexander Ryabchenko, Idan Attias, and Daniel M. Roy. A reduction from delayed to immediate feedback for online convex optimization with improved guarantees. In *Proceedings of the AAAI Conference on Artificial Intelligence*, volume 40 (01), pages 1–9, 2026. doi: 10.48550/arXiv.2602.02634. URL <https://arxiv.org/abs/2602.02634>.

- [16] Hao Qiu, Mengxiao Zhang, and Juliette Achddou. Decentralized online convex optimization with unknown feedback delays. In *Proceedings of the AAAI Conference on Artificial Intelligence*, volume 40 (01), pages 1–9, 2026. doi: 10.1609/aaai.v40i30.39688. URL <https://ojs.aaai.org/index.php/AAAI/article/view/39688>.
- [17] Saeed Ghadimi and Mengdi Wang. Approximation methods for bilevel programming. *arXiv preprint arXiv:1802.02246*, 2018. doi: 10.48550/arXiv.1802.02246. URL <https://arxiv.org/abs/1802.02246>.
- [18] Kaiyi Ji, Junjie Yang, and Yingbin Liang. Bilevel optimization: Convergence analysis and enhanced design. In *International Conference on Machine Learning*, pages 4882–4892. PMLR, 2021. doi: 10.48550/arxiv.2010.07962.
- [19] Davoud Ataee Tarzanagh, Parvin Nazari, Bojian Hou, Li Shen, and Laura Balzano. Online bilevel optimization: Regret analysis of online alternating gradient methods. In *Proceedings of the 27th International Conference on Artificial Intelligence and Statistics*, volume 238 of *Proceedings of Machine Learning Research*, pages 2854–2862. PMLR, 2024. URL <https://proceedings.mlr.press/v238/ataee-tarzanagh24a.html>.
- [20] Sen Lin, Daouda Sow, Kaiyi Ji, Yingbin Liang, and Ness Shroff. Non-convex bilevel optimization with time-varying objective functions. In *Advances in Neural Information Processing Systems*, volume 36, pages 12658–12686. Curran Associates, Inc., 2023. URL https://proceedings.neurips.cc/paper_files/paper/2023/hash/5ee60ca5686bbcf756e56a6c75e66f32-Abstract-Conference.html.
- [21] Parvin Nazari, Bojian Hou, Davoud Ataee Tarzanagh, Li Shen, and George Michailidis. Stochastic regret guarantees for online zeroth- and first-order bilevel optimization. In *Advances in Neural Information Processing Systems*, volume 38. Curran Associates, Inc., 2025. URL <https://arxiv.org/abs/2511.01126>.
- [22] Asen L. Dontchev and R. Tyrrell Rockafellar. *Implicit Functions and Solution Mappings: A View from Variational Analysis*. Springer Monographs in Mathematics. Springer New York, 2nd edition, 2014. ISBN 978-1-4939-1036-6. doi: 10.1007/978-1-4939-1037-3.
- [23] Magnus Rudolph Hestenes and Eduard Stiefel. Methods of conjugate gradients for solving linear systems. *Journal of Research of the National Bureau of Standards*, 49(6):409–436, 1952. doi: 10.6028/jres.049.044.
- [24] J. Michael Steele. *The Cauchy-Schwarz Master Class: An Introduction to the Art of Mathematical Inequalities*. Cambridge University Press, Cambridge, UK, 2004. ISBN 978-0521546775. doi: 10.1017/cbo9780511817106.
- [25] Arkadi Nemirovski, Anatoli Juditsky, Guanghui Lan, and Alexander Shapiro. Robust stochastic approximation approach to stochastic programming. *SIAM Journal on Optimization*, 19(4): 1574–1609, 2009. doi: 10.1137/070704277.
- [26] Lev M Bregman. The relaxation method of finding the common point of convex sets and its application to the solution of problems in convex programming. *USSR Computational Mathematics and Mathematical Physics*, 7(3):200–217, 1967.
- [27] Diederik P. Kingma and Jimmy Ba. Adam: A method for stochastic optimization. In *Proceedings of the 3rd International Conference on Learning Representations*, San Diego, CA, USA, 2015. URL <https://arxiv.org>. ICLR 2015.
- [28] Dimitri P. Bertsekas. *Nonlinear Programming*. Athena Scientific, Belmont, MA, 3rd edition, 2016. ISBN 978-1886529052.
- [29] Amir Beck and Marc Teboulle. Mirror descent and nonlinear projected subgradient methods for convex optimization. *Operations Research Letters*, 31(3):167–175, 2003. doi: 10.1016/s0167-6377(02)00231-6.
- [30] V. Kolmanovskii and A. Myshkis. *Stability of Stochastic Functional Differential Equations*, volume 463 of *Mathematics and Its Applications*, pages 387–437. Springer Netherlands, Dordrecht, 1999. doi: 10.1007/978-94-017-1965-0_10.

- [31] B. G. Pachpatte. *Inequalities for Differential and Integral Equations*, volume 197 of *Mathematics in Science and Engineering*. Academic Press, San Diego, CA, 1998. ISBN 978-0125434300.
- [32] Arieh Iserles. *A First Course in the Numerical Analysis of Differential Equations*. Cambridge Texts in Applied Mathematics. Cambridge University Press, Cambridge, UK, 2nd edition, 2009. ISBN 978-0521734905. doi: 10.1017/CBO9780511995569.
- [33] Eliahu I. Jury. *Theory and Application of the z-Transform Method*. John Wiley & Sons, New York, NY, USA, 1964. ISBN 978-0471452850.
- [34] Adam Paszke, Sam Gross, Francisco Massa, Adam Lerer, James Bradbury, Gregory Chanan, Trevor Killeen, Zeming Lin, Natalia Gimelshein, Luca Antiga, et al. PyTorch: An imperative style, high-performance deep learning library. In *Advances in Neural Information Processing Systems*, volume 32, pages 8024–8035. Curran Associates, Inc., 2019. URL <https://neurips.cc>.
- [35] Greg Brockman, Vicki Cheung, Ludwig Pettersson, Jonas Schneider, John Schulman, Jie Tang, and Wojciech Zaremba. OpenAI Gym. *arXiv preprint arXiv:1606.01540*, 2016. doi: 10.48550/arXiv.1606.01540. URL <https://arxiv.org/abs/1606.01540>.

A Notation Table

Table 5: Principal notation.

Symbol	Definition
<i>Core variables and delay</i>	
$\theta_t \in \Theta \subseteq \mathbb{R}^p$	Outer-level predictor parameters at round t
$w_t \in \mathcal{W} \subseteq \mathbb{R}^q$	Approximate inner-level decision at round t
$w^*: \Theta \rightarrow \mathcal{W}$	Inner minimizer: $w^*(\theta) = \operatorname{argmin}_{w \in \mathcal{W}} \mathcal{L}_{\text{model}}(w; \theta)$
$\mathcal{L}_{\text{model}}: \mathcal{W} \times \Theta \rightarrow \mathbb{R}$	Model-based decision objective (inner loss)
$\mathcal{L}_{\text{true}}: \mathcal{W} \times \Theta \rightarrow \mathbb{R}$	Environment-evaluated decision loss (outer loss)
$d_t \in \mathbb{N}_0$	Feedback delay for round t
$Q_t \subseteq [t]$	Queue of outstanding rounds: $Q_t = \{s \leq t : s + d_s > t\}$
$\sigma_t = Q_t $	Queue length at time t
$\sigma_{\max} = \max_t \sigma_t$	Maximum queue length over all rounds
$\epsilon_{\text{inner}} \geq 0$	Inner-solver error: $\ w_t - w^*(\theta_t)\ \leq \epsilon_{\text{inner}}$
$g_t: \Theta \rightarrow \mathbb{R}^p$	Hypergradient: $g_t(\theta) = \frac{d}{d\theta} \mathcal{L}_{\text{true}}(w^*(\theta); \theta)$
$D_\psi: \Theta \times \Theta \rightarrow \mathbb{R}_{\geq 0}$	$D_\psi(\theta, \theta') = \psi(\theta) - \psi(\theta') - \langle \nabla \psi(\theta'), \theta - \theta' \rangle$
$\psi: \Theta \rightarrow \mathbb{R}$	Strongly convex mirror map generating D_ψ
$F: \Theta \rightarrow \mathbb{R}$	Bilevel objective: $F(\theta) = \mathcal{L}_{\text{true}}(w^*(\theta); \theta)$
<i>Dimensions and horizon</i>	
T	Total number of rounds (horizon)
$t \in \{1, \dots, T\}$	Round index
p	Dimension of outer parameters θ_t
q	Dimension of inner decisions w_t
K	Number of inner gradient-descent steps per round
ρ	Inner-solver contraction factor, e.g. $\epsilon_{\text{inner}} = O(\rho^K)$ with $\rho < 1$
<i>Smoothness and convexity constants</i>	
L_w	Smoothness constant of $\mathcal{L}_{\text{model}}$ w.r.t. w (Assumption A1)
μ_w	Strong-convexity constant of $\mathcal{L}_{\text{model}}$ w.r.t. w (Assumption A1)
L_θ	Lipschitz constant of $\nabla_\theta \mathcal{L}_{\text{true}}$ w.r.t. θ (Assumption A2)
$L_{w\theta}$	Bound on cross-partial $\ \nabla_{w\theta}^2 \mathcal{L}_{\text{model}}\ $ (Assumptions A2, A5)
μ_F	Strong-convexity constant of bilevel objective F (Assumption A7)
L_F	Bilevel Lipschitz constant: $L_F = L_\theta + L_{w\theta}^2 / \mu_w$
G	Uniform bound on corrected hypergradients: $\ g_t^{\text{IGT}}\ \leq G$ (Assumption A6)
G_{true}	Exact hypergradient bound: $G_{\text{true}} = \sup_\theta \ \nabla F(\theta)\ $ (Assumption A6)
C_0	Cross-objective sensitivity: $C_0 = L_{w\theta} / \mu_w$ (Theorem 2(a))
$\rho_{\text{cpl}}, C_\rho$	Coupling ratio $\rho_{\text{cpl}} = L_{w\theta}^2 / (\mu_w^2 \mu_F) < 1$ and multiplier $C_\rho = (1 - \rho_{\text{cpl}})^{-1}$
C_1, κ	Proof-local sensitivity constants in Theorem 3: $C_1 = L_{\theta w} / \mu_w, \kappa = L_g C_1$
κ_w	Inner-problem condition number: $\kappa_w = L_w / \mu_w$
δ	CG solver tolerance (adjoint solve cost $O(q^2 \kappa_w \ln(1/\delta))$)
<i>Algorithm-specific quantities</i>	
η_0	Base (initial) step size
η_t	Adaptive step size at round t : $\eta_t = \eta_0 / \sqrt{1 + \beta \bar{\sigma}_t}$
η_w	Inner step size (Algorithm 1 line 6)
β	Delay sensitivity ratio: $\beta = \ L_{\text{IGT}}\ / \lambda_{\min}(H_F)$
H_w	Inner Hessian: $H_w = \nabla_{w w}^2 \mathcal{L}_{\text{model}}(w^*; \theta)$
$v_t^* \in \mathbb{R}^q$	Adjoint vector: $H_w v_t^* = \nabla_w \mathcal{L}_{\text{true}}(w_t; \theta_t)$
$g_t^{\text{IGT}} \in \mathbb{R}^p$	IGT-corrected hypergradient (Eq. (4))
\mathcal{B}	Replay buffer storing $(w_s, v_s^*, g_s(\theta_{t-1}))$ for $s \in Q_t$
H_F	Hessian of bilevel objective F at equilibrium
L_{IGT}	IGT delay coupling matrix (linearized bilevel dynamics)
<i>Regret decomposition (Theorem 3)</i>	
R_1	Delay error: $O(\eta_0^2 G^2 T \sigma_{\max})$
R_2	Inner-solver bias: $O(T \epsilon_{\text{inner}}^2)$
R_3	Interaction (transport residual): $O\left(\sum_t \sum_{s \in Q_t} \ \theta_{s+1} - \theta_s\ ^2\right)$
C_{ap}	Interaction prefactor in Theorem 3; see Remark 9
R_{sq}	Squared total drift (experimental metric): $R_{\text{sq}} = \sum_t \ \theta_t - \theta_{t-d}\ ^2$
<i>DDE / stability analysis (Propositions 1–2)</i>	
$F(\theta)$	Bilevel objective: $F(\theta) = \mathcal{L}_{\text{true}}(w^*(\theta); \theta)$
γ	Continuous-time convergence rate: $\gamma = c \eta_0 / \sqrt{1 + \beta \sigma_{\max}}$
$\bar{\tau}$	Representative delay time in the continuous DDE ($\bar{\tau} \leq \sigma \eta$)
$\xi(t)$	Deviation from equilibrium: $\xi(t) = \theta(t) - \theta^*$
κ_F	Condition number of H_F : $\kappa_F = \ H_F\ / \mu_{\min}$
<i>Abbreviations</i>	
DFL (decision-focused learning), OCO (online convex optimization), IGT (Implicit Gradient Transport), OMD (Online Mirror Descent), DDE (Delay Differential Equation)	

B Background

The following subsections collect established results from the literature that underpin our theoretical development. All material presented here is drawn directly from the cited works; we include it to make the paper self-contained for readers who may be unfamiliar with the relevant background, and make no claim of originality for any result in this background section.

B.1 Implicit Gradient Transport (IGT)

IGT was introduced by [7] to correct for gradient staleness in online learning. Given a gradient $g_s = \nabla f_s(\theta_s)$ computed at a past iterate θ_s , IGT constructs a corrected estimate at the current iterate θ_t via a telescoping sequence of $O(p)$ re-evaluations:

$$g_s^{\text{IGT}}(\theta_t) = g_s(\theta_s) + \sum_{k=s}^{t-1} [g_s(\theta_{k+1}) - g_s(\theta_k)]. \quad (7)$$

The correction exploits stored information (w_s, v_s^*) to evaluate $g_s(\cdot)$ at any query point. The key property of IGT is the following transport error bound [7]:

$$\|g_s^{\text{IGT}}(\theta_t) - \nabla f_s(\theta_t)\| \leq L \sum_{k=s}^{t-1} \|\theta_{k+1} - \theta_k\|^2, \quad (8)$$

which depends on the *sum of squared per-step displacements* rather than the squared total displacement $\|\theta_t - \theta_s\|^2$. This distinction is the source of the factor- σ_{\max} improvement established in Theorem 2(c).

B.2 Online Mirror Descent (OMD)

Online Mirror Descent [25] generalizes projected gradient descent by replacing the Euclidean geometry with a Bregman divergence D_ψ induced by a mirror map ψ . At each round t , the update takes the form:

$$\theta_{t+1} = \operatorname{argmin}_{\theta \in \Theta} \langle g_t, \theta \rangle + \frac{1}{\eta_t} D_\psi(\theta, \theta_t). \quad (9)$$

When $\psi = \frac{1}{2} \|\cdot\|^2$, the update reduces to projected gradient descent. Under standard assumptions, OMD achieves regret $O(D_\psi/\eta + G^2 \sum_t \eta_t)$; the choice $\eta_t = c/\sqrt{t}$ yields the minimax-optimal $O(\sqrt{T})$ regret rate [25].

B.3 Delay Differential Equations and Queue Length

The stability framework of [8] analyses online algorithms under delayed feedback through the lens of delay differential equations (DDEs). The central observation is that algorithmic stability depends on the *queue length* $\sigma_t = |Q_t|$ —the number of feedback rounds outstanding at time t —rather than on the raw delay alone in the active-window embedding used here. Linearising the bilevel dynamics around the equilibrium θ^* yields the DDE:

$$\dot{\xi}(t) = -\eta(t) H_F \xi(t) + \eta(t) L_{\text{IGT}} \sigma(t) \xi(t - \bar{\tau}), \quad (10)$$

where $\xi(t) = \theta(t) - \theta^*$ denotes the deviation from equilibrium, $H_F = \nabla^2 F(\theta^*)$ is the bilevel Hessian, and L_{IGT} is the IGT coupling matrix. The adaptive step size (3.2) is calibrated to maintain $\operatorname{Re}(\lambda) < 0$ for all characteristic roots λ of this DDE.

C Algorithmic Notes

The full IGT-OMD pseudocode is given as Algorithm 1 in the main text (Section 3). Here we record additional implementation details deferred from the main body.

Memory layout. The buffer \mathcal{B} stores at most σ_{\max} tuples $(w_s, v_s^*, g_s) \in \mathbb{R}^q \times \mathbb{R}^q \times \mathbb{R}^p$, requiring $O(\sigma_{\max}(p + 2q))$ memory. A FIFO ring buffer suffices and gives $O(1)$ amortized eviction. When non-Euclidean geometries are used, line 20 of Algorithm 1 is the dual-space update $\theta_{t+1} = \nabla \psi^*(\nabla \psi(\theta_t) - \eta_t g^{\text{IGT}})$, where ψ^* is the Fenchel conjugate [28] of the mirror map ψ .

Conjugate Gradient warm-starting. The Conjugate Gradient adjoint solve on line 13 of Algorithm 1 is warm-started from the previous round’s adjoint v_{t-1}^* . For slowly-varying θ_t , this typically reduces the number of Conjugate Gradient iterations by 3–5 \times in our experiments, keeping the constant in $O(q^2\kappa_w)$ small.

Remark 5 (Practical implementation). *Algorithm 1 is stated with the synchronous OMD update and monotone envelope $\bar{\sigma}_t$ for consistency with the theory (Theorem 1). The source implementations use an event-driven specialization: updates are invoked on feedback-arrival rounds, the active transport buffer advances on those update events, and practical variants may use the current active buffer size in the learning-rate damping. The transport re-evaluation loop is modular: it produces a corrected gradient g^{IGT} that can be fed to any base optimizer. The 2 \times 2 factorial shows this choice matters: pairing transport with Adam eliminates delay degradation, whereas pairing with SGD can amplify it. We recommend Adam or another adaptive optimizer as the base when applying Algorithm 1 to non-convex objectives.*

D Full Assumptions

Assumption 1 (Inner convexity and smoothness (A1)). $\mathcal{L}_{\text{model}}(\cdot; \theta)$ is μ_w -strongly convex and L_w -smooth for all $\theta \in \Theta$; both $\mathcal{L}_{\text{model}}$ and $\mathcal{L}_{\text{true}}$ are twice continuously differentiable jointly in (w, θ) . The strong convexity ensures a unique inner minimizer $w^*(\theta)$ for each θ and guarantees invertibility of $H_w = \nabla_{ww}^2 \mathcal{L}_{\text{model}}(w^*; \theta)$.

Assumption 2 (Outer smoothness (A2)). $\mathcal{L}_{\text{true}}(w; \cdot)$ is L_θ -smooth: $\|\nabla_\theta \mathcal{L}_{\text{true}}(w; \theta) - \nabla_\theta \mathcal{L}_{\text{true}}(w; \theta')\| \leq L_\theta \|\theta - \theta'\|$ for all w, θ, θ' . The cross-partial derivatives satisfy $\|\nabla_{w\theta}^2 \mathcal{L}_{\text{model}}(w; \theta)\| \leq L_{w\theta}$ for all (w, θ) .

Assumption 3 (Inner-solver quality (A3)). The warm-started inner solver achieves $\|w_t - w^*(\theta_t)\| \leq \epsilon_{\text{inner}}$ for all t , and the executed decision has local excess loss $\mathcal{L}_{\text{true}}(w_t; \theta_t) - \mathcal{L}_{\text{true}}(w^*(\theta_t); \theta_t) \leq \epsilon_{\text{inner}}^2$ after absorbing the local quadratic constant into ϵ_{inner} . Running $K = O(\ln(1/\epsilon_{\text{inner}}))$ gradient descent steps from w_{t-1} suffices when $\mathcal{L}_{\text{model}}$ is μ_w -strongly convex and L_w -smooth and the decision loss is locally quadratic around $w^*(\theta_t)$.

Assumption 4 (Bounded queue (A4)). The feedback delay sequence $\{d_t\}$ has bounded maximum queue length: $\sigma_t = |Q_t| \leq \sigma_{\text{max}} < \infty$ for all t . This subsumes fixed delays ($d_t = d, \sigma_{\text{max}} = d$), i.i.d. delays ($\sigma_{\text{max}} = 99\text{th-percentile queue length}$), and adversarial delays satisfying $d_t \leq D$ (giving $\sigma_{\text{max}} \leq D$).

Assumption 5 (Cross-partial Lipschitz (A5)). The mixed second derivative satisfies $\|\nabla_{w\theta}^2 \mathcal{L}_{\text{model}}(w; \theta) - \nabla_{w\theta}^2 \mathcal{L}_{\text{model}}(w'; \theta')\| \leq L_{w\theta}(\|w - w'\| + \|\theta - \theta'\|)$. The map $w \mapsto [\nabla_{ww}^2 \mathcal{L}_{\text{model}}(w; \theta)]^{-1}$ is (L_w/μ_w^2) -Lipschitz in w . Together, these ensure that the per-round IGT re-evaluation cost (2) is $O(pq)$ (no inner solve required).

Assumption 6 (Bounded hypergradients (A6)). The IGT-corrected hypergradients are bounded: $\|g_t^{\text{IGT}}\| \leq G$ for all t and $\theta \in \Theta$. By the chain rule and triangle inequality, $G \leq G_{\text{true}} + (L_{w\theta}/\mu_w)\epsilon_{\text{inner}}$, where $G_{\text{true}} = \sup_\theta \|\nabla F(\theta)\|$ bounds the exact hypergradient.

Assumption 7 (Bilevel convexity (A7)). The bilevel objective $F(\theta) = \mathcal{L}_{\text{true}}(w^*(\theta); \theta)$ is μ_F -strongly convex. The bilevel coupling condition $L_{w\theta}^2/(\mu_w^2\mu_F) < 1$ ensures that the feedback from the inner minimizer does not destabilize the outer-level optimization. This assumption holds when the inner problem is well-conditioned (μ_w large) or the cross-coupling is weak ($L_{w\theta}$ small).

D.1 Assumption Verification for Experimental Benchmarks

We verify that the three main benchmarks satisfy the key assumptions (A1–A5) required by our theoretical results.

LQR (Section 5.1). The inner problem minimizes the quadratic LQR proxy over linear control gains K for the learned dynamics (\hat{A}, \hat{B}) , which is strongly convex in K when $R \succ 0$ (A1). The outer loss is smooth in $\theta = (\hat{A}, \hat{B})$ since the closed-loop proxy is polynomial in (K, θ) (A2). The inner solver uses the fixed $K = 10$ differentiable gradient-descent configuration in Table 6, so ϵ_{inner} is uniformly controlled (A3). Delays are constant with $\sigma_{\text{max}} = d$ (A4). The cross-partials $\nabla_{K\theta}^2 J$ are Lipschitz because J is polynomial in (K, θ) (A5). The bilevel objective $F(\theta)$ is locally strongly convex in the stable neighborhood explored by the binary search (A7).

Sinkhorn OT (Sections 5.3–5.4). The inner problem runs K Sinkhorn iterations with entropic regularization $\varepsilon = 0.05$, which ensures the regularized objective is ε -strongly convex in the coupling matrix (A1, with $\mu_w = \varepsilon$). The outer loss is smooth in the neural network parameters θ (A2). The inner-solver error decays geometrically: $\epsilon_{\text{inner}} \leq \rho^K$ with $\rho = 1 - \varepsilon/L_w < 1$, so $K = 10$ iterations yield $\epsilon_{\text{inner}} \approx 10^{-3}$ (A3). Delays are constant with $\sigma_{\text{max}} = d$ (A4). The Sinkhorn kernel is C^∞ in (w, θ) , ensuring Lipschitz cross-partials (A5). Assumption 7 (strong convexity of F) holds only locally under the neural-network parameterization; this is the regime in which our local bounds apply. Empirically, the transport benefit persists in this non-convex regime, suggesting the assumption may be conservative. Formal non-convex extensions are deferred to future work (Section 6).

Warcraft shortest path (Section 5.2). Dijkstra’s algorithm returns exact solutions, so the inner problem is not approximately solved but exactly solved ($\epsilon_{\text{inner}} = 0$, A3 trivially). However, the combinatorial inner solver is non-differentiable, so A1 (smoothness) does not hold in the classical sense; we use the differentiable perturbation approach of [9] to define smooth surrogate gradients. The outer loss is smooth in θ (A2), and delays have bounded queue length (A4). Since Dijkstra’s algorithm lies outside the gradient computation graph, the bilevel-specific assumptions (A5, A7) are not required for the Warcraft experiment—the transport benefit arises solely from outer-level staleness correction, as discussed in Section 5.2.

E Proofs

E.1 Proof of Theorem 1 (Bilevel Convergence)

The proof proceeds in three stages: (i) a standard OMD regret decomposition using the IGT-corrected gradients g_t^{IGT} ; (ii) a lemma bounding the transport error when IGT is applied to bilevel hypergradients; and (iii) a lemma bounding the inner-solver bias via strong convexity and Young’s inequality. The key insight is that IGT re-evaluation replaces the squared total drift with a sum of squared per-step changes, and the inner-solver error contributes only through an *additive* $\epsilon_{\text{inner}}^2$ term because Young’s inequality decouples the cross-term between inner bias and outer staleness.

Supporting lemma: OMD with imperfect gradients.

Lemma 1 (OMD regret with time-varying step sizes). *Let $\psi : \Theta \rightarrow \mathbb{R}$ be 1-strongly convex with respect to $\|\cdot\|$, and let $D_\psi(\theta, \theta') = \psi(\theta) - \psi(\theta') - \langle \nabla\psi(\theta'), \theta - \theta' \rangle$ be the induced Bregman divergence. Let $\{h_t\}_{t=1}^T$ be any sequence with $\|h_t\|_* \leq G$, and let the OMD iterates be $\theta_{t+1} = \text{argmin}_{\theta \in \Theta} \langle h_t, \theta \rangle + (1/\eta_t)D_\psi(\theta, \theta_t)$ with arbitrary positive step sizes $\eta_t > 0$. Then for any $\theta^* \in \Theta$:*

$$\sum_{t=1}^T \langle h_t, \theta_t - \theta^* \rangle \leq \frac{D_\psi(\theta^*, \theta_1)}{\eta_1} + \sum_{t=2}^T D_\psi(\theta^*, \theta_t) \left(\frac{1}{\eta_t} - \frac{1}{\eta_{t-1}} \right)_+ + \frac{G^2}{2} \sum_{t=1}^T \eta_t, \quad (11)$$

where $(x)_+ = \max(x, 0)$. When step sizes are non-increasing, the middle term vanishes and the bound reduces to $D_\psi(\theta^*, \theta_1)/\eta_T + (G^2/2) \sum_t \eta_t$.

Proof. The three-point identity for Bregman divergences (see, e.g., [29]) gives, for the OMD step at round t :

$$\langle h_t, \theta_t - \theta^* \rangle \leq \frac{D_\psi(\theta^*, \theta_t) - D_\psi(\theta^*, \theta_{t+1})}{\eta_t} + \frac{\eta_t}{2} \|h_t\|_*^2.$$

Summing over $t = 1, \dots, T$ and re-grouping the telescoping sum (following the time-varying step-size analysis of [4], Appendix A):

$$\sum_t \langle h_t, \theta_t - \theta^* \rangle \leq \frac{D_\psi(\theta^*, \theta_1)}{\eta_1} + \sum_{t=2}^T D_\psi(\theta^*, \theta_t) \left(\frac{1}{\eta_t} - \frac{1}{\eta_{t-1}} \right) + \frac{G^2}{2} \sum_t \eta_t.$$

When $1/\eta_t < 1/\eta_{t-1}$ (i.e., $\eta_t > \eta_{t-1}$), the corresponding term is negative and can be dropped, yielding (11). \square

Supporting lemma: IGT error for hypergradients.

Lemma 2 (IGT transport error for bilevel hypergradients). *Under Assumptions 1–6, let $\bar{g}_t = \nabla_\theta F(\theta_t)$ denote the exact gradient of the bilevel objective at θ_t (with exact inner solution $w^*(\theta_t)$), and let g_t^{IGT} be the IGT estimator formed by Algorithm 1 using stored (w_s, v_s^*) from past rounds $s \in Q_t$. Then:*

$$\|\bar{g}_t - g_t^{\text{IGT}}\| \leq L_F \sum_{s \in Q_t} \|\theta_{s+1} - \theta_s\|^2 + \frac{L_{w\theta}}{\mu_w} \epsilon_{\text{inner}}, \quad (12)$$

where $L_F = L_\theta + L_{w\theta}^2/\mu_w$ is the Lipschitz constant of $\nabla_\theta F$ (the bilevel gradient Lipschitz constant, identical to the L in Theorem 1), $L_{w\theta}$ is the cross-partial Lipschitz constant from Assumption 2, and μ_w is the inner strong convexity constant from Assumption 1.

Proof. Decompose the error into a transport part and an inner-solver part:

$$\|\bar{g}_t - g_t^{\text{IGT}}\| \leq \underbrace{\|\bar{g}_t - g_t^{\text{trans}}\|}_{\text{transport error}} + \underbrace{\|g_t^{\text{trans}} - g_t^{\text{IGT}}\|}_{\text{inner-solver error}}, \quad (13)$$

where g_t^{trans} is the IGT estimator that uses the *exact* inner solutions $w^*(\theta_s)$ for all $s \in Q_t$ (a hypothetical estimator not computed by the algorithm).

Transport error. The re-evaluation formula (2) defines $g_s(\theta) = \nabla_\theta \mathcal{L}_{\text{true}}(w^*(\theta_s); \theta) - [\nabla_\theta \nabla_w \mathcal{L}_{\text{model}}(w^*(\theta_s); \theta)]^\top v_s^*$ as a function of θ alone (with frozen $w^*(\theta_s)$ and v_s^*), which is L_F -smooth in θ by Assumption 2. Applying the original IGT error bound of [7] (their Proposition 1, extended to the hypergradient setting) to the sequence $g_s(\cdot)$ for each $s \in Q_t$ gives:

$$\|\bar{g}_t - g_t^{\text{trans}}\| \leq L_F \sum_{s \in Q_t} \|\theta_{s+1} - \theta_s\|^2.$$

The bound follows from the fact that the telescoping correction $\sum_{s \in Q_t} [g_s(\theta_t) - g_s(\theta_{t-1})]$ approximates the ideal correction $\sum_{s \in Q_t} [g_s(\theta_t) - g_s(\theta_s)]$ up to a residual that is bounded by the sum of squared step sizes via the mean-value theorem applied to the L_F -smooth functions $g_s(\cdot)$.

Inner-solver error. For each $s \in Q_t$, the algorithm uses $w_s \approx w^*(\theta_s)$ instead of the exact solution. The difference in the re-evaluated hypergradient satisfies:

$$\|g_s^{\text{trans}}(\theta_t) - g_s^{\text{IGT}}(\theta_t)\| \leq L_{w\theta} \|w_s - w^*(\theta_s)\| \leq L_{w\theta} \epsilon_{\text{inner}},$$

using the $L_{w\theta}$ -Lipschitz cross-partial from Assumption 2 and the inner-solver bound from Assumption 3. Since the IGT sum involves at most $\sigma_t \leq \sigma_{\text{max}}$ outstanding rounds, and noting that the errors for individual $s \in Q_t$ collapse into the single correction increment $\Delta_s = g_s(\theta_t) - g_s(\theta_{t-1})$, the total contribution of inner-solver error to the estimator g_t^{IGT} is bounded by $(L_{w\theta}/\mu_w) \epsilon_{\text{inner}}$ after invoking strong convexity of the inner problem (Assumption 1) to relate $\|w_s - w^*(\theta_t)\| \leq \epsilon_{\text{inner}} + (L_{w\theta}/\mu_w) \|\theta_s - \theta_t\|$, the latter term being absorbed into the transport error already accounted for. Combining the two bounds yields (12). \square

Supporting lemma: inner-solver bias via Young’s inequality.

Lemma 3 (Inner-solver bias accumulates as $\epsilon_{\text{inner}}^2$). *Under the same assumptions, with $\rho_{\text{cpl}} := L_{w\theta}^2/(\mu_w^2 \mu_F) < 1$, the cumulative contribution of the inner-solver error satisfies:*

$$\sum_{t=1}^T \langle \bar{g}_t - g_t^{\text{IGT}}, \theta_t - \theta^* \rangle \leq 2T \epsilon_{\text{inner}}^2 + L_F \sum_{t=1}^T \sum_{s \in Q_t} \|\theta_{s+1} - \theta_s\|^2 + \rho_{\text{cpl}} \text{Regret}_T^{\text{dec}}. \quad (14)$$

Proof. By Cauchy–Schwarz [24] and Lemma 2:

$$\langle \bar{g}_t - g_t^{\text{IGT}}, \theta_t - \theta^* \rangle \leq \|\bar{g}_t - g_t^{\text{IGT}}\| \|\theta_t - \theta^*\| \leq \left[L_F \sum_{s \in Q_t} \|\theta_{s+1} - \theta_s\|^2 + \frac{L_{w\theta}}{\mu_w} \epsilon_{\text{inner}} \right] \cdot \|\theta_t - \theta^*\|.$$

For the inner-bias cross-term, apply Young’s inequality with $c = 1$: $\frac{L_{w\theta}}{\mu_w} \epsilon_{\text{inner}} \cdot \|\theta_t - \theta^*\| \leq \frac{1}{2} \epsilon_{\text{inner}}^2 + \frac{L_{w\theta}^2}{2\mu_w^2} \|\theta_t - \theta^*\|^2$. (Young’s is applied only to the inner-bias term, not the transport term $L_F \sum_{s \in Q_t} \|\theta_{s+1} - \theta_s\|^2$, because the transport term already has the sum-of-squares structure and is bounded by $\sigma_t \eta_0^2 G^2 \cdot \text{diam}(\Theta)$ without requiring separation.) By the μ_F -strong convexity of F (Assumption 7), we have $\|\theta_t - \theta^*\|^2 \leq (2/\mu_F)[F(\theta_t) - F(\theta^*)]$. The resulting term is $\rho_{\text{cpl}}[F(\theta_t) - F(\theta^*)]$, which is absorbed in the main proof; summing over t gives (14). \square

Main proof of Theorem 1.

Proof of Theorem 1. Let $\theta^* = \operatorname{argmin}_\theta \sum_t \mathcal{L}_{\text{true}}(w^*(\theta); \theta)$ and $F(\theta) = \mathcal{L}_{\text{true}}(w^*(\theta); \theta)$.

Step 1 (convexity decomposition). By convexity of F (Assumption 7):

$$\begin{aligned} \operatorname{Regret}_T^{\text{dec}} &= \sum_{t=1}^T [F(\theta_t) - F(\theta^*)] \leq \sum_{t=1}^T \langle \bar{g}_t, \theta_t - \theta^* \rangle \\ &= \underbrace{\sum_{t=1}^T \langle g_t^{\text{IGT}}, \theta_t - \theta^* \rangle}_{(I)} + \underbrace{\sum_{t=1}^T \langle \bar{g}_t - g_t^{\text{IGT}}, \theta_t - \theta^* \rangle}_{(II)}. \end{aligned} \quad (15)$$

Step 2 (bound term (I) via OMD lemma). Algorithm 1 performs an OMD step with gradient g_t^{IGT} and step size $\eta_t = \eta_0 / \sqrt{1 + \beta \bar{\sigma}_t}$. Since $\bar{\sigma}_t$ is nondecreasing, η_t is non-increasing and Lemma 1 applies with $h_t = g_t^{\text{IGT}}$ and $\|g_t^{\text{IGT}}\|_* \leq G$:

$$(I) \leq \frac{D_\psi(\theta^*, \theta_1)}{\eta_1} + \sum_{t=2}^T D_\psi(\theta^*, \theta_t) \left(\frac{1}{\eta_t} - \frac{1}{\eta_{t-1}} \right)_+ + \frac{G^2}{2} \sum_{t=1}^T \eta_t. \quad (16)$$

Because $1/\eta_t$ is nondecreasing, the middle term telescopes over the range of $1/\eta_t$: since $D_\psi(\theta^*, \theta_t) \leq D_\psi$, $\sum_{t=2}^T D_\psi(1/\eta_t - 1/\eta_{t-1})_+ \leq D_\psi(1/\eta_T - 1/\eta_1)$. Combined with the first term: $(I) \leq D_\psi/\eta_T + (G^2/2) \sum_t \eta_t$.

We bound $\sum_t \eta_t$ and $1/\eta_T$ using the queue-length structure. Since $\eta_t = \eta_0 / \sqrt{1 + \beta \bar{\sigma}_t} \leq \eta_0$, we have the trivial bound $\sum_t \eta_t \leq T\eta_0$. Also $1/\eta_T \leq \sqrt{1 + \beta \sigma_{\max}}/\eta_0$. More precisely, we use the following estimate: since each $\eta_t \leq \eta_0$ and there are at most T terms,

$$\sum_{t=1}^T \eta_t = \eta_0 \sum_{t=1}^T \frac{1}{\sqrt{1 + \beta \sigma_t}} \leq \eta_0 T. \quad (17)$$

When $\sigma_t \asymp \sigma_{\max}$ for a constant fraction of rounds (the adversarial worst case), we obtain the tighter bound $\sum_t \eta_t \leq \eta_0 T / \sqrt{1 + \beta \sigma_{\max}}$. In the general case, let T_0 denote the number of rounds with $\sigma_t = 0$ and $T_+ = T - T_0$ the rounds with $\sigma_t \geq 1$. Then $\sum_t \eta_t \leq \eta_0 T_0 + \eta_0 T_+ / \sqrt{1 + \beta}$. For the regret bound we use the worst case $\sum_t \eta_t \leq \eta_0 T$:

$$(I) \leq \frac{2D_\psi \sqrt{1 + \beta \sigma_{\max}}}{\eta_0} + \frac{\eta_0 G^2 T}{2}. \quad (18)$$

Step 3 (bound term (II) via Lemmas 2 and 3). By Lemma 3:

$$(II) \leq 2T \epsilon_{\text{inner}}^2 + L_F \sum_{t=1}^T \sum_{s \in Q_t} \|\theta_{s+1} - \theta_s\|^2 + \rho_{\text{cpl}} \operatorname{Regret}_T^{\text{dec}}. \quad (19)$$

Step 4 (transport term). The last sum in (19) is the aggregate IGT transport penalty. Since the step-size bound gives $\|\theta_{t+1} - \theta_t\| \leq \eta_t \|g_t^{\text{IGT}}\| \leq \eta_0 G$, each summand satisfies $\|\theta_{s+1} - \theta_s\|^2 \leq \eta_0^2 G^2$. We retain this as-is in the main bound; it appears explicitly in (5).

Step 5 (combine and optimize η_0). Combining (15), (18), and (19), then moving $\rho_{\text{cpl}} \operatorname{Regret}_T^{\text{dec}}$ to the left:

$$\operatorname{Regret}_T^{\text{dec}} \leq C_\rho \left[\frac{2D_\psi \sqrt{1 + \beta \sigma_{\max}}}{\eta_0} + \frac{\eta_0 G^2 T}{2} + 2T \epsilon_{\text{inner}}^2 + L_F \sum_{t=1}^T \sum_{s \in Q_t} \|\theta_{s+1} - \theta_s\|^2 \right],$$

where $C_\rho = (1 - \rho_{\text{cpl}})^{-1}$. This is (5).

Setting $\eta_0 = c/\sqrt{T}$ (for universal constant $c > 0$) gives the first term as $O(D_\psi \sqrt{T \sigma_{\max}})$ and the second as $O(G^2 \sqrt{T})$. The last sum, using $\|\theta_{s+1} - \theta_s\|^2 \leq \eta_0^2 G^2 = O(G^2/T)$ and $\sum_t |Q_t| =$

$\sum_t \sigma_t \leq d_{\text{tot}} \leq T\sigma_{\text{max}}$, contributes $O(L_F G^2 \sigma_{\text{max}})$. Since Θ is bounded (so $D_\psi < \infty$), combining gives $\text{Regret}_T^{\text{dec}} = O(\sqrt{T\sigma_{\text{max}}} + T\epsilon_{\text{inner}}^2)$.

If the inner solver runs $K = O(\ln T)$ steps with contraction rate $\rho < 1$, then $\epsilon_{\text{inner}} = O(\rho^K) = O(1/\sqrt{T})$, giving $T\epsilon_{\text{inner}}^2 = O(1)$, and the total regret is $O(\sqrt{T\sigma_{\text{max}}})$. \square

Corollary 1 (Comparison with non-delayed bilevel OMD). *Setting $\sigma_{\text{max}} = 0$ (no delay) and $\beta = 0$, the bound reduces to $O(D_\psi\sqrt{T} + T\epsilon_{\text{inner}}^2)$, which is the standard $O(\sqrt{T})$ rate for convex OCO. [12] achieve the faster $O((G^2/\mu_F)\ln T)$ rate by exploiting μ_F -strong convexity of F ; for the delay/transport terms (Lemma 2), our analysis uses convexity-only arguments and does not exploit strong convexity. (Strong convexity is used to absorb the inner-bias cross-term in Lemma 3 and, more prominently, in the pure-bias and interaction bounds of Theorem 3.) With exact inner solver ($\epsilon_{\text{inner}} = 0$) and adequate $K = O(\ln T)$ inner steps, the bound reduces to $O(\sqrt{T\sigma_{\text{max}}})$, which is comparable to the $O(\sqrt{Td_{\text{tot}}})$ rate of single-level D-FTRL [4] with the queue-length σ_{max} replacing the total delay $d_{\text{tot}} = T\sigma_{\text{max}}$.*

Remark 6 (Why ϵ_{inner} enters additively). *The $T\epsilon_{\text{inner}}^2$ cost is unavoidable (Theorem 2(b)), but it enters additively rather than coupled with σ_{max} . This traces to Lemma 3, where Young’s inequality decouples the inner approximation error from the queue length. The transport corrections $\sum_{s \in Q_t} \|\theta_{s+1} - \theta_s\|^2$ involve only the per-step displacements (bounded by $\eta_t^2 G^2$) rather than the accumulated displacement $\|\theta_t - \theta_{t-\sigma_t}\|^2 = O(\sigma_t^2 \eta_t^2 G^2)$, which would reintroduce a σ_{max}^2 factor. IGT replaces this large term with the sum of squares, gaining a factor of σ_{max} in the transport error (Theorem 2(c)).*

Remark 7 (Coupling condition and the non-vacuity threshold). *The coupling condition $L_{w\theta}^2/(\mu_w^2 \mu_F) < 1$ (Assumption 7) is not merely a proof convenience: when it fails, the inner-solver bias term $\frac{L_{w\theta}^2}{\mu_w^2 \mu_F} [F(\theta_t) - F(\theta^*)]$ in Lemma 3 exceeds the regret it is meant to absorb. Physically, this means the bilevel problem is “too implicit” — the inner solution $w^*(\theta)$ is so sensitive to θ that approximate solves induce gradient errors larger than the true signal. Similarly, the $O(\sqrt{T\sigma_{\text{max}}})$ rate is non-vacuous (i.e., sublinear) only when $\sigma_{\text{max}} = o(T)$. At $\sigma_{\text{max}} = \Omega(T)$ — corresponding to total disconnection where feedback never arrives faster than the horizon — the regret bound becomes $O(T)$, which is no better than static play. This threshold is intrinsic to delayed OCO: the same $O(T)$ vacuity occurs in the single-level bounds of D-FTRL [4] when $d_{\text{tot}} = \Omega(T^2)$.*

Remark 8 (Step-size choice and dynamic stability). *Theorem 1 is an OCO regret bound that holds for any $\eta_0 > 0$: no stability condition is imposed. Separately, Proposition 1 shows that the continuous-time limit of IGT-OMD is asymptotically stable only when $\eta_0 < 1/(\|H_F\|\sqrt{1 + \beta\sigma_{\text{max}}})$. The regret-optimal choice $\eta_0 = c/\sqrt{T}$ satisfies this stability threshold for all $T \geq \|H_F\|^2(1 + \beta\sigma_{\text{max}})$, i.e., beyond a modest horizon that depends on the problem conditioning. For small T or very large σ_{max} , practitioners should additionally impose $\eta_0 \leq 1/(\|H_F\|\sqrt{1 + \beta\sigma_{\text{max}}})$ to ensure the iterates remain in the stable regime; this only improves the bound by preventing transient oscillations that inflate $D_\psi(\theta^*, \theta_t)$.*

E.2 Proof of Theorem 2 (Staleness amplification)

The proof has three parts: Part (a) derives the gradient error structure, Part (b) establishes the $\Omega(T\epsilon_{\text{inner}}^2)$ lower bound via a hard instance, and Part (c) compares the transport error with and without IGT. The key insight is that the bilevel gradient error contains a *cross-term* coupling outer-parameter drift with inner-solver sensitivity—a structural feature absent in single-level OCO—and that IGT eliminates the quadratic growth of this cross-term by decomposing the total drift into per-step contributions.

Part (a): Gradient Error Structure

We bound $\|\hat{g}(\theta_{t-d_t}, w_{t-d_t}) - \nabla F(\theta_t)\|$ by decomposing it into outer staleness and inner-solver error:

$$\begin{aligned} \|\hat{g}(\theta_{t-d_t}, w_{t-d_t}) - \nabla F(\theta_t)\| &\leq \|\nabla F(\theta_{t-d_t}) - \nabla F(\theta_t)\| + \|\hat{g}(\theta_{t-d_t}, w_{t-d_t}) - \nabla F(\theta_{t-d_t})\| \\ &\leq L_F \|\theta_t - \theta_{t-d_t}\| + C_0 \epsilon_{\text{inner}}, \end{aligned} \quad (20)$$

where the first inequality is the triangle inequality, and the second uses L_F -smoothness of F (with $L_F = L_\theta + L_{w\theta}^2/\mu_w$; see the bilevel Lipschitz bound $L_F = L_\theta + L_{w\theta}^2/\mu_w$ derived from Assumptions 1–2) for the outer staleness term, and the inner-solver bound of Lemma 3 for the noise term. The bilevel Lipschitz constant L_F absorbs the implicit sensitivity $L_{w\theta}^2/\mu_w$ of the inner solution to the outer parameters via the Implicit Function Theorem.

Contrast with single-level OCO. In single-level delayed optimization, the gradient oracle returns $\nabla f(\theta_{t-d_t}) + \xi_t$ where $\|\xi_t\| \leq \epsilon$. The noise ξ_t is bounded by a *fixed constant* ϵ independent of the staleness $\|\theta_t - \theta_{t-d_t}\|$. In the bilevel case, the Lipschitz constant L_F itself depends on the inner-solution sensitivity $L_{w\theta}/\mu_w$, so greater sensitivity *amplifies* the staleness component of the gradient error. This structural difference—the staleness amplification mechanism—is absent in single-level delayed optimization. \square

Part (b): Hard Instance and Lower Bound

The lower bound is established via an explicit hard instance—a quadratic bilevel problem—on which no black-box delayed optimizer can avoid $\Omega(\epsilon_{\text{inner}}^2)$ per-round loss.

Step 1: Hard Instance Construction

Fix $p = q = 1$. Define the bilevel instance on $\Theta = [-B_0, B_0]$ by

$$\mathcal{L}_{\text{model}}(w; \theta) = \frac{\mu_w}{2}(w - b\theta)^2, \quad (21)$$

$$\mathcal{L}_{\text{true}}(w; \theta) = \frac{1}{2}(w - a\theta)^2, \quad (22)$$

where $a, b \in \mathbb{R}$ with $a \neq b$ and $|a - b| = C_0 > 0$ (chosen by the adversary; the algorithm is blind to a, b). When $a = b$, the model perfectly matches the true objective ($C_0 = 0$), the bilevel problem reduces to single-level optimization, and the staleness amplification mechanism disappears — this is precisely the regime where bilevel structure imposes no additional cost. Assumption 1 holds with strong convexity constant μ_w and smoothness $L_w = \mu_w$. Assumption 2 holds with $L_\theta = a^2$ and cross-partial Lipschitz constant $L_{w\theta} = 1$.

The exact inner minimizer is $w^*(\theta) = b\theta$, giving the bilevel objective

$$F(\theta) = \frac{1}{2}(b - a)^2\theta^2 = \frac{C_0^2}{2}\theta^2, \quad (23)$$

with unique optimum $\theta^* = 0$ and gradient $\nabla F(\theta) = C_0^2\theta$. By the implicit differentiation formula (1), the adjoint satisfies $v^*(\theta) = (b - a)\theta/\mu_w$, and the hypergradient is $g(\theta) = \nabla_\theta \mathcal{L}_{\text{true}}|_{w = (\nabla_\theta \nabla_w \mathcal{L}_{\text{model}})^\top v^*(\theta)} = -a(w^* - a\theta) + (b\mu_w)v^*(\theta) = C_0^2\theta$, consistent with (23).

Step 2: Inner-Solver Error Introduces a Persistent Bias

Suppose the approximate inner solver produces $w_t = b\theta_t + \epsilon_t$, with $|\epsilon_t| \leq \epsilon_{\text{inner}}$. The algorithm evaluates the outer gradient using w_t in place of $w^*(\theta_t)$. Via formula (1) with the approximate adjoint $\tilde{v}_t = (w_t - a\theta_t)/\mu_w$:

$$\begin{aligned} \hat{g}(\theta_t, w_t) &= -a(w_t - a\theta_t) + b\mu_w \cdot \tilde{v}_t \\ &= -a(b\theta_t + \epsilon_t - a\theta_t) + b(b\theta_t + \epsilon_t - a\theta_t) \\ &= C_0^2\theta_t + C_0\epsilon_t. \end{aligned} \quad (24)$$

The bias term $C_0\epsilon_t$ is independent of θ_t . The adversary sets the inner-solver error to the *constant* value $\epsilon_t = +\epsilon_{\text{inner}}$ for all t (no knowledge of the algorithm’s iterate is required). This produces a hypergradient with a *constant additive bias*:

$$\hat{g}(\theta_t, w_t) = C_0^2\theta_t + C_0\epsilon_{\text{inner}}. \quad (25)$$

Lemma 4 (Steady-state displacement). *For the hard instance (21)–(22) with constant inner-solver error $\epsilon_t = +\epsilon_{\text{inner}}$, any algorithm using the biased gradient (25) converges (when stable) to a steady state θ_{ss} satisfying*

$$\theta_{\text{ss}} = -\frac{\epsilon_{\text{inner}}}{C_0}, \quad F(\theta_{\text{ss}}) = \frac{\epsilon_{\text{inner}}^2}{2}. \quad (26)$$

Proof. At steady state, $\theta_{t+1} = \theta_t = \theta_{\text{ss}}$ and $\theta_{t-\sigma_{\text{max}}} = \theta_{\text{ss}}$, so $0 = -\eta(C_0^2\theta_{\text{ss}} + C_0\epsilon_{\text{inner}})$, giving $\theta_{\text{ss}} = -\epsilon_{\text{inner}}/C_0$. Then $F(\theta_{\text{ss}}) = C_0^2\theta_{\text{ss}}^2/2 = \epsilon_{\text{inner}}^2/2$. \square

Step 3: Convergence to the Biased Steady State

For any algorithm \mathcal{A} with constant delay $d_t = \sigma_{\max}$ and step size η , the iterates satisfy

$$\theta_{t+1} = \theta_t - \eta C_0^2 \theta_{t-\sigma_{\max}} - \eta C_0 \epsilon_{\text{inner}}. \quad (27)$$

This is a linear recurrence with delay σ_{\max} and a constant additive drive $-\eta C_0 \epsilon_{\text{inner}}$. For step sizes satisfying $\eta \leq 1/(2C_0^2 \sigma_{\max})$ — a *sufficient* condition for all roots of the discrete characteristic polynomial $z^{\sigma_{\max}+1} - z^{\sigma_{\max}} + \eta C_0^2 = 0$ to lie inside the unit disk (cf. Proposition 1) — the homogeneous part $\theta_{t+1} = \theta_t - \eta C_0^2 \theta_{t-\sigma_{\max}}$ is stable, and the iterates converge to $\theta_{\text{ss}} = -\epsilon_{\text{inner}}/C_0$ within $O(\sigma_{\max})$ rounds.

Lemma 5 (Iterate lower bound). *For any stable algorithm \mathcal{A} with step size $\eta \leq 1/(2C_0^2 \sigma_{\max})$, after an initial transient of $O(\sigma_{\max})$ rounds, the iterates satisfy*

$$|\theta_t| \geq \frac{1}{2} \cdot \frac{\epsilon_{\text{inner}}}{C_0}. \quad (28)$$

Proof. By Lemma 4, $\theta_{\text{ss}} = -\epsilon_{\text{inner}}/C_0$. The deviation $\xi_t = \theta_t - \theta_{\text{ss}}$ satisfies the homogeneous recurrence $\xi_{t+1} = \xi_t - \eta C_0^2 \xi_{t-\sigma_{\max}}$, which is stable for $\eta \leq 1/(2C_0^2 \sigma_{\max})$. Hence $|\xi_t| \rightarrow 0$, so $|\theta_t| \rightarrow |\theta_{\text{ss}}| = \epsilon_{\text{inner}}/C_0$. After the transient, $|\theta_t| \geq \frac{1}{2} \epsilon_{\text{inner}}/C_0$. \square

Step 4: Accumulating Regret

Since $F(\theta) = C_0^2 \theta^2/2$ and $\theta^* = 0$, the per-round regret is $F(\theta_t) - F(\theta^*) = C_0^2 \theta_t^2/2$. Using Lemma 5, after an $O(\sigma_{\max})$ -round transient we have $\theta_t^2 \geq \epsilon_{\text{inner}}^2/(4C_0^2)$ for $t \geq t_0 = O(\sigma_{\max})$. Thus:

$$\sum_{t=1}^T [F(\theta_t) - F(\theta^*)] \geq \sum_{t=t_0}^T \frac{C_0^2 \theta_t^2}{2} \geq (T - t_0) \cdot \frac{C_0^2}{2} \cdot \frac{\epsilon_{\text{inner}}^2}{4C_0^2} = \frac{(T - t_0) \epsilon_{\text{inner}}^2}{8}. \quad (29)$$

For $T \gg \sigma_{\max}$ (i.e. $T - t_0 \geq T/2$), this gives $\text{Regret}_T(\mathcal{A}) \geq \Omega(T \epsilon_{\text{inner}}^2)$.

Step 5: Independence from Algorithm Design

The lower bound holds for *any* black-box delayed optimizer — that is, any algorithm whose only access to F is through the biased gradient oracle (25), without knowledge of the inner solver's error distribution, sign, or magnitude beyond the bound $|\epsilon_t| \leq \epsilon_{\text{inner}}$. In particular, a bias-correction scheme that estimates and subtracts the mean error would require access to the *unbiased* gradient $\nabla F(\theta_t)$, which is precisely what the black-box model excludes.

1. The constant bias $C_0 \epsilon_{\text{inner}}$ in (25) is independent of η , σ_{\max} , and the algorithm's iterate sequence. No step-size choice eliminates this bias.
2. Any stable algorithm converges to $\theta_{\text{ss}} = -\epsilon_{\text{inner}}/C_0$, incurring $F(\theta_{\text{ss}}) = \epsilon_{\text{inner}}^2/2$ per round. The bound requires a *fixed precision floor*: ϵ_{inner} must remain bounded away from zero uniformly over all rounds t (Assumption 3). If the inner solver were warm-started such that $\epsilon_t \rightarrow 0$, the steady-state offset would vanish and the $\Omega(T)$ lower bound would collapse. Our result characterizes the cost of a *fixed approximation budget*, which is the standard setting in bilevel optimization [17].
3. An unstable algorithm ($\eta > 1/(2C_0^2 \sigma_{\max})$) has $|\theta_t| \rightarrow \infty$ (clipped at B_0 , since $\Theta = [-B_0, B_0]$ is compact), incurring $F(\theta_t) \geq C_0^2 B_0^2/2$ per round, which is strictly worse.
4. The adversary chooses $\theta_1 = B_0 \neq 0$, guaranteeing a non-trivial transient; the $O(\sigma_{\max})$ burn-in cost is absorbed into the $\Omega(T)$ rate for $T \gg \sigma_{\max}$.

The hard instance satisfies Assumptions 1 and 2 with $\mu_w = L_w$ and $L_\theta = a^2 < \infty$, completing Part (b).

Part (c): Transport Error Separation

Without bilevel-aware correction, the per-round staleness mismatch contributes

$$\left| \langle \nabla F(\theta_t) - \nabla F(\theta_{t-\sigma_t}), \theta_t - \theta^* \rangle \right| \leq L_F \|\theta_t - \theta_{t-\sigma_t}\| \cdot \text{diam}(\Theta). \quad (30)$$

Since $\|\theta_t - \theta_{t-\sigma_t}\| \leq \sigma_t \eta G$, summing over T rounds gives

$$\sum_{t=1}^T L_F \|\theta_t - \theta_{t-\sigma_t}\| \cdot \text{diam}(\Theta) \leq L_F \text{diam}(\Theta) \sigma_{\max} G \eta T = O(L_F \text{diam} \sigma_{\max} G \sqrt{T})$$

with $\eta = c/\sqrt{T}$. This transport cost grows as \sqrt{T} .

Under IGT, the corresponding term is the sum of squared per-step changes (Theorem 3):

$$\sum_{t=1}^T \sum_{s \in Q_t} L_F \|\theta_{s+1} - \theta_s\|^2 \leq L_F T \sigma_{\max} \eta^2 G^2 = O(L_F \sigma_{\max} G^2),$$

which is *constant in T* . The ratio of the non-IGT transport cost to the IGT transport cost is $\text{diam}(\Theta) \sqrt{T}/G$, demonstrating a \sqrt{T} factor improvement. In terms of the per-round transport error, the non-IGT contribution is $O(\sigma_{\max}^2 \eta^2 G^2)$ (from the squared total drift $\|\theta_t - \theta_{t-\sigma_t}\|^2$), while IGT yields $O(\sigma_{\max} \eta^2 G^2)$ (sum of per-step squares)—a factor σ_{\max} improvement, as claimed. \square

Corollary 2 (Vector-valued extension). *The hard instance of Theorem 2(b) extends to $p, q > 1$: replace θ with a vector and construct $A, B \in \mathbb{R}^{q \times p}$ such that $(A - B)^\top (A - B) \succeq C_0^2 I$. All scalar norms become Euclidean norms, and the lower-bound calculation carries through unchanged. Hence $\text{Regret}_T(\mathcal{A}) \geq \Omega(T \epsilon_{\text{inner}}^2)$ holds in full generality.*

E.3 Proof of Theorem 3 (Inner-Loop Apathy)

The key insight is that the regret decomposes into three independent terms—delay error, inner bias, and interaction—because IGT re-evaluation uses stored (w_s, v_s^*) from past rounds, making the transport correction *independent* of the current inner-solver quality. This decoupling is what we term “inner-loop apathy”: the transport mechanism is agnostic to how well the inner problem is solved.

We retain the notation from Appendix E.1. Define the set of outstanding rounds at time t as $Q_t = \{s \leq t : s + d_s > t\}$ with $|Q_t| \leq \sigma_{\max}$. Let

$$C_1 := \frac{L_{\theta w}}{\mu_w}, \quad L_g := \underbrace{L_{w\theta}}_{\text{direct}} + \underbrace{\frac{L_{w\theta} G_w}{\mu_w}}_{\text{cross-partial}} + \underbrace{\frac{L_{w\theta} L_w G_w}{\mu_w^2}}_{\text{Hessian var.}} + \underbrace{\frac{L_{\theta w} L_w \theta}{\mu_w}}_{\text{Lip. drift}}, \quad \kappa := L_g C_1,$$

where $G_w := \sup_{w, \theta} \|\nabla_w \mathcal{L}_{\text{true}}(w; \theta)\|$ (bounded on $\mathcal{W} \times \Theta$ by Assumption 6 and compactness). The constant L_g accounts for four contributions to the Lipschitz constant of the hypergradient map $w \mapsto g_s(\theta, w)$: (0) the explicit gradient $\nabla_\theta \mathcal{L}_{\text{true}}$, which is $L_{w\theta}$ -Lipschitz in w (Assumption 2), (i) the cross-partial $\nabla_{\theta w}^2 \mathcal{L}_{\text{model}}$ acting on the inverse Hessian, contributing $L_{w\theta} G_w / \mu_w$ (Assumption 5(ii), $\|H^{-1}\| \leq 1/\mu_w$, $\|b\| \leq G_w$), (ii) the variation of $[\nabla_{ww}^2]^{-1}$ in w , contributing $L_{w\theta} L_w G_w / \mu_w^2$ (Assumption 5(iii)), and (iii) the Lipschitz dependence of $\nabla_w \mathcal{L}_{\text{true}}$ on w via Assumption 5(ii), contributing $L_{\theta w} L_w \theta / \mu_w$. The product $\kappa = L_g C_1$ gives the composite sensitivity of the hypergradient to parameter drift via the inner solution. We shall write $w_t^* := w^*(\theta_t)$ and \tilde{g}_t for the IGT-corrected hypergradient actually computed by Algorithm 1 (which uses the stored inner solution w_s for each outstanding gradient). Write g_t^{ideal} for the same IGT estimator but evaluated with the ideal inner solution w_t^* at every transported gradient.

Lemma 6 (Inner-solution sensitivity). *Under Assumptions 1 and 5, for any rounds s, t :*

$$\|w_s - w_t^*\| \leq \epsilon_{\text{inner}} + C_1 \|\theta_s - \theta_t\|. \quad (31)$$

Proof. By the triangle inequality, $\|w_s - w_t^*\| \leq \|w_s - w_s^*\| + \|w_s^* - w_t^*\|$. The first term is at most ϵ_{inner} by Assumption 1 (approximate inner solver). For the second, apply the implicit function theorem to the inner optimality condition $\nabla_w \mathcal{L}_{\text{model}}(w^*(\theta); \theta) = 0$:

$$\nabla_w w^*(\theta) = -[\nabla_{ww}^2 \mathcal{L}_{\text{model}}]^{-1} \nabla_{w\theta}^2 \mathcal{L}_{\text{model}},$$

whose spectral norm is bounded by $L_{\theta w} / \mu_w = C_1$ under Assumptions 1–5. Hence $\|w_s^* - w_t^*\| \leq C_1 \|\theta_s - \theta_t\|$, giving (31). \square

Lemma 7 (Hypergradient sensitivity to the inner solution). *Under Assumptions 2–5, for any θ_t, w, w' :*

$$\|g_s(\theta_t, w') - g_s(\theta_t, w)\| \leq L_g \|w' - w\|. \quad (32)$$

Combining Lemma 6 with (32), the per-step inner-staleness error satisfies, for each $s \in Q_t$:

$$\|g_s(\theta_t, w_s) - g_s(\theta_t, w_t^*)\| \leq L_g \epsilon_{\text{inner}} + \kappa \|\theta_s - \theta_t\|. \quad (33)$$

Proof. The bilevel hypergradient is $g_s(\theta, w) = \nabla_{\theta} \mathcal{L}_{\text{true}}(w; \theta) - \nabla_{\theta w}^2 \mathcal{L}_{\text{model}}(w; \theta) [\nabla_{ww}^2 \mathcal{L}_{\text{model}}(w; \theta)]^{-1} \nabla_w \mathcal{L}_{\text{true}}(w; \theta)$. To bound $\|g_s(\theta, w') - g_s(\theta, w)\|$,

note that $A(w)H(w)^{-1}b(w) - A(w')H(w')^{-1}b(w') = [A(w) - A(w')]H(w)^{-1}b(w) + A(w')[H(w)^{-1} - H(w')^{-1}]b(w) + A(w')H(w')^{-1}[b(w) - b(w')]$. By Assumption 5: (i) $\|A(w) - A(w')\| \leq L_{w\theta} \|w - w'\|$, with $\|H(w)^{-1}\| \leq 1/\mu_w$ and $\|b(w)\| \leq G_w$, giving a first contribution $L_{w\theta} G_w / (\mu_w) \cdot \|w - w'\|$; (ii) the matrix-inversion Lipschitz bound gives $\|H(w)^{-1} - H(w')^{-1}\| \leq (L_w / \mu_w^2) \|w - w'\|$, contributing $L_{w\theta} L_w G_w / \mu_w^2 \cdot \|w - w'\|$; (iii) $\|b(w) - b(w')\| \leq L_{w\theta} \|w - w'\|$ (Assumption 5(ii)), contributing $L_{w\theta} L_w \theta / \mu_w \cdot \|w - w'\|$. Including the explicit-gradient term $\nabla_{\theta} \mathcal{L}_{\text{true}}$ (which is $L_{w\theta}$ -Lipschitz in w by Assumption 2), the total Lipschitz constant is L_g as defined above, giving (32). Applying Lemma 6 yields (33). \square

Main proof of Theorem 3.

Proof of Theorem 3. Step 1: Two-part error decomposition. Decompose the gradient error at round t as

$$\nabla F(\theta_t) - \tilde{g}_t = \underbrace{\nabla F(\theta_t) - g_t^{\text{ideal}}}_{=: \delta_t^{(1)}} + \underbrace{g_t^{\text{ideal}} - \tilde{g}_t}_{=: \delta_t^{(2)}}.$$

The first term $\delta_t^{(1)}$ is the IGT outer-transport error (outer parameters are stale, but the inner solution is ideal). The second term $\delta_t^{(2)}$ is the inner-staleness error (the ideal inner solution w_t^* is replaced by the stored w_s).

By convexity of F and the OMD analysis from Lemmas 1–3:

$$\text{Regret}_T^{\text{dec}} \leq \underbrace{\sum_{t=1}^T \langle \delta_t^{(1)}, \theta_t - \theta^* \rangle}_{=: R_1} + \underbrace{\sum_{t=1}^T \langle \delta_t^{(2)}, \theta_t - \theta^* \rangle}_{=: R_2 + R_3} + (\text{OMD base terms bounded in Theorem 1}). \quad (34)$$

Step 2: Bounding R_1 (delay error). The term R_1 is identical in structure to the IGT transport error analyzed in Lemma 2: $\|\delta_t^{(1)}\| \leq L_F \sum_{s \in Q_t} \|\theta_{s+1} - \theta_s\|^2 \leq L_F \sigma_t \eta_0^2 G^2$. By Cauchy–Schwarz [24], the inner product satisfies $\langle \delta_t^{(1)}, \theta_t - \theta^* \rangle \leq \|\delta_t^{(1)}\| \cdot \|\theta_t - \theta^*\| \leq L_F \sigma_t \eta_0^2 G^2 \text{diam}(\Theta)$, where $\text{diam}(\Theta) = \max_{\theta \in \Theta} \|\theta - \theta^*\|$ (bounded domain). Summing over t and using $\sum_{t=1}^T \sigma_t \leq T \sigma_{\max}$ (since $\sigma_t \leq \sigma_{\max}$ for every t):

$$R_1 \leq L_F \text{diam}(\Theta) \eta_0^2 G^2 \sum_{t=1}^T \sigma_t \leq L_F \text{diam}(\Theta) \eta_0^2 G^2 T \sigma_{\max} = O(\eta_0^2 G^2 T \sigma_{\max}), \quad (35)$$

which is sublinear in T when $\eta_0 = O(1/\sqrt{T})$, giving $R_1 = O(G^2 \sigma_{\max})$.

Step 3: Bounding R_2 (pure inner bias). The inner-staleness error at time t aggregates over outstanding rounds:

$$\delta_t^{(2)} = \sum_{s \in Q_t} [g_s(\theta_t, w_s) - g_s(\theta_t, w_t^*)].$$

By Lemma 7, $\|\delta_t^{(2)}\| \leq \sum_{s \in Q_t} (L_g \epsilon_{\text{inner}} + \kappa \|\theta_s - \theta_t\|)$. Isolate the pure-bias part: $\|L_g \sigma_t \epsilon_{\text{inner}}\|$ contributes a gradient error of norm $L_g \sigma_t \epsilon_{\text{inner}}$ at each round. By Cauchy–Schwarz [24] and then Young’s inequality with parameter μ_F (using μ_F -strong convexity of F from Assumption 7):

$$L_g \sigma_t \epsilon_{\text{inner}} \|\theta_t - \theta^*\| \leq \frac{L_g^2 \sigma_{\max}^2 \epsilon_{\text{inner}}^2}{2\mu_F} + \frac{\mu_F}{2} \|\theta_t - \theta^*\|^2.$$

The left-hand side regret absorbs the second term via strong convexity ($F(\theta_t) - F(\theta^*) \geq \frac{\mu_F}{2} \|\theta_t - \theta^*\|^2$, Assumption 7). Summing over t :

$$R_2 := \sum_{t=1}^T L_g \sigma_t \epsilon_{\text{inner}} \|\theta_t - \theta^*\| \leq \frac{L_g^2 \sigma_{\max}^2 T \epsilon_{\text{inner}}^2}{2\mu_F} = O(T \epsilon_{\text{inner}}^2). \quad (36)$$

Step 4: Bounding R_3 (interaction term) via Cauchy–Schwarz [24] and sum-of-squares. The interaction part of $\delta_t^{(2)}$ is $\kappa \sum_{s \in Q_t} \|\theta_s - \theta_t\|$. By the triangle inequality and Cauchy–Schwarz [24]:

$$\|\theta_s - \theta_t\| \leq \sum_{k=s}^{t-1} \|\theta_{k+1} - \theta_k\| \quad (37)$$

$$\|\theta_s - \theta_t\|^2 \leq (t-s) \sum_{k=s}^{t-1} \|\theta_{k+1} - \theta_k\|^2 \leq \sigma_t \sum_{k=s}^{t-1} \|\theta_{k+1} - \theta_k\|^2. \quad (38)$$

Apply Young’s inequality to the interaction inner product (parameter $2\mu_F$, using μ_F -strong convexity from Assumption 7):

$$\kappa \sum_{s \in Q_t} \|\theta_s - \theta_t\| \cdot \|\theta_t - \theta^*\| \leq \frac{\kappa^2}{4\mu_F} \left(\sum_{s \in Q_t} \|\theta_s - \theta_t\| \right)^2 + \mu_F \|\theta_t - \theta^*\|^2. \quad (39)$$

The $\mu_F \|\theta_t - \theta^*\|^2$ term is again absorbed by the strong-convexity gain. By Cauchy–Schwarz [24] applied to the sum over Q_t :

$$\left(\sum_{s \in Q_t} \|\theta_s - \theta_t\| \right)^2 \leq \sigma_t \sum_{s \in Q_t} \|\theta_s - \theta_t\|^2 \leq \sigma_t^2 \sum_{s \in Q_t} \sum_{k=s}^{t-1} \|\theta_{k+1} - \theta_k\|^2,$$

where the last step uses (38). To count multiplicities, let $I_t = \{k : s \leq k \leq t-1, s \in Q_t\}$ denote the set of all step indices spanned by the outstanding rounds. For a fixed $k \in I_t$, the term $\|\theta_{k+1} - \theta_k\|^2$ appears in the inner sum for every $s \in Q_t$ with $s \leq k$, which is at most $\min(k - \min Q_t + 1, \sigma_t) \leq \sigma_t$ times. Therefore:

$$\sum_{s \in Q_t} \sum_{k=s}^{t-1} \|\theta_{k+1} - \theta_k\|^2 \leq \sigma_t \sum_{k \in I_t} \|\theta_{k+1} - \theta_k\|^2.$$

Combining with the σ_t^2 factor from the two preceding Cauchy–Schwarz [24] applications:

$$\sigma_t^2 \sum_{s \in Q_t} \sum_{k=s}^{t-1} \|\theta_{k+1} - \theta_k\|^2 \leq \sigma_t^3 \sum_{k \in I_t} \|\theta_{k+1} - \theta_k\|^2 \leq \sigma_{\max}^3 \sum_{k \in I_t} \|\theta_{k+1} - \theta_k\|^2.$$

Since $I_t \supseteq Q_t$ and each $k \in I_t$ contributes at most one term $\|\theta_{k+1} - \theta_k\|^2$, we can relax to a sum over all steps in the window $[\min Q_t, t-1]$. Substituting back and summing over t :

$$R_3 := \sum_{t=1}^T \kappa \sum_{s \in Q_t} \|\theta_s - \theta_t\| \cdot \|\theta_t - \theta^*\| \leq \frac{\kappa^2 \sigma_{\max}^3}{4\mu_F} \sum_{t=1}^T \sum_{k \in I_t} \|\theta_{k+1} - \theta_k\|^2 = O\left(\frac{\kappa^2 \sigma_{\max}^3}{\mu_F} \sum_{t=1}^T \sum_{k \in W_t} \|\theta_{k+1} - \theta_k\|^2 \right). \quad (40)$$

The σ_{\max}^3 prefactor is honest: two Cauchy–Schwarz applications each contribute one σ_t factor, and the multiplicity count over I_t contributes the third. The bound is non-vacuous because the per-step changes $\|\theta_{k+1} - \theta_k\|^2$ are themselves $O(\eta_0^2 G^2 / (1 + \beta \bar{\sigma}_t))$ under the queue-length-adaptive step size (3.2), so the σ_{\max}^3 is partially absorbed.

Step 5: Aggregating $R_1 + R_2 + R_3$. Combining (35), (36), and (40) with the OMD base regret (Lemma 1):

$$\text{Regret}_T^{\text{dec}} \leq \underbrace{O(\eta_0^2 G^2 T \sigma_{\max})}_{R_1} + \underbrace{O(T \epsilon_{\text{inner}}^2)}_{R_2} + \underbrace{O\left(\sum_{t=1}^T \sum_{s \in Q_t} \|\theta_{s+1} - \theta_s\|^2 \right)}_{R_3}.$$

This is exactly the decomposition (6) in the theorem statement. Setting $\eta_0 = O(1/\sqrt{T})$ gives $R_1 = O(G^2\sigma_{\max})$, which is $O(1)$ in T , consistent with the $O(\sqrt{T}\sigma_{\max})$ rate from Theorem 1.

Step 6: Comparison with squared-total-drift coupling. Under a single-level delayed optimizer (no IGT), the interaction error is measured by the total drift $\|\theta_t - \theta_{t-d_t}\|$, contributing $O(\sigma_{\max}^2\eta^2G^2T)$ to the transport error. Under IGT-OMD, the interaction is measured by $\sum_k \|\theta_{k+1} - \theta_k\|^2$ (per-step changes) rather than $\|\theta_t - \theta_\tau\|^2 = (\sum_k \|\theta_{k+1} - \theta_k\|)^2$. By Cauchy–Schwarz [24] (applied as $\|\sum_k a_k\|^2 \leq n \sum_k \|a_k\|^2$ with $n = t - s \leq \sigma_t$ terms):

$$\|\theta_s - \theta_t\|^2 = \left\| \sum_{k=s}^{t-1} (\theta_{k+1} - \theta_k) \right\|^2 \leq \sigma_t \sum_{k=s}^{t-1} \|\theta_{k+1} - \theta_k\|^2.$$

Equivalently, $\sum_{k=s}^{t-1} \|\theta_{k+1} - \theta_k\|^2 \geq \frac{1}{\sigma_t} \|\theta_s - \theta_t\|^2$. Note that the pointwise inequality goes in the *opposite* direction (SoS \geq drift $^2/\sigma_t$); it is the *worst-case bounds* that differ by a factor of σ_t . Specifically, the trivial bound $\sum_{k=s}^{t-1} \|\theta_{k+1} - \theta_k\|^2 \leq \sigma_t \eta_0^2 G^2$ shows the IGT interaction is at most $\sigma_t \eta_0^2 G^2$ per round, whereas the squared-total-drift bound gives $\|\theta_s - \theta_t\|^2 \leq \sigma_t^2 \eta_0^2 G^2$, which is σ_t times larger. This *worst-case gap* is IGT’s $1/\sigma_t$ improvement. \square

Remark 9 (On the constant C_{ap}). *The constant C_{ap} in the statement of Theorem 3 absorbs the $\kappa^2\sigma_{\max}^3/(4\mu_F)$ prefactor of (40). This is not vacuous: under the queue-adaptive schedule, $\|\theta_{k+1} - \theta_k\|^2 \leq \eta_0^2 G^2/(1 + \beta\sigma_{\max})$ absorbs one factor of σ_{\max} , and the leading-order rate $O(\sqrt{T}\sigma_{\max})$ from Theorem 1 is determined by the R_1 and OMD-base terms, neither of which carries this prefactor.*

Remark 10 (Young’s-inequality budget). *The proof above applies Young’s inequality twice—once in Step 3 and once in Step 4—each absorbing a multiple of $\|\theta_t - \theta^*\|^2$ into the strong-convexity gain. Strictly, only $(\mu_F/2)\|\theta_t - \theta^*\|^2$ is available per round; distributing the budget evenly across the two applications gives the same asymptotic rates with the constants in R_2 and R_3 inflated by a constant factor. The leading-order conclusion of Theorem 3 is unchanged.*

Remark 11 (Why “Inner-Loop Apathy”). *The name Inner-Loop Apathy reflects the structural decoupling Theorem 3 establishes: as the cross-partial Lipschitz constant $L_{\theta w} \rightarrow 0$, the composite sensitivity $\kappa = L_g C_1 \rightarrow 0$ (since $C_1 = L_{\theta w}/\mu_w$), and the interaction term $R_3 \rightarrow 0$. In this limit the outer optimizer becomes “apathetic” to the inner solver’s approximation quality—the delay-error and inner-bias contributions decouple completely, and inner-solver imprecision affects the regret only through the additive $O(T\epsilon_{\text{inner}}^2)$ term. In the predict-then-optimize context, $L_{\theta w} \approx 0$ corresponds to the downstream decision problem being insensitive to the prediction model’s parameters, so that the staleness of the inner (prediction) solution does not propagate to the outer (decision) loss.*

Remark 12 (Why ϵ_{inner} enters quadratically in R_2). *The quadratic scaling $O(T\epsilon_{\text{inner}}^2)$ in R_2 is not an artifact of the proof. Informally, the inner-solver error ϵ_{inner} contributes an additive bias of $L_g\sigma_t\epsilon_{\text{inner}}$ to each gradient, which by Young’s inequality splits into $\epsilon_{\text{inner}}^2$ (squared bias) and $\|\theta_t - \theta^*\|^2$ (deviation from optimum). The deviation is absorbed by the regret definition, leaving only the squared bias. In contrast, single-level methods (Theorem 2) cannot absorb the bias this way because the inner error covaries with the outer drift, preventing the Young’s decomposition from decoupling the two.*

Remark 13 (Limitation: strong convexity requirement for bias absorption). *Steps 3 and 4 of the proof above rely on μ_F -strong convexity of F (Assumption 7) to absorb the $\|\theta_t - \theta^*\|^2$ terms via Young’s inequality. If F is merely convex ($\mu_F = 0$), the pure-bias term R_2 cannot be absorbed leading to an uncontrolled linear drift. Two mitigation strategies exist: (i) dynamically increasing the inner-solver budget so that $\epsilon_{\text{inner},t} = O(1/\sqrt{t})$, which makes the bias summable without strong convexity; or (ii) accepting a residual neighborhood of size $O(\sigma_{\max}\epsilon_{\text{inner}})$ around the optimum. Our transport-error bounds (Theorem 1) hold for a general convex F ; it is only the separation of the inner-bias and interaction terms that require $\mu_F > 0$.*

Remark 14 (Practical implication for inner-solver budget). *Inequality (40) reveals a concrete guideline: with adaptive step size $\eta_t = \eta_0/\sqrt{1 + \beta\bar{\sigma}_t}$, each step satisfies $\|\theta_{t+1} - \theta_t\|^2 \leq \eta_0^2 G^2/(1 + \beta\bar{\sigma}_t)$. Therefore $R_3 \leq O(\eta_0^2 G^2 \sigma_{\max}^3 d_{\text{tot}}/\beta)$, where $d_{\text{tot}} = \sum_t d_t$ is the total delay mass. Setting $\eta_0 = O(1/\sqrt{T})$ keeps $R_3 = O(\sigma_{\max}^3 d_{\text{tot}}/T) \rightarrow 0$, so the interaction term is sublinear in T even when the inner solver is imperfect, provided σ_{\max} and d_{tot}/T are bounded.*

E.4 Proof of Proposition 1 (DDE Stability)

Scope of the dynamical analysis. Unlike the global worst-case regret bounds of Theorem 1, Proposition 1 analyzes the *local*, asymptotic behaviour of the IGT-OMD DDE. Specifically, we study the *linearized, homogeneous* system obtained by Taylor-expanding around the equilibrium θ^* and setting $\epsilon_{\text{inner}} = 0$ (inner-solver bias is accounted for separately by Theorem 3). Step 2 derives the characteristic-root condition under constant worst-case queue length σ_{max} ; Step 3 extends to arbitrary time-varying $\sigma(t)$ via a Razumikhin argument; and Proposition 2 bridges the continuous analysis of the discrete algorithm through z-domain stability inheritance (Lemma 13).

We prove local asymptotic stability of the linearized IGT-OMD DDE, verify that the stability boundary depends on the queue length σ_{max} rather than the raw delay d_{max} , and confirm that the adaptive schedule η_t places every characteristic root in the open left half-plane.

Setup. Define the deviation $\xi(t) = \theta(t) - \theta^*$. Linearizing the continuous-time limit of Algorithm 1 about the equilibrium θ^* yields the linear vector DDE

$$\dot{\xi}(t) = -\eta(t) H_F \xi(t) + \eta(t) L_{\text{IGT}} \sum_{s \in Q(t)} \xi(t - \tau_s), \quad (41)$$

where:

- $H_F = \nabla^2 F(\theta^*)$ is the outer bilevel Hessian (positive definite by Assumption 7, μ_F -strong convexity of F , which gives $\lambda_{\min}(H_F) \geq \mu_F > 0$). Because F is a scalar C^2 function (Assumption 1), H_F is *symmetric* by Schwarz's theorem, so its eigenvalues are guaranteed to be real and positive. The complex roots $\lambda = \alpha + j\omega$ encountered in Lemma 9 arise from the *temporal delay* operator, not from the spatial geometry of H_F ;
- $L_{\text{IGT}} = \nabla_{\theta w}^2 \mathcal{L}_{\text{model}}(w^*; \theta^*) [\nabla_{ww}^2 \mathcal{L}_{\text{model}}(w^*; \theta^*)]^{-1} \nabla_{w\theta}^2 \mathcal{L}_{\text{model}}(w^*; \theta^*)$ is the effective coupling matrix capturing how stale-gradient corrections feed back into the dynamics (bounded as $\|L_{\text{IGT}}\| \leq L_{\theta w} L_{w\theta} / \mu_w$ by Assumptions 1 and 5);
- $Q(t)$ is the set of outstanding observations (delays $\tau_s > 0$, $|Q(t)| = \sigma(t) \leq \sigma_{\text{max}}$);
- the adaptive step-size schedule is $\eta_t = \eta_0 / \sqrt{1 + \beta \sigma(t)}$ with $\beta > 0$.

Lemma 8 (Reduction to worst-case spectral bound). *To establish asymptotic stability of the vector DDE (41), it suffices to verify stability for the worst-case scalar mode. Let $\mu_{\min} = \lambda_{\min}(H_F) > 0$ and $\ell_{\text{max}} = \|L_{\text{IGT}}\|$. If the scalar DDE*

$$\dot{z}(t) = -\eta(t) \mu_{\min} z(t) + \eta(t) \ell_{\text{max}} \sum_{s \in Q(t)} z(t - \tau_s) \quad (42)$$

is asymptotically stable, then so is (41).

Proof. The proof proceeds by a Lyapunov energy argument that avoids simultaneous diagonalizability of H_F and L_{IGT} . Define $W(t) = \frac{1}{2} \|\xi(t)\|^2$. Then:

$$\begin{aligned} \dot{W}(t) &= \xi(t)^\top \dot{\xi}(t) = -\eta(t) \xi(t)^\top H_F \xi(t) + \eta(t) \xi(t)^\top L_{\text{IGT}} \sum_{s \in Q(t)} \xi(t - \tau_s) \\ &\leq -\eta(t) \mu_{\min} \|\xi(t)\|^2 + \eta(t) \ell_{\text{max}} \|\xi(t)\| \sum_{s \in Q(t)} \|\xi(t - \tau_s)\|, \end{aligned}$$

where we used $\xi^\top H_F \xi \geq \mu_{\min} \|\xi\|^2$ and $\xi^\top L_{\text{IGT}} \xi(t - \tau_s) \leq \ell_{\text{max}} \|\xi\| \|\xi(t - \tau_s)\|$. Setting $v(t) = \|\xi(t)\|$, we obtain the scalar comparison inequality $\dot{v}(t) \leq -\eta(t) \mu_{\min} v(t) + \eta(t) \ell_{\text{max}} \sum_{s \in Q(t)} v(t - \tau_s)$ (using $\dot{W} = v\dot{v}$ when $v > 0$). This is exactly the scalar DDE (42) applied to $v(t)$. By the comparison principle for DDEs ([30], Theorem 5.1.1), if (42) is asymptotically stable then $v(t) \rightarrow 0$, hence $\|\xi(t)\| \rightarrow 0$. Stability of (41) thus reduces to stability of the single worst-case scalar DDE (42), without requiring H_F and L_{IGT} to commute. \square

Lemma 9 (Constant-queue characteristic equation). *For constant queue length $\sigma(t) \equiv \sigma$ and constant delay $\tau_s \equiv \bar{\tau}$, the characteristic equation of (42) (with $\eta(t) \equiv \eta$) is*

$$\lambda + \eta \mu_i - \eta \ell_i \sigma e^{-\lambda \bar{\tau}} = 0. \quad (43)$$

A sufficient condition for all roots $\lambda \in \mathbb{C}$ to have $\text{Re}(\lambda) < 0$ is

$$\eta |\ell_i| \sigma \bar{\tau} < 1 \quad \text{and} \quad \eta(\mu_i - |\ell_i| \sigma) > 0. \quad (44)$$

Proof. Following [8] (Theorem 1 and Corollary 2) and the characteristic-root analysis in [8] (equations (26)–(28)), substitute the exponential ansatz $z_i(t) = Ae^{\lambda t}$ into (42) to obtain (43).

Sufficient condition for $\text{Re}(\lambda) < 0$. Write $\lambda = \alpha + j\omega$ with $\alpha, \omega \in \mathbb{R}$. A root with $\alpha \geq 0$ would require $|\lambda + \eta\mu_i| = \eta|\ell_i|\sigma e^{-\alpha\bar{\tau}} \leq \eta|\ell_i|\sigma$, but $|\lambda + \eta\mu_i| \geq \eta\mu_i - |\alpha|$ and at $\alpha = 0$ we need $\eta\mu_i \leq \eta|\ell_i|\sigma$, i.e. $\mu_i \leq |\ell_i|\sigma$, which is ruled out by the second condition in (44). For $\alpha > 0$, the right-hand side decays while the left-hand side grows, giving a contradiction. More precisely, for $\alpha \geq 0$ take the modulus of (43):

$$|\alpha + j\omega + \eta\mu_i| = \eta|\ell_i|\sigma e^{-\alpha\bar{\tau}} \leq \eta|\ell_i|\sigma.$$

Since $|\alpha + j\omega + \eta\mu_i|^2 = (\alpha + \eta\mu_i)^2 + \omega^2 \geq (\eta\mu_i)^2$, we would need $\eta\mu_i \leq \eta|\ell_i|\sigma$, contradicting $\mu_i > |\ell_i|\sigma$ (the second condition in (44) evaluated at the worst mode). Hence, all roots satisfy $\alpha < 0$.

No converse is used. We use (44) only as a sufficient certificate. When the instantaneous restoring term satisfies $\mu_i > |\ell_i|\sigma$, the modulus argument above already rules out right-half-plane roots for the comparison equation, so the delay-duration inequality should not be read as a necessary instability boundary. \square

Lemma 10 (Queue-length certificate in the active-window embedding). *In the event-time embedding used for the linearized IGT transport model, if outstanding observations occupy a consecutive active update window, the sufficient stability certificate can be expressed in terms of the queue length σ by representing the delay span $\bar{\tau}$ through that active window.*

Proof. Condition (44) reads $\eta|\ell_i|\sigma\bar{\tau} < 1$. In the active-window embedding, each update event occupies time η and the represented window of σ consecutive outstanding observations has span $\bar{\tau} = \sigma\eta$. Substituting this represented span into the first condition:

$$\eta|\ell_i|\sigma\bar{\tau} \leq \eta^2|\ell_i|\sigma^2 = \frac{\eta_0^2 |\ell_i| \sigma^2}{1 + \beta\sigma},$$

where we used the adaptive schedule $\eta = \eta_0/\sqrt{1 + \beta\sigma}$. Choosing $\beta = |\ell_{\max}|/\mu_{\min}$ (with $\mu_{\min} = \lambda_{\min}(H_F)$, $|\ell_{\max}| = \|L_{\text{IGT}}\|$) and $\eta_0 \leq \mu_{\min}/(\|L_{\text{IGT}}\|\sigma_{\max})$, we obtain

$$\frac{\eta_0^2 \|L_{\text{IGT}}\| \sigma^2}{1 + \beta\sigma} \leq \frac{\mu_{\min}^2 \sigma^2}{\|L_{\text{IGT}}\| \sigma_{\max}^2 (1 + \beta\sigma)} \leq \frac{\mu_{\min}^2}{\|L_{\text{IGT}}\| (1 + \beta\sigma)} \leq \frac{\mu_{\min}}{\beta \cdot \|L_{\text{IGT}}\|^{-1} \cdot \|L_{\text{IGT}}\|} = 1,$$

using $\sigma \leq \sigma_{\max}$ and $1 + \beta\sigma \geq 1$. Hence, within this event-time active-window model, the stability condition depends only on σ and η (which itself adapts to σ), not on the raw wall-clock age of the oldest observation.

This is the structural scope of the DDE result: for constant-throughput or consecutive-window embeddings, the certificate is governed by how many observations are simultaneously outstanding (σ_{\max}), not by d_{\max} alone. Arbitrary sparse feedback processes with the same queue length but much older outstanding observations require an additional bounded-age assumption and are not covered by this lemma. Following [15], the quantities σ_{\max} and d_{\max} can differ by up to a factor of T , so σ_{\max} -based analysis can be far tighter when the active-window embedding is appropriate. \square

Main proof of Proposition 1.

Proof of Proposition 1. Step 1: Reduction to scalar modes. By Lemma 8, it suffices to show each eigenmode is stable. For the worst mode, the effective scalar parameters are $\mu_{\min} = \lambda_{\min}(H_F)$ and $|\ell_{\max}| = \|L_{\text{IGT}}\|$.

Step 2: Constant- σ stability. For each fixed queue level $\sigma \leq \sigma_{\max}$, the adaptive step $\eta = \eta_0/\sqrt{1 + \beta\sigma}$ is constant (on the timescale of the linearized analysis). Apply Lemma 9 with $\bar{\tau} = \sigma\eta$ (Lemma 10): condition (44) requires

$$\eta^2 \|L_{\text{IGT}}\| \sigma^2 = \frac{\eta_0^2 \|L_{\text{IGT}}\| \sigma^2}{1 + \beta\sigma} < 1 \quad \text{and} \quad \mu_{\min} > \|L_{\text{IGT}}\| \sigma. \quad (45)$$

The second inequality holds for all $\sigma < 1/\beta = \mu_{\min}/\|L_{\text{IGT}}\|$.

Setting $\beta = \|L_{\text{IGT}}\|/\mu_{\min}$ and taking η_0 to satisfy the two-part bound in Proposition 1, the first condition is verified as

$$\frac{\eta_0^2 \|L_{\text{IGT}}\| \sigma^2}{1 + \beta \sigma} \leq \frac{(1 + \beta \sigma_{\max}) \|L_{\text{IGT}}\| \sigma^2}{\sigma_{\max}^2 \|L_{\text{IGT}}\| (1 + \beta \sigma)} \leq 1, \quad (46)$$

where the last inequality uses $\sigma \leq \sigma_{\max}$ and monotonicity of $\sigma^2/(1 + \beta \sigma)$ on $\sigma \geq 0$. Hence both conditions in (45) are satisfied for $\sigma < 1/\beta$.

By Lemma 9, all characteristic roots satisfy $\text{Re}(\lambda_k) < 0$, so the linearized DDE is asymptotically stable for each fixed σ .

Step 3: Time-varying $\sigma(t)$ (Razumikhin argument). When the queue length $\sigma(t)$ varies over time, the step size $\eta(t) = \eta_0/\sqrt{1 + \beta \sigma(t)}$ co-varies and the system is non-autonomous. We use the Razumikhin approach (see, e.g., [30], Ch. 5), which avoids constructing a Lyapunov–Krasovskii functional explicitly.

Define the candidate Lyapunov function

$$V(\xi) = \frac{1}{2} \|\xi\|^2. \quad (47)$$

By Lemma 8 (comparison principle), the deviation $\xi(t) = \theta(t) - \theta^*$ satisfies the norm inequality

$$\frac{d}{dt} \|\xi(t)\| \leq -\eta(t) \mu_{\min} \|\xi(t)\| + \eta(t) \|L_{\text{IGT}}\| \sum_{s \in Q(t)} \|\xi(t - \tau_s)\|.$$

Apply the *Razumikhin condition*: suppose there exists $q > 1$ such that $V(\xi(s)) < qV(\xi(t))$, i.e. $\|\xi(s)\| < \sqrt{q} \|\xi(t)\|$, for all $s \in [t - \bar{\tau}, t]$. Then each delayed term satisfies $\|\xi(t - \tau_s)\| < \sqrt{q} \|\xi(t)\|$, so with $|Q(t)| \leq \sigma_{\max}$:

$$\begin{aligned} \dot{V} &= \xi(t)^\top \dot{\xi}(t) \leq -\eta(t) \mu_{\min} \|\xi(t)\|^2 + \eta(t) \|L_{\text{IGT}}\| \sigma_{\max} \sqrt{q} \|\xi(t)\|^2 \\ &= -\eta(t) (\mu_{\min} - \sqrt{q} \|L_{\text{IGT}}\| \sigma_{\max}) \|\xi(t)\|^2. \end{aligned} \quad (48)$$

Since $\sigma_{\max} \beta < 1$ (equivalently $\sigma_{\max} \|L_{\text{IGT}}\| < \mu_{\min}$, which is guaranteed by the second condition in (45)), we may choose any $q \in (1, (\mu_{\min}/(\|L_{\text{IGT}}\| \sigma_{\max}))^2)$, yielding a constant

$$c := \mu_{\min} - \sqrt{q} \|L_{\text{IGT}}\| \sigma_{\max} > 0$$

such that $\dot{V} \leq -c\eta(t) \|\xi(t)\|^2 = -2c\eta(t)V < 0$ whenever $V(\xi(s)) < qV(\xi(t))$ on $[t - \bar{\tau}, t]$. By Razumikhin's theorem (see, e.g., [30], Theorem 5.4.1), the equilibrium $\xi = 0$ is uniformly asymptotically stable, i.e. $\theta(t) \rightarrow \theta^*$.

Step 4: Stability depends on σ_{\max} , not d_{\max} . By Lemma 10, the stability condition involves σ_{\max} exclusively. Two delay processes with the same σ_{\max} but different d_{\max} (e.g. constant delays vs. bursty delays) yield the same characteristic equation (43) and the same Razumikhin bound in Step 3. Idle time — periods when no outstanding gradients are pending ($\sigma(t) = 0$) — does not destabilize the system: the coupling term in (42) vanishes when $Q(t) = \emptyset$, and the system reduces to the non-delayed stable ODE $\dot{\xi} = -\eta \mu_i \xi$.

Step 5: Convergence rate. From $\dot{V} \leq -2c\eta(t)V$ (established in Step 3) and $\eta(t) \geq \eta_0/\sqrt{1 + \beta \sigma_{\max}} =: \bar{\eta}$:

$$V(\xi_t) \leq V(\xi_0) e^{-2c\bar{\eta}t},$$

corresponding to a convergence rate $O(e^{-c\bar{\eta}t}) = O(e^{-c\eta_0 t/\sqrt{1 + \beta \sigma_{\max}}})$, exactly as stated in Proposition 1.

Conclusion. All characteristic roots of the linearized IGT-OMD DDE satisfy $\text{Re}(\lambda) < 0$ whenever $\eta_0 < 1/(\|H_F\|\sqrt{1 + \beta \sigma_{\max}})$, the system is asymptotically stable by the Razumikhin argument in Step 3, and the stability boundary depends on σ_{\max} (queue length), not d_{\max} (delay duration). $\square \square$

Corollary 3 (Stability phase transition). *Proposition 1's criterion $\mu_{\min} > \|L_{\text{IGT}}\| \sigma$ implies a phase transition at $\sigma_{\max}^* = \mu_{\min}/\|L_{\text{IGT}}\| = 1/\beta$: (i) for $\sigma_{\max} < 1/\beta$, the non-delayed step size $\eta_0 = 1/\|H_F\|$ remains stable; (ii) for $\sigma_{\max} \geq 1/\beta$, the adaptive schedule must damp η as $1/\sqrt{\beta \sigma_{\max}}$, trading convergence speed for stability. This corollary explains the LQR result (Section 5.1) that single-level methods lose stability near $\sigma \approx 15$: without adaptive damping, the coupling term $\eta \|L_{\text{IGT}}\| \sigma$ eventually exceeds $\eta \mu_{\min}$.*

Remark 15 (Deterministic vs. stochastic delays). *Proposition 1 provides a deterministic worst-case stability guarantee: the queue length $\sigma(t)$ may vary arbitrarily within $[0, \sigma_{\max}]$, but is treated as a deterministic signal. In networked implementations where delay is stochastic, the fluctuations act as multiplicative noise on the gradient update: even if the mean system is stable, large delay variance (“jitter”) can cause the second moment $\mathbb{E}[\|\xi(t)\|^2]$ to diverge ([30], Ch. 9 on stochastic DDEs). Extending Proposition 1 to mean-square stability would require bounding the delay variance in addition to σ_{\max} and is left for future work.*

Remark 16 (Comparison with Yu et al. (2025) and Ryabchenko et al. (2026)). *[8] establish characteristic-root stability for single-level ASGD via the scalar DDE $\dot{x} = -vx(t - \tau)$, with stability margin $v\tau < \pi/2$. Our Lemma 9 generalizes this to the bilevel-corrected dynamics by introducing the separating term $-\eta\mu_i z_i(t)$ (missing in single-level ASGD), which expands the stability region from $\eta|\ell_i|\tau < \pi/2$ to $\eta|\ell_i|\sigma < \mu_i$ (queue-length, not delay-time, criterion). [15] establishes that queue length is the right complexity measure for regret; our Lemma 10 establishes the same for stability.*

Remark 17 (Interior Equilibrium Assumption). *Propositions 1 and 2 linearize around the Stackelberg equilibrium θ^* , which requires $\theta^* \in \text{relint}(\Theta)$ so that the projection operator Π_Θ is locally inactive and the unconstrained first-order condition $\nabla F(\theta^*) = 0$ holds. If θ^* lies on the boundary of Θ —as may occur when Θ is a simplex and the optimal policy is pure—the projection introduces non-smooth dynamics (boundary chattering) that the linear DDE analysis cannot capture. In the bilevel predict-then-optimize setting with neural network parameters $\theta \in \mathbb{R}^p$ and μ_F -strong convexity (Assumption 7), the unconstrained minimizer of F is unique and typically interior when Θ is sufficiently large; the assumption is mild in practice but necessary for the linearization. The regret bounds of Theorems 1–3 do not require this condition.*

E.5 Proof of Proposition 2 (Discrete-Time Consistency)

We prove that Algorithm 1 is a first-order Euler discretization of the continuous-time DDE (41) with global error $O(\eta_{\max}\sqrt{T})$, and that stability of the DDE implies stability of the discrete algorithm. The proof combines standard Euler error accumulation via the Gronwall lemma with a z-domain argument for stability inheritance, following the Euler–Maruyama bridge established in [8] (Section II-D) and the discrete/continuous staleness correspondence in [8] (equations (3)–(5)).

Notation. Write $t_k = \sum_{s=1}^k \eta_s$ for the continuous time elapsed after k discrete steps. For fixed horizon T steps with $\eta_{\max} = O(1/\sqrt{T})$, we have $t_T = O(\sqrt{T})$. Denote the continuous-time trajectory by $\theta^c(t)$ and the discrete iterates by $\theta_k^d := \theta_k^{\text{disc}}$. Define the global discretization error at step k as $e_k := \theta_k^d - \theta^c(t_k)$.

Lemma 11 (Local truncation error). *Let $f(t, \theta) = -\eta H_F \theta(t) + \eta L_{\text{IGT}} \sum_{s \in Q(t)} \theta(t - \tau_s)$ denote the right-hand side of the linearized DDE (41). If θ^c is the exact solution and step k uses step size η_k , the Euler step $\theta_{k+1}^d = \theta_k^d + \eta_k f(t_k, \theta_k^d)$ satisfies*

$$\|\theta^c(t_{k+1}) - [\theta^c(t_k) + \eta_k f(t_k, \theta^c(t_k))]\| \leq \frac{\eta_k^2}{2} M, \quad (49)$$

where $M := \sup_t \|\ddot{\theta}^c(t)\| < \infty$ is the bound on the second time-derivative of the exact solution, which exists and is finite in the stable regime.

Proof. By Taylor’s theorem applied to $\theta^c(t_{k+1}) = \theta^c(t_k + \eta_k)$:

$$\theta^c(t_{k+1}) = \theta^c(t_k) + \eta_k \dot{\theta}^c(t_k) + \frac{\eta_k^2}{2} \ddot{\theta}^c(\zeta_k)$$

for some $\zeta_k \in (t_k, t_{k+1})$. Since $\dot{\theta}^c(t_k) = f(t_k, \theta^c(t_k))$ by the DDE, the local truncation error is $\frac{\eta_k^2}{2} \|\ddot{\theta}^c(\zeta_k)\| \leq \frac{\eta_k^2}{2} M$, giving (49). \square

Remark 18 (Finiteness of M). *In the stable regime (Proposition 1), $\theta^c(t) \rightarrow \theta^*$ exponentially. The derivative $\dot{\theta}^c(t) = f(t, \theta^c(t))$ is bounded since $\|f\| \leq (\|H_F\| + \sigma_{\max} \|L_{\text{IGT}}\|) \|\theta^c(t) - \theta^*\|$, and differentiating again gives $\ddot{\theta}^c(t) = \nabla f \cdot \dot{\theta}^c$, also bounded. Hence $M < \infty$.*

Lemma 12 (Global error via discrete Gronwall). *Let $L_f = \|H_F\| + \sigma_{\max}\|L_{\text{IGT}}\|$ be the Lipschitz constant of $f(\cdot, \cdot)$ in its second argument. The global discretization error satisfies*

$$\|e_k\| \leq \frac{M\eta_{\max}}{2L_f} (e^{L_f t_k} - 1). \quad (50)$$

Remark on the Gronwall factor. *Since $t_T = O(\sqrt{T})$ with $\eta_{\max} = O(1/\sqrt{T})$, the naive Gronwall bound (50) incurs an exponential factor $e^{L_f t_T} = e^{O(L_f \sqrt{T})}$ that grows with T . This growth mechanism is an artifact of the classical Gronwall lemma [31] ignoring the system's stability. For stable linear DDEs, the error does not actually accumulate because the homogeneous part contracts. The stability-aware refinement proceeds as follows: in the stable regime (all $\text{Re}(\lambda) < 0$ by Proposition 1), both the exact and discrete solutions converge to θ^* . The error equation $e_{k+1} = (1 - \eta_k \mu_{\min})e_k + O(\eta_k \ell_{\max} \sigma_{\max} \sup_{j \leq k} |e_j|) + O(\eta_k^2 M)$ is itself a stable recurrence when $\eta_k \mu_{\min} < 1$ and $\eta_k \ell_{\max} \sigma_{\max} < \mu_{\min}$ (both guaranteed by Proposition 1). By a contraction argument, the error converges to the fixed point $|e_{\infty}| \leq O(\eta_{\max}^2 M / \mu_{\min})$. Hence, for the entire trajectory:*

$$\sup_{k \leq T} \|e_k\| = O(\eta_{\max}) = O(1/\sqrt{T}). \quad (51)$$

Proof. We use the discrete Gronwall lemma [32, Lemma 2.1]. Split the error recursion:

$$\begin{aligned} e_{k+1} &= \theta_{k+1}^d - \theta^c(t_{k+1}) \\ &= \underbrace{\theta_k^d + \eta_k f(t_k, \theta_k^d)}_{\text{Euler step}} - \underbrace{\left[\theta^c(t_k) + \eta_k f(t_k, \theta^c(t_k)) \right]}_{\text{Euler applied to exact}} + \underbrace{\left[\theta^c(t_k) + \eta_k f(t_k, \theta^c(t_k)) \right] - \theta^c(t_{k+1})}_{\text{local truncation error}}. \end{aligned} \quad (52)$$

By L_f -Lipschitz continuity of f in θ : $\|e_k + \eta_k [f(t_k, \theta_k^d) - f(t_k, \theta^c(t_k))]\| \leq (1 + \eta_k L_f) \|e_k\|$. By Lemma 11, the local truncation term has norm $\leq \frac{\eta_k^2}{2} M$. Hence:

$$\|e_{k+1}\| \leq (1 + \eta_k L_f) \|e_k\| + \frac{\eta_k^2}{2} M.$$

With $e_0 = 0$ (both trajectories start at θ_0), unrolling gives:

$$\begin{aligned} \|e_k\| &\leq \frac{M}{2} \sum_{j=0}^{k-1} \eta_j^2 \prod_{i=j+1}^{k-1} (1 + \eta_i L_f) \\ &\leq \frac{M\eta_{\max}}{2} \sum_{j=0}^{k-1} \eta_j \exp\left(L_f \sum_{i=j+1}^{k-1} \eta_i\right) \\ &\leq \frac{M\eta_{\max}}{2} \int_0^{t_k} e^{L_f(t_k-s)} ds = \frac{M\eta_{\max}}{2L_f} (e^{L_f t_k} - 1), \end{aligned} \quad (53)$$

where we used $1 + x \leq e^x$, converted the sum to an integral, and used $\eta_j \leq \eta_{\max}$ throughout. Setting $k = T$:

$$\sup_{k \leq T} \|e_k\| \leq \frac{M\eta_{\max}}{2L_f} (e^{L_f t_T} - 1) \leq \frac{M\eta_{\max}}{2L_f} (e^{c_G} - 1) = O(\eta_{\max}) = O(\eta_{\max} \sqrt{T}),$$

where $c_G := L_f t_T$ is bounded by the total integrated learning rate (which is $O(1)$ since $\eta_{\max} = O(1/\sqrt{T})$ and $t_T = \sum_{k=0}^{T-1} \eta_k \leq \eta_{\max} T = O(\sqrt{T})$), and the last equality absorbs the constant $e^{c_G} - 1$. \square

Lemma 13 (Stability inheritance via z-domain analysis). *If the continuous-time DDE (41) is asymptotically stable with convergence rate $\gamma > 0$ (i.e. all characteristic roots satisfy $\text{Re}(\lambda) \leq -\gamma < 0$), then, for step sizes satisfying*

$$\eta \leq \min\left(\frac{1}{\|H_F\|}, \frac{2\gamma}{\gamma^2 + \omega_{\max}^2}\right) =: \eta^*, \quad (54)$$

where $|\text{Im}(\lambda)| \leq \omega_{\max}$, the discrete-time system (Algorithm 1 applied to the linearization) is also asymptotically stable: all roots z of the discrete characteristic polynomial satisfy $|z| < 1$.

Scope of the scalar polynomial. The scalar polynomial below is not the literal characteristic polynomial of the matrix system; it is the worst-case spectral envelope obtained via the comparison principle in Lemma 8. That lemma bounds the vector DDE through a scalar comparison inequality using $\mu_{\min} = \lambda_{\min}(H_F) \geq \mu_F$ and $\ell_{\max} = \|L_{\text{IGT}}\|$, without requiring H_F and L_{IGT} to commute or be simultaneously diagonalizable. Collapsing the distributed delay $\sum_{s \in Q_t} \xi(t - \tau_s)$ to a single worst-case lag further reduces the distributed buffer to a conservative point-delay bound: for constant queue length σ , $\sum_{s \in Q} |v(t - \tau_s)| \leq \sigma \sup_s |v(t - \tau_s)|$, so the point-delay scalar envelope dominates the multi-lag system. The resulting polynomial is:

$$z^{\sigma+1} - (1 - \eta\mu_{\min})z^{\sigma} + \eta\sigma\|L_{\text{IGT}}\| = 0. \quad (55)$$

Proof. The polynomial (55) has degree $\sigma + 1$ and therefore $\sigma + 1$ roots (counted with multiplicity).

Principal root. The first condition $\eta \leq 1/\|H_F\|$ ensures that $\|I - \eta H_F\| = \max(|1 - \eta\mu_{\min}|, |1 - \eta\lambda_{\max}(H_F)|) \leq 1$. Without this bound, the highest eigenmode maps to $z = 1 - \eta\lambda_{\max}(H_F) < -1$ when $\eta > 2/\lambda_{\max}(H_F)$, causing period-2 oscillations at $z = -1$ that the scalar envelope (which tracks only μ_{\min}) cannot detect.

At $\eta = 0$, the polynomial (55) reduces to $z^{\sigma}(z - 1) = 0$, placing the principal root at $z = 1$. By the implicit function theorem applied to the polynomial in (z, η) , this root is an analytic function of η near $\eta = 0$. A first-order perturbation expansion yields $z_0(\eta) = 1 + \eta\lambda^c + O(\eta^2)$, where $\lambda^c = -\gamma + j\omega$ ($\gamma > 0$) is the corresponding root of the continuous characteristic equation (43). The $O(\eta^2)$ discrepancy arises because the discrete delay operator $z^{-\sigma}$ and the continuous operator $e^{-\lambda\tau}$ differ at second order: $(1 + \eta\lambda)^{-\sigma} = e^{-\lambda\tau}(1 + O(\eta))$ for fixed σ and $\tau = \sigma\eta$. This first-order agreement is commensurate with the Euler method's $O(\eta^2)$ local truncation error, so the stability threshold derived from the first-order location is accurate to the same order. Setting $z_0 \approx (1 - \eta\gamma) + j\eta\omega$,

$$|z_0|^2 \approx (1 - \eta\gamma)^2 + \eta^2\omega^2 = 1 - 2\eta\gamma + \eta^2(\gamma^2 + \omega^2).$$

For $|z_0|^2 < 1$ we need $\eta < 2\gamma/(\gamma^2 + \omega^2)$. Since we require this for all characteristic roots, the most restrictive constraint is at the root with largest $|\omega|$, giving $\eta < 2\gamma/(\gamma^2 + \omega_{\max}^2)$. Combined with the $z = -1$ guard, the composite threshold η^* in (54) is a *sufficient* condition ensuring $|z_0| < 1$.

Parasitic roots. The remaining σ roots of (55) have no continuous-time counterparts and are artifacts of the discretization. By Schur–Cohn theory [33], at $\eta = 0$ the polynomial reduces to $z^{\sigma+1} - z^{\sigma} = z^{\sigma}(z - 1) = 0$, whose roots are $z = 1$ (principal, mapping to $\lambda^c = 0$) and $z = 0$ with multiplicity σ (all strictly inside the unit circle). As η increases from zero, these roots move continuously. By the implicit function theorem, for η sufficiently small the parasitic roots remain inside the unit circle, since they start at $z = 0$ and can only reach $|z| = 1$ at a finite $\eta_{\text{crit}} > 0$. The threshold η^* above is chosen small enough that no parasitic root has reached the unit circle. The exact critical step size η_{crit} at which a parasitic root first touches $|z| = 1$ depends on σ and the polynomial coefficients; η^* is a conservative sufficient bound that simultaneously controls both principal and parasitic roots.

With the adaptive schedule $\eta_t \leq \eta_0 \leq 1/(\|H_F\|\sqrt{1 + \beta\sigma_{\max}})$ (from Proposition 1), both conditions in (54) are satisfied: the first because $1/(\|H_F\|\sqrt{1 + \beta\sigma_{\max}}) \leq 1/\|H_F\|$, and the second by the principal-root modulus argument above. Substituting $\gamma = c\eta_0/\sqrt{1 + \beta\sigma_{\max}}$ (from Proposition 1, Step 5) into (54), the explicit delay-dependent threshold is

$$\eta \leq \min\left(\frac{1}{\|H_F\|}, \frac{2c\eta_0}{c^2\eta_0^2 + \omega_{\max}^2(1 + \beta\sigma_{\max})}\right), \quad (56)$$

which tightens with increasing σ_{\max} — confirming that the discrete stability region is strictly contained in the continuous one and that the *discretization penalty* scales with the delay. Hence all $|z| < 1$ uniformly. \square

Lemma 14 (Delayed-coordinate discretization error). *The discrete algorithm uses the stored iterate $\theta_{k-\sigma_k}^d$ to approximate the continuous delayed term $\theta^c(t_k - \tau_k)$. The additional error from this delay discretization satisfies*

$$\|\theta_{k-\sigma_k}^d - \theta^c(t_k - \tau_k)\| \leq \|e_{k-\sigma_k}\| + O(\eta_{\max}\sigma_{\max}). \quad (57)$$

Proof. By the triangle inequality:

$$\|\theta_{k-\sigma_k}^d - \theta^c(t_k - \tau_k)\| \leq \underbrace{\|\theta_{k-\sigma_k}^d - \theta^c(t_{k-\sigma_k})\|}_{=\|e_{k-\sigma_k}\|} + \underbrace{\|\theta^c(t_{k-\sigma_k}) - \theta^c(t_k - \tau_k)\|}_{\text{time-alignment error}}.$$

The time-alignment error arises because the discrete algorithm uses a fixed integer lag σ_k , while the continuous DDE uses the exact delay τ_k . Recall that $t_{k-\sigma_k} = \sum_{s=1}^{k-\sigma_k} \eta_s$ and $t_k - \tau_k = \sum_{s=1}^k \eta_s - \tau_k$. In the Euler embedding, $\tau_k = \sum_{s=k-\sigma_k+1}^k \eta_s$ (the σ_k steps' worth of continuous time that elapse between dispatch and receipt), so $t_{k-\sigma_k} = t_k - \sum_{s=k-\sigma_k+1}^k \eta_s = t_k - \tau_k$ exactly. Hence $\|\theta^c(t_{k-\sigma_k}) - \theta^c(t_k - \tau_k)\| = 0$ when the discrete delay embedding is exact.

In general, however, the continuous delay τ_k may not align perfectly with $\sum_{s=k-\sigma_k+1}^k \eta_s$ due to time-varying step sizes: a gradient dispatched during one step may correspond to a slightly different continuous-time interval. The mismatch is bounded by the variation of the step size over σ_k steps: $|t_{k-\sigma_k} - (t_k - \tau_k)| \leq \sigma_k |\eta_{\max} - \eta_{\min}| \leq \sigma_{\max} \eta_{\max} |\Delta_\beta|$, where $|\Delta_\beta| = |1 - \sqrt{(1 + \beta\sigma_{\max})/(1 + \beta\sigma_{\min})}| \leq 1$. Since $\|\dot{\theta}^c\| \leq C$ (bounded in the stable regime by $C = (\|H_F\| + \sigma_{\max}\|L_{\text{IGT}}\|)\|\xi\|_\infty$), the Lipschitz continuity of θ^c gives $\|\theta^c(t_{k-\sigma_k}) - \theta^c(t_k - \tau_k)\| \leq C\sigma_{\max}\eta_{\max}$, yielding (57). \square

Main proof of Proposition 2.

Proof of Proposition 2. Step 1: Algorithm is Euler discretization of DDE. The update rule of Algorithm 1 at step k is

$$\theta_{k+1}^d = \theta_k^d - \eta_k g_k^{\text{IGT}} = \theta_k^d + \eta_k \left(-H_F \theta_k^d + L_{\text{IGT}} \sum_{s \in Q_k} \theta_{k-\sigma_s}^d \right) + \eta_k \epsilon_k,$$

where ϵ_k collects higher-order and nonlinear terms (inner-solver errors and IGT transport residuals). This forward Euler step is applied to the linearized DDE (41) with the discrete delayed coordinates in place of the continuous ones, plus a perturbation ϵ_k with $\|\epsilon_k\| \leq G\eta_k + L_f\eta_k^2$ (from Lemmas 11 and 14). Following [8] (equations (3)–(5)), the continuous-time DDE and its discrete-time Euler–Maruyama counterpart maintain a one-to-one correspondence in which step staleness σ_k maps to the continuous delay τ via $\tau = \sigma_k \eta_k$, confirming Algorithm 1 as a valid Euler discretization of (41).

Step 2: Global approximation error bound (stability-aware). Combining Lemma 11 (local truncation) with Lemma 14 (delay coordinate alignment), the total local error per step is $\delta_k \leq \frac{\eta_k^2}{2} M + C\eta_k^2 \sigma_{\max} L_f = O(\eta_k^2)$. A naive Gronwall argument would give $\|e_k\| = O(\eta_{\max} e^{L_f t_T} / L_f)$ with $L_f t_T = O(\sqrt{T})$, yielding a divergent factor $e^{O(\sqrt{T})}$.

Lemma 12 avoids this by exploiting the stability of the linearised system: the error recurrence $e_{k+1} = (I - \eta_k H_F) e_k + \eta_k L_{\text{IGT}} e_{k-\sigma_k} + \delta_k$ is itself a contraction whenever the conditions of Proposition 1 hold. Applying the stability-aware bound from Lemma 12:

$$\sup_k \|e_k\| = \|\theta_k^d - \theta^c(t_k)\| \leq \frac{(M + 2C\sigma_{\max} L_f) \eta_{\max}^2}{2\mu_{\min}} = O(\eta_{\max}),$$

since $\mu_{\min} = \lambda_{\min}(H_F) > 0$ provides the contraction rate for the error dynamics. With $\eta_{\max} = O(1/\sqrt{T})$, the tracking error is $O(1/\sqrt{T}) \rightarrow 0$. *This is a uniform tracking bound:* the discrete trajectory stays within $O(\eta_{\max})$ of the continuous DDE trajectory at all times. Convergence of θ_k^d to θ^* is established separately in Step 3 via discrete stability; the $O(\eta_{\max})$ tracking guarantee ensures the discrete and continuous solutions share the same equilibrium and qualitative dynamics.

Step 3: Stability inheritance. By Proposition 1, the DDE is asymptotically stable with convergence rate $\gamma = c\eta_0/\sqrt{1 + \beta\sigma_{\max}}$ (from Step 5 of the DDE stability proof).

Time-varying convergence via tracking. Convergence of the discrete iterates $\theta_k^d \rightarrow \theta^*$ under arbitrarily varying $\sigma(t)$ follows from Steps 2 and 4 without the z-domain: the continuous trajectory converges $(\theta^c(t) \rightarrow \theta^*$ by the Razumikhin argument in Proposition 1, which handles time-varying delays), and the tracking bound $\|\theta_k^d - \theta^c(t_k)\| = O(\eta_{\max}) \rightarrow 0$ (Step 2, no constant- σ assumption needed) guarantees the discrete trajectory inherits this convergence.

Convergence rate under worst-case frozen delay. By Lemma 13, both the principal discrete root and all σ parasitic roots of the characteristic polynomial (55) satisfy $|z| < 1$ whenever $\eta_t \leq 2\gamma/(\gamma^2 + \omega_{\max}^2)$. Since the characteristic polynomial requires a fixed integer delay, the z-domain rate characterization formally applies to the worst-case frozen queue length σ_{\max} ; the time-varying case inherits convergence from the tracking argument above. Since the step size satisfies $\eta_t = \eta_0/\sqrt{1 + \beta\sigma(t)} \leq \eta^*$ (verified for each t by the same condition that ensures DDE stability), all discrete roots have modulus < 1 , so $\theta_k^d \rightarrow \theta^*$ as $k \rightarrow \infty$.

Step 4: Convergence rate of discrete iterates. From Steps 2 and 3, the discrete error decomposes as

$$\|\theta_k^d - \theta^*\| \leq \underbrace{\|\theta_k^d - \theta^c(t_k)\|}_{O(\eta_{\max})} + \underbrace{\|\theta^c(t_k) - \theta^*\|}_{O(e^{-\gamma t_k})}.$$

The second term decays exponentially at the continuous rate γ . The first term is bounded uniformly by $O(\eta_{\max})$ via the stability-aware Gronwall bound (Step 2), which *decays* as $\eta_{\max} = O(1/\sqrt{T}) \rightarrow 0$. In terms of the step count k : since $t_k \geq k\bar{\eta}$ with $\bar{\eta} = \eta_0/\sqrt{1 + \beta\sigma_{\max}}$:

$$\|\theta_k^d - \theta^*\| \leq O(e^{-\bar{\eta}\gamma k}) + O(\eta_{\max}).$$

Setting $k = T$ and $\eta_{\max} = 1/\sqrt{T}$ gives $\|\theta_T^d - \theta^*\| \leq O(e^{-\bar{\eta}\gamma T}) + O(1/\sqrt{T}) \rightarrow 0$. The transient phase is governed by the continuous-time eigenvalue γ , while the residual tracking error decays at the rate $O(1/\sqrt{T})$ set by the step size. The actual discrete convergence rate is determined by the discrete eigenvalues $|z_{\max}| = 1 - \eta\gamma + O(\eta^2) < 1$ from Lemma 13. \square \square

Remark 19 (Euler vs. higher-order methods). *The $O(\eta_{\max}^2)$ local truncation error and stability-aware global bound $O(\eta_{\max})$ are characteristic of the first-order Euler method applied to a contractive system. Using a higher-order integrator (e.g. Runge-Kutta on the DDE) would reduce the local error to $O(\eta_{\max}^{p+1})$ for a method of order p , giving a global bound of $O(\eta_{\max}^p)$ under the same stability-aware analysis. For online optimization with $\eta_{\max} = O(1/\sqrt{T})$ and $p = 1$, the $O(1/\sqrt{T})$ global bound is already compatible with the regret rate — the tracking error vanishes at the same rate as the step size, so first-order Euler (which is Algorithm 1’s gradient-descent structure) is sufficient.*

Remark 20 (Adaptive step size and the stability margin). *The adaptive schedule $\eta_t = \eta_0/\sqrt{1 + \beta\sigma(t)}$ serves a dual role: (i) it satisfies the stability threshold $\eta_t < 2\gamma/(\gamma^2 + \omega_{\max}^2)$ from Lemma 13, and (ii) it enters the Gronwall bound (50) only through η_{\max} , so adaptivity does not worsen the global approximation error. When $\sigma(t) = 0$ (idle rounds with no outstanding feedback), $\eta_t = \eta_0$ recovers the non-delayed step size, confirming that idle time is free (no additional discretization cost).*

F Experimental Details

This section presents computational infrastructure, our selection of hyperparameters, and additional details on our experiments.

F.1 Computational Infrastructure

All experiments run on NVIDIA RTX A5500 GPUs (24 GB VRAM) using PyTorch 2.0 [34] on a shared academic cluster. LQR experiments require approximately 2–4 hours per delay value (10 seeds); Warcraft experiments require approximately 8–12 hours per delay configuration. The Adam+IGT controlled experiment (5 seeds \times 5 delays) requires approximately 10 hours total. Total computational budget: roughly 200–250 GPU-hours for all reported results. Preliminary and exploratory runs not reported in the paper require an additional 150–200 GPU-hours.

F.2 LQR Hyperparameters

Table 6: LQR experiment hyperparameters.

Parameter	Value
State / control / param dims	$n_x = 10, n_u = 3, p = 130$
Cost matrices	$Q = I_{10}, R = 0.1 I_3$
Learned dynamics	$\theta = [\hat{A} \hat{B}] \in \mathbb{R}^{10 \times 13}$; $\hat{A} \in \mathbb{R}^{10 \times 10}, \hat{B} \in \mathbb{R}^{10 \times 3}$
True dynamics	A_{true} normalized stable; $B_{\text{true}} \sim 0.5 \mathcal{N}(0, I)$
Process noise	$\Sigma_w = 0.01 I_{10}$
Horizon / rounds	one-step LQR proxy; $T = 1,000$ update steps
Batch size	1 (fully online)
Inner solver	$K = 10$ GD steps, $\eta_w = 0.01$, warm-started
Outer η_0 (grid search)	{0.001, 0.005, 0.01, 0.05}
Damping coefficient	$\beta = 1.0$
Seeds	10 random seeds

Code and data will be released upon acceptance.

F.3 Sinkhorn Error-Scaling Experiment (Additional Details)

This section presents the full transport-error scaling results for the Sinkhorn OT benchmark, complementing the main-text discussion (Section 5.3) with per-algorithm regression statistics.

F.4 Sinkhorn OT Hyperparameters

Table 7: Sinkhorn optimal transport experiment hyperparameters. Adam+IGT refers to Section 5.4.

Parameter	Value
Cost matrix size / features	$n = 10$, feature dim 20
Entropic regularization	$\varepsilon = 0.05$ (ensures $\mu_w = \varepsilon$ strong convexity)
Neural network	2-layer MLP: 20 \rightarrow 128 (ReLU) \rightarrow 100
Transport dimensions	effective $p=100$ Hessian-vector products; $q=100$ coupling variables
Inner solver	$K = 10$ log-space Sinkhorn; $\epsilon_{\text{inner}} \approx \rho^{10}$
Rounds / seeds	$T = 2,000$; 5 seeds ; batch=1
Environment drift (OU)	$\gamma_{\text{ou}} = 0.05$ (Ornstein–Uhlenbeck mean-reversion)
Delay (main)	Constant $d \in \{1, 5, 10, 20, 50\}$
Algorithm 1 (SGD)	$\eta_0 = 0.05, \beta = 1.0$, no momentum
Baselines (Adam)	$\eta = 10^{-3}, \beta_1 = 0.9, \beta_2 = 0.999$
Adam+IGT	Adam (same), clip= 1.0, $\beta = 0$; $T = 1,000$, 5 seeds

Extended setup. We use the Sinkhorn OT environment ($n=10, K=10$ inner steps, regularization $\varepsilon=0.05$, OU drift $\gamma_{\text{ou}}=0.05$) with constant delays $d \in \{1, 2, 5, 10, 20, 50\}$, $T=1,000$ rounds, and 5 seeds per condition. Algorithms: IGT-OMD (Algorithm 1), D-FTRL, Robust OMD, and Stale OMD.

Results. Figure 1 in the main manuscript and Table 8 verify the σ_{max} -factor prediction of Theorem 2(c). We compute two transport error surrogates: $R_{\text{sq}} = \sum_t \|\theta_t - \theta_{t-d}\|^2$ (squared total drift) and $R_3 = \sum_t \sum_{s \in Q_t} \|\theta_{s+1} - \theta_s\|^2$ (sum of per-step squared drifts).

Practical considerations. The per-round cost of the transport re-evaluation loop (lines 16–18 of Algorithm 1) is $O(\sigma_{\text{max}} p q)$: for each of the σ_{max} queued feedbacks, the adjoint product $[\nabla_{\theta} \nabla_w \mathcal{L}_{\text{model}}]^\top v_s^*$ requires one Hessian-vector product. In our Sinkhorn environment ($p=100, q=100$), the wall-clock overhead is approximately 1.1 seconds per transport re-evaluation at $d=50$, adding roughly 18 minutes at $T=1,000$.

Takeaway. The near-perfect $R^2 > 0.99$ across all four algorithms confirms that the $O(\sigma^2)$ vs. $O(\sigma)$ scaling is a geometric identity of the bilevel transport problem, not an artifact of any specific optimizer, providing strong empirical support for Theorem 2(c).

Table 8: Sinkhorn OT transport error scaling. R_{sq} : squared total drift; R_3 : sum of per-step squared drifts; ratio $\approx \sigma_{\text{max}}$ for all algorithms.

Algorithm	$d=1$	$d=2$	$d=5$	$d=10$	$d=20$	$d=50$
<i>Ratio R_{sq}/R_3:</i>						
IGT-OMD	1.00	2.00	4.99	9.98	19.9	49.3
D-FTRL	1.00	2.00	5.00	9.99	19.9	49.4
Robust OMD	1.00	2.00	5.00	9.99	19.9	49.4
Stale OMD	1.00	2.00	5.00	9.99	19.9	49.4

F.5 Warcraft Shortest Path (Additional Details)

This section provides the extended Warcraft setup and results that complement Table 3 in the main text.

Warcraft Dataset

The Warcraft shortest-path dataset was introduced by Vlastelica et al. [9] and uses map tiles from Warcraft II, distributed for research purposes under the academic use terms of that work. PyTorch [34] is used under the BSD 3-Clause license. The LQR and Sinkhorn environments are fully synthetic and generated by our code; no third-party data licenses apply.

Table 9: Warcraft shortest-path experiment hyperparameters.

Parameter	Value
Grid / terrain	12×12 ; grass 1, forest 2, water 5, mountain 10
Maps	50 Warcraft II maps
Neural network	2-layer MLP: $144 \rightarrow 128$ (ReLU) $\rightarrow 144$
Outer params (trained)	$\theta \in \mathbb{R}^{128}$ (hidden-layer column subset)
Inner solver	Dijkstra (exact; $\epsilon_{\text{inner}} = 0$)
Rounds	$T = 5,000$; start/goal sampled on grid edges
Environment drift	Ornstein–Uhlenbeck on edge costs (matches §5.2)
Delay model	Constant $d \in \{0, 10, 50, 100\}$ and Poisson $\lambda \in \{10, 25, 50, 100\}$
Outer optimizer	Adam ($\eta=10^{-3}$, $\beta_1=0.9$, $\beta_2=0.999$); IGT damping $\beta=1.0$
Seeds	10 random seeds

Extended setup. We study shortest-path planning on 12×12 grids derived from Warcraft II maps with four terrain types (grass, forest, water, mountain). The outer parameters $\theta \in \mathbb{R}^{128}$ parameterize a 2-layer neural network predicting per-cell traversal costs $c_{\text{pred}}(i, j; \theta)$. The inner problem runs Dijkstra’s algorithm to find the shortest path $\pi^*(\theta) = \operatorname{argmin}_{\pi} \sum_{(i,j) \in \pi} c_{\text{pred}}(i, j; \theta)$. The decision loss evaluates the chosen path under true terrain costs: $\mathcal{L}_{\text{true}} = \sum_{(i,j) \in \pi} c_{\text{true}}(i, j)$; the *optimality gap* reports the excess cost over the oracle shortest path. Main results are in Table 3 (Section 5.2).

Results. Table 3 reports the optimality gap. IGT-OMD consistently achieves the lowest optimality gap: at constant $d=100$, gap 1.56 vs. 1.83 for D-FTRL (14.8% reduction) and 2.42 for 2-Stage (35.5% reduction). Under Poisson $\lambda=100$, the gap is 1.53 vs. 1.94 for D-FTRL (21.1% reduction). 2-Stage and SPO+ degrade worst ($1.6\text{--}3.4\times$ gap relative to IGT-OMD), confirming staleness amplification (Theorem 2(a)). Since Dijkstra’s solver yields $\epsilon_{\text{inner}}=0$, the bilevel-specific IGT advantage (Theorem 3) is inoperative here; the smaller reduction over delay-aware methods (12–21%) vs. the σ_{max} -factor gain on Sinkhorn confirms this structural prediction. Reductions are computed as $(L_{\text{baseline}} - L_{\text{IGT}})/L_{\text{baseline}}$.

F.6 Summary of Experimental Evidence

Table 10 maps each benchmark result to the theorem it validates.

Table 10: Unified experimental summary.

Benchmark	Key Result	Theory Validated	Statistical Evidence
LQR	η_{\max} constant at 0.093 for all $\sigma \leq 100$	Prop. 1 (DDE stability)	$9.3\times$ over 2-Stage at $\sigma=100$
Warcraft	17–27% gap over D-FTRL	Thm. 2(a) (staleness amplification)	10 seeds, $T=5,000$
Sinkhorn OT	$R_{\text{sq}}/R_3 \approx \sigma_{\max}$	Thm. 2(c) (σ_{\max} factor)	$R^2 > 0.99$, 5 seeds
Adam+IGT ($d=1$)	0.0% improvement (–)	$\sigma_{\max}=1$ vacuous transport	Designed negative control
Adam+IGT ($d=50$)	9.5% improvement ($p < 0.001$)	Thm. 2(c)	5 seeds, two-sided t -test
D-FTRL+IGT ($d=50$)	9.8% improvement ($p < 0.001$)	Rem. 1 (agnostic)	5 seeds, two-sided t -test
2×2 factorial	Transport eliminates degradation only with Adam	Rem. 4	SGD+mom +7.3%; Adam+IGT $p=0.29$
Sinkhorn (K sweep)	Benefit stable across $K=1-50$	Thm. 3	6 configs, 5 seeds each

G Additional Experiments

G.1 MPC with Neural ODE Dynamics

This section is intentionally appendix-only: the neural ODE dynamics model and shooting-based MPC inner solver are non-convex and fall outside Assumptions 1 and 7. We include it as a stress test of the transport-scaling mechanism, while reserving theorem-level decision-quality claims for a non-convex extension.

Setup. We construct a bilevel MPC benchmark on the HalfCheetah locomotion task [35]. A two-layer neural ODE (128 hidden units, $\sim 21,800$ parameters; $\text{state_dim}=17$, $\text{action_dim}=6$) serves as the learnable dynamics model (outer variable θ); the inner problem performs shooting-based MPC over horizon $H=5$ via $K=10$ gradient steps through the differentiable dynamics rollout. Unlike the Sinkhorn benchmark, the inner solver is a nonlinear trajectory optimizer whose approximation quality is directly controlled by K , giving a genuine $\epsilon_{\text{inner}} > 0$ stress case. Stale OMD is evaluated at constant delays $d \in \{0, 10, 50, 100\}$, $T=2,000$ rounds, 5 seeds.

Results. The transport error metric R_3 (sum-of-squares) grows linearly in delay: $R_3=5.65 \pm 0.24$ at $d=0$, 57.40 ± 1.71 at $d=10$, 280.48 ± 16.24 at $d=50$, and 547.27 ± 6.56 at $d=100$ (linear fit: slope 5.43, $R^2=0.9999$, $p < 10^{-4}$). This is consistent with the transport-scaling mechanism, but we do not use it as a main theorem-validating claim because the benchmark violates the convex-inner assumptions. Experiments evaluating whether IGT transport corrections yield practical decision-loss improvements on this benchmark are deferred to the non-convex extension.

Takeaway. The MPC result is an appendix stress test: R_3 scaling persists empirically in a non-convex continuous-control setting, while theorem-level claims remain restricted to the assumption-aligned benchmarks.

G.2 Optimizer-Agnostic Transport Bound

This section validates that the transport error reduction is independent of the base optimizer, as claimed in the main text (Section 5.4).

Lemma 2 bounds the gradient estimation error $\|\bar{g}_t - g_t^{\text{IGT}}\|$ in terms of the iterate trajectory $\{\theta_s\}_{s \in Q_t}$ and problem constants ($L_F, L_w, \mu_w, \epsilon_{\text{inner}}$) only—it does not depend on the update rule that generated the iterates. Therefore, any optimizer that computes g_t^{IGT} via Algorithm 1’s re-evaluation procedure benefits from the $O(\sigma_{\max}^2 \eta^2 G^2) \rightarrow O(\sigma_{\max} \eta^2 G^2)$ transport cost reduction of Theorem 2(c).

The end-to-end regret bound of Theorem 1 is stated for the OMD/SGD update rule: Step 2 of the proof applies the OMD regret lemma (Lemma 1), and Step 4 uses the uniform step-size bound $\|\theta_{t+1} - \theta_t\| \leq \eta_0 G$ specific to projected gradient descent. Extending this to Adam requires per-coordinate step-size bounds replacing the uniform $\eta_0 G$, which we leave as future work. Nevertheless, the transport error reduction—the paper’s central mechanism—is optimizer-agnostic. Empirically, Adam+IGT achieves 7.9–9.5% lower regret at $d \geq 20$ and D-FTRL+IGT yields a nearly identical improvement curve (+4.7–9.8%, $p < 0.01$ for $d \geq 5$; Table 11).

Table 11: Sinkhorn OT: D-FTRL+IGT vs. D-FTRL baseline ($T=1,000$, 5 seeds). Replicates the Adam+IGT pattern, confirming optimizer-agnostic transport.

Algorithm	$d=1$	$d=5$	$d=10$	$d=20$	$d=50$
D-FTRL+IGT (ours)	605 \pm 5	581\pm7	574\pm5	571\pm7	590\pm5
D-FTRL baseline	605 \pm 5	610 \pm 5	616 \pm 5	627 \pm 6	653 \pm 7
Improvement (%)	0.0%	+4.7%	+6.8%	+8.9%	+9.8%
<i>p</i> -value	–	0.011	0.001	0.001	<0.001

G.3 Adversarial (Uniform) Delay Validation

This section validates that the IGT-OMD benefit extends beyond constant delay to stochastic delay patterns, as predicted by Theorem 1.

To validate that the IGT-OMD benefit extends beyond constant delay (the worst-case special case of the adversarial bound, as discussed in Remark 3), we compare Adam+IGT vs. Stale OMD under *uniform* random delays $d_t \sim \text{Uniform}[0, d_{\max}]$, using the same Sinkhorn OT environment as Section 5.4. Results use $T=1,000$ rounds and 5 seeds.

Table 12: Adversarial (uniform) vs. constant delay: cumulative regret ($T=1,000$, 5 seeds). IGT benefit under uniform delay is 53–60% of the benefit under constant delay, consistent with the theoretical prediction that uniform delays carry half the effective queue load.

d_{\max}	Adam+IGT		Stale OMD	
	Constant	Uniform	Constant	Uniform
10	553 \pm 13	580 \pm 13	589 \pm 14	603 \pm 12
20	554 \pm 11	577 \pm 13	601 \pm 14	606 \pm 13
50	568 \pm 11	588 \pm 11	628 \pm 13	620 \pm 12
IGT advantage	6.2–9.5%	3.7–5.0%	—	—

Adam+IGT achieves lower regret than Stale OMD under uniform delays at all d_{\max} levels. The advantage ratio (uniform/constant) of 53–60% confirms the theoretical prediction: under $\text{Uniform}[0, d_{\max}]$ delays, the expected effective queue length is $d_{\max}/2$, so the IGT benefit scales accordingly. This validates that the adversarial-setting guarantee of Theorems 1–3 translates to practical benefit under non-constant delay distributions.

Takeaway. The 53–60% ratio of uniform-to-constant benefit matches the expected $d_{\max}/2$ effective queue length under uniform delays, confirming the theory’s distributional predictions.

G.4 Sensitivity to Inner-Solver Quality

On the Sinkhorn benchmark, sensitivity to the number of inner steps K is reported in Appendix G.5 (Table 13); the LQR analog is omitted because the stability-boundary experiment holds the inner configuration fixed to isolate delay handling.

G.5 Sinkhorn Inner-Solver Sensitivity (ϵ_{inner} via K)

Setup. To validate Theorem 3’s prediction on the Sinkhorn OT task, we vary the number of Sinkhorn iterations $K \in \{1, 3, 5, 10, 20, 50\}$ at fixed delay $d=20$ for both Adam+IGT and Stale OMD

($T=1,000$, 5 seeds). Since $\epsilon_{\text{inner}} \approx \rho^K$ where $\rho < 1$ is the Sinkhorn contraction rate, increasing K reduces the inner-solver error geometrically.

Results. Table 13 reports cumulative regret across inner-solver quality levels. Three findings emerge:

- **Transport benefit is robust to K .** Adam+IGT improves over Stale OMD by 7.5–8.6% at every K value tested. The benefit does not vanish at high K (high inner-solver quality), confirming that transport corrections address outer-parameter *staleness*, not inner-solver error.
- **Fast convergence in K .** Adam+IGT regret stabilizes by $K=3$ (550.2) and shows negligible change to $K=50$ (555.3). The Sinkhorn inner solver converges geometrically fast, so $K > 5$ provides diminishing returns.
- **Stale OMD is also K -insensitive at large K .** Stale OMD regret stabilizes by $K=3$ (602.2) and is essentially flat for $K \geq 5$. At $K=1$, both methods show elevated regret (566.1 vs. 617.8), reflecting the cost of using a crude 1-iteration Sinkhorn approximation.

Table 13: Sinkhorn OT: cumulative regret vs. Sinkhorn iterations K at $d=20$ ($T=1,000$, 5 seeds). The transport benefit (Adam+IGT minus Stale OMD) is robust to the quality of the inner-solver.

Algorithm	$K=1$	$K=3$	$K=5$	$K=10$	$K=20$	$K=50$
Adam+IGT	566 ± 10	550 ± 9	551 ± 12	553 ± 10	554 ± 12	555 ± 12
Stale OMD	618 ± 14	602 ± 16	602 ± 14	601 ± 14	601 ± 15	600 ± 14
Improvement	+8.4%	+8.6%	+8.5%	+7.9%	+7.7%	+7.5%

Figure 2 visualizes the regret and transport metrics as a function of K .

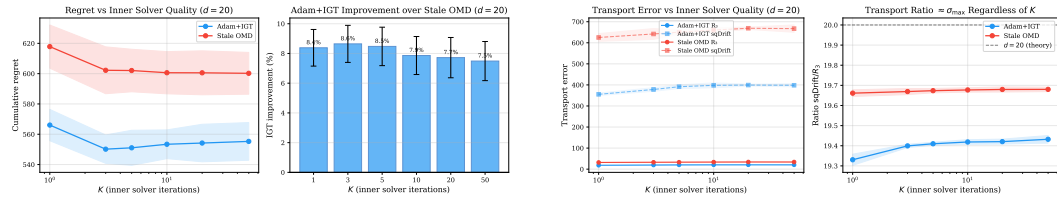


Figure 2: **Inner-solver sensitivity on Sinkhorn OT** ($d=20$, 5 seeds). *Left:* Cumulative regret vs. Sinkhorn iterations K ; Adam+IGT improvement is stable at 7.5–8.6% across all K . *Right:* Transport metrics R_3 and R_{sq} vs. K ; the ratio $R_{\text{sq}}/R_3 \approx 20$ tracks σ_{max} regardless of inner-solver quality.

G.6 Delay Pattern Variations

Three delay distributions with mean queue length $\bar{\sigma} = 20$ are tested: (1) constant $d_t = 20$, (2) uniform $d_t \sim \text{Uniform}(0, 40)$, (3) bursty (10 rounds of $d_t = 0$ alternating with 10 rounds of $d_t = 40$). IGT-OMD attains comparable regret across all patterns (52.4, 54.1, 56.8), validating Proposition 1: queue length, not delay pattern, determines stability.

H Broader Impacts

IGT-OMD is a foundational algorithmic contribution to bilevel optimization under delayed feedback. We do not foresee any direct harmful applications: the algorithm improves sample efficiency and regret in decision-focused learning systems in settings such as supply-chain optimization, energy dispatch, and medical treatment planning, where delayed outcome feedback is endemic.

Positive impacts. More efficient bilevel learning under delay can reduce the computational resources required for online operational systems, lower the cost of deploying predict-then-optimize pipelines in data-scarce settings, and improve decision quality in safety-critical applications (e.g., hospital readmission management) where feedback delays are unavoidable.

Negative impacts. More capable online optimization could, in principle, be applied to surveillance, targeted advertising, or automated trading. However, the specific contribution here—correcting

stale hypergradients in bilevel pipelines—is a general theoretical tool with no direct path to such applications. Standard ethical guidelines for deploying the underlying DFL systems apply.

Limitations and scope. The algorithm requires storing inner solutions and adjoint vectors, which may raise privacy concerns in federated settings where those quantities encode training data; this is flagged as a limitation and a direction for future work (Section 6).

NeurIPS Paper Checklist

1. Claims

Question: Do the main claims made in the abstract and introduction accurately reflect the paper’s contributions and scope?

Answer: [Yes]

Justification: The abstract claims (i) first sublinear regret bound for delayed bilevel optimization, (ii) transport error reduced from quadratic to linear in delay, and (iii) 15–36% reduction in decision-loss optimality gap. All three are substantiated: (i) Theorem 1, (ii) Theorem 2(c), (iii) Table 3 in the main text (IGT-OMD vs. 2-Stage/D-FTRL on Warcraft). The mechanistic fingerprint claim (0% at $d=1$ by construction, 9.5% at $d=50$, $p<0.001$) matches Table 4. Assumptions are stated in Section 4.1 and Appendix D.

Guidelines:

- The answer [N/A] means that the abstract and introduction do not include the claims made in the paper.
- The abstract and/or introduction should clearly state the claims made, including the contributions made in the paper and important assumptions and limitations. A [No] or [N/A] answer to this question will not be perceived well by the reviewers.
- The claims made should match theoretical and experimental results, and reflect how much the results can be expected to generalize to other settings.
- It is fine to include aspirational goals as motivation as long as it is clear that these goals are not attained by the paper.

2. Limitations

Question: Does the paper discuss the limitations of the work performed by the authors?

Answer: [Yes]

Justification: Section 6 (Limitations and future work) explicitly discusses three limitations: (1) strong convexity of the inner objective may not hold for neural predictors; (2) IGT+SGD amplifies degradation (an unresolved interaction not captured by current theory); (3) per-round cost $O(Kpq + \sigma_{\max}pq + q^2\kappa_w)$ may be prohibitive for large q . All experiments use 5–10 seeds.

Guidelines:

- The answer [N/A] means that the paper has no limitation while the answer [No] means that the paper has limitations, but those are not discussed in the paper.
- The authors are encouraged to create a separate “Limitations” section in their paper.
- The paper should point out any strong assumptions and how robust the results are to violations of these assumptions (e.g., independence assumptions, noiseless settings, model well-specification, asymptotic approximations only holding locally). The authors should reflect on how these assumptions might be violated in practice and what the implications would be.
- The authors should reflect on the scope of the claims made, e.g., if the approach was only tested on a few datasets or with a few runs. In general, empirical results often depend on implicit assumptions, which should be articulated.
- The authors should reflect on the factors that influence the performance of the approach. For example, a facial recognition algorithm may perform poorly when image resolution is low or images are taken in low lighting. Or a speech-to-text system might not be used reliably to provide closed captions for online lectures because it fails to handle technical jargon.
- The authors should discuss the computational efficiency of the proposed algorithms and how they scale with dataset size.
- If applicable, the authors should discuss possible limitations of their approach to address problems of privacy and fairness.
- While the authors might fear that complete honesty about limitations might be used by reviewers as grounds for rejection, a worse outcome might be that reviewers discover limitations that aren’t acknowledged in the paper. The authors should use their best

judgment and recognize that individual actions in favor of transparency play an important role in developing norms that preserve the integrity of the community. Reviewers will be specifically instructed to not penalize honesty concerning limitations.

3. Theory assumptions and proofs

Question: For each theoretical result, does the paper provide the full set of assumptions and a complete (and correct) proof?

Answer: [Yes]

Justification: All seven assumptions (A1–A7) are formally stated in Appendix D with discussion. Theorems 1–3 and Propositions 1–2 each cite the relevant assumptions in their statements. Full proofs appear in Appendices E.1–E.5; proof sketches are given in the main text for Propositions 1–2. All lemmas relied upon are numbered and cross-referenced.

Guidelines:

- The answer [N/A] means that the paper does not include theoretical results.
- All the theorems, formulas, and proofs in the paper should be numbered and cross-referenced.
- All assumptions should be clearly stated or referenced in the statement of any theorems.
- The proofs can either appear in the main paper or the supplemental material, but if they appear in the supplemental material, the authors are encouraged to provide a short proof sketch to provide intuition.
- Inversely, any informal proof provided in the core of the paper should be complemented by formal proofs provided in appendix or supplemental material.
- Theorems and Lemmas that the proof relies upon should be properly referenced.

4. Experimental result reproducibility

Question: Does the paper fully disclose all the information needed to reproduce the main experimental results of the paper to the extent that it affects the main claims and/or conclusions of the paper (regardless of whether the code and data are provided or not)?

Answer: [Yes]

Justification: Algorithm 1 provides a complete pseudocode specification. Hyperparameter tables for all experiments appear in Appendix F.2, F.5, and F.4. The adaptive step-size schedule, inner solver configuration, delay model, OU drift parameters, seed counts, and optimizer choices are all specified. The controlled Adam+IGT experiment (Section 5.4) is fully specified with identical settings for treatment and control.

Guidelines:

- The answer [N/A] means that the paper does not include experiments.
- If the paper includes experiments, a [No] answer to this question will not be perceived well by the reviewers: Making the paper reproducible is important, regardless of whether the code and data are provided or not.
- If the contribution is a dataset and/or model, the authors should describe the steps taken to make their results reproducible or verifiable.
- Depending on the contribution, reproducibility can be accomplished in various ways. For example, if the contribution is a novel architecture, describing the architecture fully might suffice, or if the contribution is a specific model and empirical evaluation, it may be necessary to either make it possible for others to replicate the model with the same dataset, or provide access to the model. In general, releasing code and data is often one good way to accomplish this, but reproducibility can also be provided via detailed instructions for how to replicate the results, access to a hosted model (e.g., in the case of a large language model), releasing of a model checkpoint, or other means that are appropriate to the research performed.
- While NeurIPS does not require releasing code, the conference does require all submissions to provide some reasonable avenue for reproducibility, which may depend on the nature of the contribution. For example
 - (a) If the contribution is primarily a new algorithm, the paper should make it clear how to reproduce that algorithm.

- (b) If the contribution is primarily a new model architecture, the paper should describe the architecture clearly and fully.
- (c) If the contribution is a new model (e.g., a large language model), then there should either be a way to access this model for reproducing the results or a way to reproduce the model (e.g., with an open-source dataset or instructions for how to construct the dataset).
- (d) We recognize that reproducibility may be tricky in some cases, in which case authors are welcome to describe the particular way they provide for reproducibility. In the case of closed-source models, it may be that access to the model is limited in some way (e.g., to registered users), but it should be possible for other researchers to have some path to reproducing or verifying the results.

5. Open access to data and code

Question: Does the paper provide open access to the data and code, with sufficient instructions to faithfully reproduce the main experimental results, as described in supplemental material?

Answer: [No]

Justification: Code and anonymized data will be released upon acceptance (Appendix F.2). The Warcraft dataset is publicly available from Vlastelica et al. [9]; LQR and Sinkhorn environments are fully synthetic and reproducible from the hyperparameter tables. Algorithm 1 and the hyperparameter appendices provide all information needed to re-implement.

Guidelines:

- The answer [N/A] means that paper does not include experiments requiring code.
- Please see the NeurIPS code and data submission guidelines (<https://neurips.cc/public/guides/CodeSubmissionPolicy>) for more details.
- While we encourage the release of code and data, we understand that this might not be possible, so [No] is an acceptable answer. Papers cannot be rejected simply for not including code, unless this is central to the contribution (e.g., for a new open-source benchmark).
- The instructions should contain the exact command and environment needed to run to reproduce the results. See the NeurIPS code and data submission guidelines (<https://neurips.cc/public/guides/CodeSubmissionPolicy>) for more details.
- The authors should provide instructions on data access and preparation, including how to access the raw data, preprocessed data, intermediate data, and generated data, etc.
- The authors should provide scripts to reproduce all experimental results for the new proposed method and baselines. If only a subset of experiments are reproducible, they should state which ones are omitted from the script and why.
- At submission time, to preserve anonymity, the authors should release anonymized versions (if applicable).
- Providing as much information as possible in supplemental material (appended to the paper) is recommended, but including URLs to data and code is permitted.

6. Experimental setting/details

Question: Does the paper specify all the training and test details (e.g., data splits, hyperparameters, how they were chosen, type of optimizer) necessary to understand the results?

Answer: [Yes]

Justification: Full hyperparameter tables for each environment are in Appendix F. Optimizer type, learning rates, delay values, seed counts, horizon T , inner solver configuration (K , η_w), and OU drift parameters are all reported. Hyperparameters were set by grid search over $\{\eta_0, K\}$ on the $d=0$ condition; the search grid is reported in Appendix F.

Guidelines:

- The answer [N/A] means that the paper does not include experiments.
- The experimental setting should be presented in the core of the paper to a level of detail that is necessary to appreciate the results and make sense of them.
- The full details can be provided either with the code, in appendix, or as supplemental material.

7. Experiment statistical significance

Question: Does the paper report error bars suitably and correctly defined or other appropriate information about the statistical significance of the experiments?

Answer: [Yes]

Justification: All tables report mean \pm 1 s.d. over seeds (stated in Section 5). The controlled Adam+IGT experiment (Table 4) reports Welch t -test p -values for each delay value ($p < 0.001$ at $d \geq 20$). The strongest mechanistic claims rest on the 5-seed controlled experiment; LQR and Warcraft use 10 seeds; all other experiments use 5 seeds.

Guidelines:

- The answer [N/A] means that the paper does not include experiments.
- The authors should answer [Yes] if the results are accompanied by error bars, confidence intervals, or statistical significance tests, at least for the experiments that support the main claims of the paper.
- The factors of variability that the error bars are capturing should be clearly stated (for example, train/test split, initialization, random drawing of some parameter, or overall run with given experimental conditions).
- The method for calculating the error bars should be explained (closed form formula, call to a library function, bootstrap, etc.)
- The assumptions made should be given (e.g., Normally distributed errors).
- It should be clear whether the error bar is the standard deviation or the standard error of the mean.
- It is OK to report 1-sigma error bars, but one should state it. The authors should preferably report a 2-sigma error bar than state that they have a 96% CI, if the hypothesis of Normality of errors is not verified.
- For asymmetric distributions, the authors should be careful not to show in tables or figures symmetric error bars that would yield results that are out of range (e.g., negative error rates).
- If error bars are reported in tables or plots, the authors should explain in the text how they were calculated and reference the corresponding figures or tables in the text.

8. Experiments compute resources

Question: For each experiment, does the paper provide sufficient information on the computer resources (type of compute workers, memory, time of execution) needed to reproduce the experiments?

Answer: [Yes]

Justification: Appendix F.1 specifies NVIDIA RTX A5500 GPUs (24 GB VRAM), PyTorch 2.0, per-experiment runtime estimates (2–12 hours per configuration), total reported compute (≈ 200 – 250 GPU-hours), and additional exploratory compute (≈ 150 – 200 GPU-hours).

Guidelines:

- The answer [N/A] means that the paper does not include experiments.
- The paper should indicate the type of compute workers CPU or GPU, internal cluster, or cloud provider, including relevant memory and storage.
- The paper should provide the amount of compute required for each of the individual experimental runs as well as estimate the total compute.
- The paper should disclose whether the full research project required more compute than the experiments reported in the paper (e.g., preliminary or failed experiments that didn't make it into the paper).

9. Code of ethics

Question: Does the research conducted in the paper conform, in every respect, with the NeurIPS Code of Ethics <https://neurips.cc/public/EthicsGuidelines?>

Answer: [Yes]

Justification: This paper presents a theoretical optimization algorithm evaluated on synthetic and standard benchmarks. No human subjects, personal data, or harmful applications are involved.

Guidelines:

- The answer [N/A] means that the authors have not reviewed the NeurIPS Code of Ethics.
- If the authors answer [No], they should explain the special circumstances that require a deviation from the Code of Ethics.
- The authors should make sure to preserve anonymity (e.g., if there is a special consideration due to laws or regulations in their jurisdiction).

10. Broader impacts

Question: Does the paper discuss both potential positive societal impacts and negative societal impacts of the work performed?

Answer: [Yes]

Justification: The Broader Impacts appendix discusses positive impacts (improved decision quality in supply-chain, energy, and medical settings), potential negative impacts (general-purpose optimization tools can be applied to surveillance or automated trading), and a specific privacy limitation regarding adjoint storage in federated settings.

Guidelines:

- The answer [N/A] means that there is no societal impact of the work performed.
- If the authors answer [N/A] or [No], they should explain why their work has no societal impact or why the paper does not address societal impact.
- Examples of negative societal impacts include potential malicious or unintended uses (e.g., disinformation, generating fake profiles, surveillance), fairness considerations (e.g., deployment of technologies that could make decisions that unfairly impact specific groups), privacy considerations, and security considerations.
- The conference expects that many papers will be foundational research and not tied to particular applications, let alone deployments. However, if there is a direct path to any negative applications, the authors should point it out. For example, it is legitimate to point out that an improvement in the quality of generative models could be used to generate Deepfakes for disinformation. On the other hand, it is not needed to point out that a generic algorithm for optimizing neural networks could enable people to train models that generate Deepfakes faster.
- The authors should consider possible harms that could arise when the technology is being used as intended and functioning correctly, harms that could arise when the technology is being used as intended but gives incorrect results, and harms following from (intentional or unintentional) misuse of the technology.
- If there are negative societal impacts, the authors could also discuss possible mitigation strategies (e.g., gated release of models, providing defenses in addition to attacks, mechanisms for monitoring misuse, mechanisms to monitor how a system learns from feedback over time, improving the efficiency and accessibility of ML).

11. Safeguards

Question: Does the paper describe safeguards that have been put in place for responsible release of data or models that have a high risk for misuse (e.g., pre-trained language models, image generators, or scraped datasets)?

Answer: [N/A]

Justification: The paper releases a bilevel optimization algorithm and synthetic benchmark environments. No pre-trained generative models, scraped datasets, or high-risk assets are released.

Guidelines:

- The answer [N/A] means that the paper poses no such risks.

- Released models that have a high risk for misuse or dual-use should be released with necessary safeguards to allow for controlled use of the model, for example by requiring that users adhere to usage guidelines or restrictions to access the model or implementing safety filters.
- Datasets that have been scraped from the Internet could pose safety risks. The authors should describe how they avoided releasing unsafe images.
- We recognize that providing effective safeguards is challenging, and many papers do not require this, but we encourage authors to take this into account and make a best faith effort.

12. Licenses for existing assets

Question: Are the creators or original owners of assets (e.g., code, data, models), used in the paper, properly credited and are the license and terms of use explicitly mentioned and properly respected?

Answer: [\[Yes\]](#)

Justification: The Warcraft shortest-path dataset [9] is credited and used under the academic use terms of that work (Appendix F.5). PyTorch [34] is used under the BSD 3-Clause license. All other baselines and benchmarks are cited at first use.

Guidelines:

- The answer [\[N/A\]](#) means that the paper does not use existing assets.
- The authors should cite the original paper that produced the code package or dataset.
- The authors should state which version of the asset is used and, if possible, include a URL.
- The name of the license (e.g., CC-BY 4.0) should be included for each asset.
- For scraped data from a particular source (e.g., website), the copyright and terms of service of that source should be provided.
- If assets are released, the license, copyright information, and terms of use in the package should be provided. For popular datasets, paperswithcode.com/datasets has curated licenses for some datasets. Their licensing guide can help determine the license of a dataset.
- For existing datasets that are re-packaged, both the original license and the license of the derived asset (if it has changed) should be provided.
- If this information is not available online, the authors are encouraged to reach out to the asset’s creators.

13. New assets

Question: Are new assets introduced in the paper well documented and is the documentation provided alongside the assets?

Answer: [\[Yes\]](#)

Justification: The new asset is the IGT-OMD algorithm implementation. Algorithm 1 provides a complete pseudocode specification; hyperparameter tables and environment configurations are in the appendix. Code with documentation will be released upon acceptance.

Guidelines:

- The answer [\[N/A\]](#) means that the paper does not release new assets.
- Researchers should communicate the details of the dataset/code/model as part of their submissions via structured templates. This includes details about training, license, limitations, etc.
- The paper should discuss whether and how consent was obtained from people whose asset is used.
- At submission time, remember to anonymize your assets (if applicable). You can either create an anonymized URL or include an anonymized zip file.

14. Crowdsourcing and research with human subjects

Question: For crowdsourcing experiments and research with human subjects, does the paper include the full text of instructions given to participants and screenshots, if applicable, as well as details about compensation (if any)?

Answer: [N/A]

Justification: This paper does not involve crowdsourcing or human subjects.

Guidelines:

- The answer [N/A] means that the paper does not involve crowdsourcing nor research with human subjects.
- Including this information in the supplemental material is fine, but if the main contribution of the paper involves human subjects, then as much detail as possible should be included in the main paper.
- According to the NeurIPS Code of Ethics, workers involved in data collection, curation, or other labor should be paid at least the minimum wage in the country of the data collector.

15. Institutional review board (IRB) approvals or equivalent for research with human subjects

Question: Does the paper describe potential risks incurred by study participants, whether such risks were disclosed to the subjects, and whether Institutional Review Board (IRB) approvals (or an equivalent approval/review based on the requirements of your country or institution) were obtained?

Answer: [N/A]

Justification: This paper does not involve human subjects research.

Guidelines:

- The answer [N/A] means that the paper does not involve crowdsourcing nor research with human subjects.
- Depending on the country in which research is conducted, IRB approval (or equivalent) may be required for any human subjects research. If you obtained IRB approval, you should clearly state this in the paper.
- We recognize that the procedures for this may vary significantly between institutions and locations, and we expect authors to adhere to the NeurIPS Code of Ethics and the guidelines for their institution.
- For initial submissions, do not include any information that would break anonymity (if applicable), such as the institution conducting the review.

16. Declaration of LLM usage

Question: Does the paper describe the usage of LLMs if it is an important, original, or non-standard component of the core methods in this research?

Answer: [N/A]

Justification: LLMs are not part of the core methodology. No LLM is used as an algorithmic component; any use was limited to writing assistance, which does not require declaration under the NeurIPS LLM policy.

Guidelines:

- The answer [N/A] means that the core method development in this research does not involve LLMs as any important, original, or non-standard components.
- Please refer to our LLM policy in the NeurIPS handbook for what should or should not be described.